UNIVERSITÀ DEGLI STUDI DI PADOVA

FACOLTÀ DI INGEGNERIA

CORSO DI LAUREA MAGISTRALE IN INGEGNERIA ELETTRICA

Measurements and numerical models for the evaluation of performance in microwave ovens

Relatore: *Ch.mo Prof. Ing. Fabrizio Dughiero*

Correlatori: *Ing. Marco Bullo*

Ing. Fernando Bressan

Laureando: *Fabio Pullano Colao*

ANNO ACCADEMICO 2011/2012

INDEX

Summary

Electromagnetic and thermal information are very important aspects to analyze heating processes on household microwave ovens. In this work are evaluated the system efficiency and the distribution of heat sources in the load, using different MWOs. In order to reach this aim, are developed numerical simulations and several experimental experiences. In particular, regarding this latter part are compared two different measurement methods: the use of IR camera and a set of measures using thermocouple probes. This project is also interesting because it allows us to validate a tool for numerical simulations, so called COMSOL Multi-physics, which is often used in order to design electromagnetic devices and for investigation about multi-physics problems.

The first chapter is a general background that introduces to microwave heating engineering.

In the second chapter is presented a wide theoretical part about microwave ovens. Here are also described the three main components that characterize the physical process: the magnetron as E-field's source, the waveguide that carries waves from the feeding to the last component, the resonant cavity.

The third chapter introduces to the dielectric and thermal properties which characterize the heating process in the load. Are also shown the phenomena that influence heating process performances and uniformity of heat sources.

The fourth chapter covers the part of experimental measurements using the different test equipment, comparing the results obtained.

The fifth chapter describes the numerical software (COMSOL Multi-physics), are presented the results obtained and, finally, will be done the validation of the tools.

The sixth final chapter provides the comparison between experimental tests and numerical models. Here are developed some conclusions and are presented outlooks for next investigations in the microwaves field of study.

Sommario

Le informazioni elettromagnetiche e termiche sono aspetti molto importanti per analizzare i processi di riscaldamento in forni a microonde ad uso domestico. In questo lavoro vengono valutati l'efficienza del sistema e la distribuzione delle fonti di calore nel carico, utilizzando differenti forni a microonde. Per raggiungere questo obiettivo, sono stati sviluppati simulazioni numeriche e diversi test sperimentali. In particolare, per quanto riguarda quest'ultima parte si confrontano due diversi metodi di misura: l'uso di telecamera a infrarossi e una serie di misure mediante sonde a termocoppia. Questo progetto è anche interessante perché ci permette di validare uno strumento per simulazioni numeriche, COMSOL Multi-phisics, che viene spesso utilizzato per la progettazione di dispositivi elettromagnetici e per l'indagine sui problemi multi-fisici.

Il primo capitolo è un background generale che introduce alle microonde.

Nel secondo capitolo viene presentata una larga parte teorica circa i forni a microonde. Qui vengono anche descritti i tre componenti principali che caratterizzano il processo fisico: il magnetron come sorgente di campo, la guida d'onda che porta le onde dall'alimentazione all'ultimo componente, la cavità risonante.

Il terzo capitolo introduce alle proprietà dielettriche e termiche che caratterizzano il processo di riscaldamento del carico. Sono inoltre descritti i fenomeni che influenzano le prestazioni del processo di riscaldamento e l'uniformità delle fonti di calore.

Il quarto capitolo riguarda la parte di misure sperimentali con diverse attrezzature di prova, confrontando i risultati ottenuti.

Il quinto capitolo descrive il software numerico (COMSOL Multi-phisics), vengono presentati i risultati ottenuti e la validazione delle simulazioni .

Il sesto e ultimo capitolo presenta il confronto tra le prove sperimentali e i modelli numerici. Qui vengono sviluppate alcune conclusioni e vengono presentate le prospettive per le indagini successive nel campo di studio delle microonde.

Introduction

Nowadays, the majority of applications of microwaves are related to radar and communication systems. Radar systems are used for detecting and locating air, ground, or seagoing targets and for air-traffic control systems, missile tracking radars, automobile collision-avoidance systems, weather prediction, motion detectors, and a wide variety of remote sensing systems. Microwave communication systems handle a large fraction of the world's international and other long-haul telephone, data and television transmission. And most of the currently developing wireless telecommunication systems, such as direct broadcast satellite (DBS) television, personal communication systems (PCSs), wireless local area computer networks (WLANS), cellular video (CV) systems, and global positioning satellite (GPS) systems, operate in the frequency range 1.5 to 94 GHz, and thus rely heavily on microwave technology.

Microwave heating of foods results from conversion of electromagnetic energy to thermal one through increased agitation of water molecules and charged ions when exposed to microwaves. Direct penetration of microwaves into food materials enables us to heat foods much faster than conventional heating methods.

The convenience brought about by fast microwave heating makes microwaves ovens a household necessity in modern society. Microwave heating systems are also commonly used in the food service and processing industry for fast heating applications. However, users of microwave ovens also experience various problems, in particular non-uniform heating.

Factors that influence uneven microwave heating include microwave cavity design, food physical properties, and food geometry. Those factors determine how the electrical field is distributed in oven and within foods.

The aims of this thesis are:

- Compare different kinds of household microwave ovens by means experimental tests, evaluating the energy efficiency of the heating process and uniformity of temperature distribution in the load.
- Develop numerical model in order to simulate as accurately as possible the process of microwave heating, including rotation of the turntable.

Chapter 1

General Background

1.1 – Introduction to microwave engineering

Microwave are electromagnetic waves at frequencies between 300 and 300.000 MHz (Decareau, 1985), with corresponding wavelengths of 1 to 0.001 m, respectively. (Figure 1 shows the microwave frequency band in the electromagnetic spectrum).

Because of the high frequencies (and short wavelengths), standard circuit theory generally cannot be used directly to solve microwave network problems. In a sense, standard circuit theory is an approximation or special use of the broader theory of electromagnetics as described by Maxwell's equations. This is due to the fact that, in general, the lumped circuit element approximations of circuit theory are not valid at microwave frequencies. Microwave components are often distributed elements, where the phase of a voltage or current changes significantly over the physical extent of the device, because the device dimension are on the order of the microwave wavelength. At much lower frequencies, the wavelength is large enough that there is insignificant phase variation across the dimension of a component.

The other extreme of frequency can be identified as optical engineering, in which the wavelength is much shorter than the dimension of the component. In this case Maxwell's equations can be simplified to the geometrical optics regime, and optical systems can be designed with the theory of geometrical optics.

Table 1 lists ISM bands used in different food applications. Industrial equipment for the listed frequency band is readily available from commercial suppliers.

Frequency (MHz)	Frequency tolerance (MHz)	Example of industrial applications	Countries
896	±10	Tempering of frozen products	Great Britain
915	±13	Precooking of bacon, tempering of frozen products	North and South America, China
2375	±50	Domestic microwave ovens	Albania, Bulgaria, Hungary, Romania, Czechoslovakia, former USSR
2450	±50	Domestic microwave ovens, industrial precooking of bacon, pasteurization and sterilization of packaged foods	Worldwide, except where 2375 MHz is used

Table 1: Important microwave frequency allocation for industrial, scientific and medical (ISM) use (Decareau, 1985; Metaxas and Meredith, 1993; Buffler, 1993)

EM waves propagate in space at speed of light ($3 \cdot 10^8$ m/s) and travelling in space without obstruction approximate the behaviour of plane waves. Electromagnetic waves have an electric (**E**) field component and a magnetic (**H**) field component that oscillate in phase and in directions perpendicular each other.

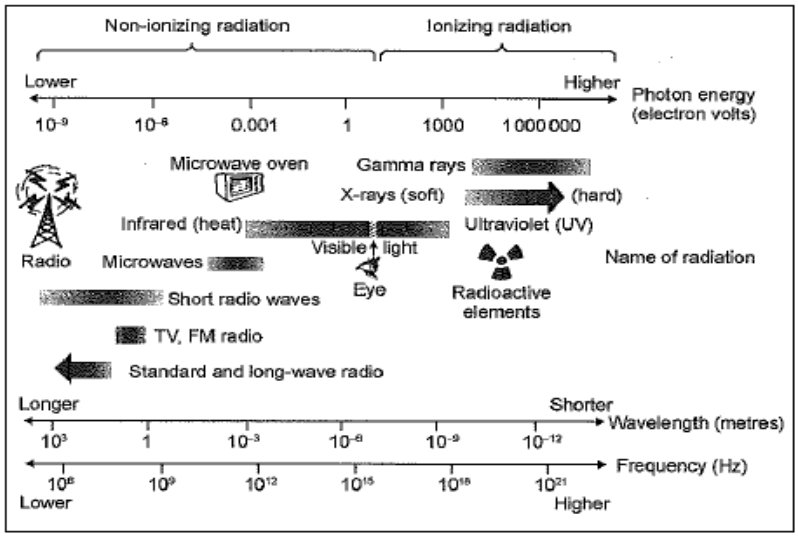

Fig. 1: Electromagnetic wave spectrum (The National Physical Laboratory, NPL).

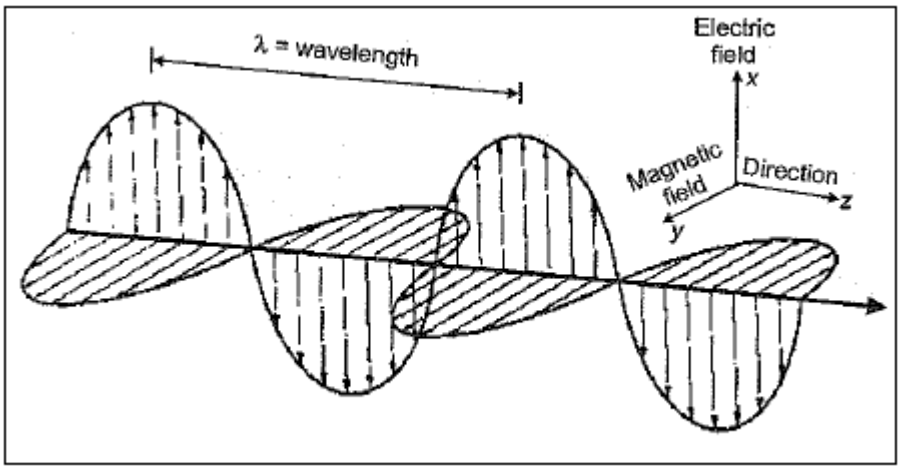

Fig. 2: Electromagnetic wave propagation.

1.2 - The history of the microwave oven

An original version about the history of the microwave oven has been described by John M.Osepchuk, member of IEEE (Institute of Electrical and Electronics Engineers), in his paper: " The History of the microwave oven: a critical review".

<<Who Made the First Microwave Oven?

The answer by almost universal acknowledgement is Raytheon Manufacturing Company in 1945-46 with Percy Spencer as inventor and those who helped design and build the first model and almost any history of the microwave oven. Yet in 2003 in the IEEE Virtual Museum it was stated that the Germans had operated microwave ovens in the 1930's. This version of history was deleted in early 2004 and replaced by the conventional view centering on Raytheon.

Where did this story come from? There existed and probably still exist websites that view "microwaves" as dangerous and their history claimed that the Nazis invented the machine and the Soviets banned it. A more genteel source of misinformation is found in a recent book by Bodanis who described some of the notable technical achievements in the electrical engineering professions through history. For some reason he chose not to relate the story of the magnetron and radar developed in the U.K. Instead he chronicled the dramatic development by the Germans of the Wurzburg radar and linked it to the microwave oven; "A close descendant of the Wurzburg radar sits in our kitchens today." This is false. First of all the Wurzburg radar operated just below 600 MHz far from the frequency of today's ovens.

Furthermore, the Germans were forbidden under Hitler to work above 1 GHz. This amazing fact has been confirmed by several personal communications as well as in history books.

With regard to the rumor on the banning of the microwave oven, that is also equally false. In fact in my history I cite the existence of microwave ovens in the 1970's in the USSR, and I displayed a photograph of such an oven procured by Raytheon at that time. Furthermore we had ample discussion with scientists from Eastern Europe with discussion on the microwave oven.

Who Designed and Built the First Oven?

Though Percy Spencer is the inventor of the microwave oven, there were many people who contributed to the design and construction of that first oven at Raytheon, (Note that Spencer was the manager of hundreds of people who were manufacturing magnetrons for the war effort but still found time for many inventions, mostly on magnetrons). Some are mentioned in and Marvin Bock is named as the engineer who "built" the first oven model. Recently there appeared rumors in the U.K. that someone other than Spencer was the true inventor—e.g. perhaps Bock. Then followed a history article by Hammack that claimed that Bock made most of the design decisions. My criticism of Hammack'a history was then published along with his response. My view is that many people were involved and I named some. Hammack claims that somebody outside of an organization is better able to make historical judgments but I disagree.

Who Marketed the First Microwave Oven for the Home?

This is a more confusing subject. First of all it is acknowledged, (and also in the historical museum in Baltimore) that the first microwave oven for the home was marketed in 1955 by Tappan (and later Westinghouse) under license from Raytheon. That oven, however, was a wall mounted oven and expensive (e.g. ~$1295). The more interesting question is who marketed the first countertop oven that triggered the dramatic growth in the market for consumer microwave ovens. My answer is Amana which had been acquired by Raytheon in 1965 under the leadership of its CEO,Thomas Phillips. As shown in my paper logarithmic growth in sales followed the introduction by Raytheon of the first Amana Radarange in 1967. Most historical accounts agree.

Are Microwave Oven Legends True?

Over the years much attention has been given to the legends about how Percy Spencer "discovered" microwave heating, especially the one featuring a candy bar. After interviewing many of the associates of Percy Spencer, I believe that a number of people were experiencing warmth and therefore heating of objects on their person. The reason is that in World War II there was no fear of "microwaves". Therefore in the manufacture of magnetrons, at some stage, many tubes simultaneously were allowed to radiate into space creating indeed a "hot environment". (A legendary story, which is undoubtedly true, is that during "blackout" exercises the fluorescent lamps in that part of the factory continued to glow under the presence of the microwave radiation.) Some have claimed that one or more of these events (with chocolate, popcorn, frankfurters…) could not have occurred as claimed because they failed to replicate the alleged heating. But all these alleged replications are done at 2.45 GHz. On the other hand in the Raytheon factory magnetrons operating at all bands from 1 to 10 GHz, at least, were being manufactured. If frequency is a variable then we are quite confident the legends can be confirmed—especially that about the chocolate. One must be careful, however, in recreating such legends. A few years ago there was such a recreation aired on the History Channel. The chocolate bar shown was a modern product wrapped in aluminized paper. A microwave engineer knows that there will be no microwave heating of the chocolate in this case.>>

1.3 – Maxwell's equations

A set of four Maxwell equation governs the general characteristics of electromagnetic waves travelling in a medium. These equations are:

- $\nabla \cdot \overline{\mathbf{D}} = \rho$ (1.1)
- $\nabla \cdot \overline{\mathbf{B}} = 0$ (1.2)
- $\nabla \times \overline{\mathbf{E}} = -\mu \frac{\partial \overline{\mathbf{H}}}{\partial t}$ (1.3)
- $\nabla \times \overline{\mathbf{H}} = \sigma \overline{\mathbf{E}} + \dot{\varepsilon} \frac{\partial \overline{\mathbf{E}}}{\partial t}$ (1.4)

where:

- **E** is the Electric field intensity [V/m];
- **D** is the Electric flux density [C/m^2];
- **H** is the Magnetic field intensity [A/m];
- **B** is the magnetic flux density [Wb/m^2];
- **ρ** is the Volume charge density [C/m^3];
- **μ** is the Permeability [H/m];
- **ε** is the Permittivity [F/m];
- **σ** is the conductivity [S/m];

For the above equation to be valid the medium should have a uniform property that is linear, homogenous, and isotropic. Linearity means that the electric flux density **D** is directly proportional to the electric field intensity **E** and magnetic flux density **B** is directly proportional to the magnetic field intensity **H**. Homogeneity means that the dielectric properties of the medium (permittivity, permeability and conductivity) at all points in the path of the EM wave are the same. Isotropicity means that permittivity and permeability are independent of orientation of the EM wave.

Equation (1.1) describes that the source of an electric field s from the charge density in a given volume, while equation (1.2) denotes that magnetic monopole does not exist. They are collectively known as Gauss' laws. Equation (1.3) called Faraday's law explains that a time-varying magnetic field would induce a time-varying electric field. Finally Equation (1.4) or Ampere's law describes the conservation of charge in term of magnetic field, current flow, and variable electric field. These laws had been discovered from experimental observations 40-50 years before by James Clerk Maxwell published a unified electromagnetic theory in 1873.

1.4 – Wave equations

Specific wave equations can be derived from Maxwell's equations. For simplification, the medium in which the EM wave travels is assumed to have no charged density and current density. By applying curl-operation on equation 1.3 and 1.4, wave equation in terms of electric field intensity or magnetic field intensity are expressed as:

$$- \quad \nabla^2\overline{\mathbf{E}} = \mu\sigma\frac{\partial\overline{\mathbf{E}}}{\partial t} + \mu\dot{\varepsilon}\frac{\partial^2\overline{\mathbf{E}}}{\partial t^2} \tag{1.5}$$

$$- \quad \nabla^2\overline{\mathbf{H}} = \mu\sigma\frac{\partial\overline{\mathbf{H}}}{\partial t} + \mu\dot{\varepsilon}\frac{\partial^2\overline{\mathbf{H}}}{\partial t^2} \tag{1.6}$$

The above two equations are not independent; the knowledge of electric field intensity leads to the magnetic field intensity, or vice versa, as indicated in the Maxwell's equations 1.3 and 1.4.

For simplicity we only consider sinusoidal time-varying fields (referred to as time-harmonic fields). Equations 1.5 and 1.6 can then be written in the following forms:

$$- \quad \nabla^2\overline{\mathbf{E}} = \dot{\gamma}^2\overline{\mathbf{E}} \tag{1.7}$$

$$- \quad \nabla^2\overline{\mathbf{H}} = \dot{\gamma}^2\overline{\mathbf{H}} \tag{1.8}$$

Where γ is referred to as propagation constant and

$$\dot{\gamma} = \sqrt{j\omega\mu(\sigma + j\omega\varepsilon)} = \alpha + j\beta \tag{1.9}$$

In the equation 1.9 ω is the angular frequency of the sine wave ($\omega=2\pi f$) and j denotes imaginary number ($j=\sqrt{-1}$). Metaxas (1996) shows detailed derivation of the general Maxwell's equations to obtain the above two equations for time-harmonic field.

The propagation number γ is a complex number. The real part α, referred to as the attenuation constant, describes the decrease in the amplitude of the wave (due to absorption and thus generation of heat) as it travels in a certain medium. The imaginary part β, referred to as phase constant, characterizes the propagation of the wave. Both parts are related to the permittivity, permeability and electric conductivity in the medium in question:

$$\alpha = 2\pi f\sqrt{\frac{\mu\varepsilon}{2}\left[\sqrt{1+\left(\frac{\sigma}{\omega\varepsilon}\right)^2}-1\right]} \tag{1.10a}$$

$$\beta = 2\pi f\sqrt{\frac{\mu\varepsilon}{2}\left[\sqrt{1+\left(\frac{\sigma}{\omega\varepsilon}\right)^2}+1\right]} \tag{1.10b}$$

The wave velocity is related to the phase constant by:

$$U_P = \frac{2\pi f}{\beta} \tag{1.10c}$$

And wavelength by:

$$\lambda = \frac{2\pi}{\beta} \tag{1.10d}$$

The magnitude of the electric field in an EM wave is proportional to that of the magnetic field. The proportionality constant is the intrinsic impedance (η), and is function of the medium properties ε and μ. The intrinsic impedance is a complex number (consisting of real and imaginary parts) with corresponding magnitude and angle:

$$\dot{\eta} = \frac{\overline{\mathbf{E}}}{\overline{\mathbf{H}}} = \frac{j\omega\mu}{\dot{\gamma}} = \sqrt{\frac{j\omega\mu}{\sigma + j\omega\varepsilon}} \tag{1.11}$$

With the propagation constants and intrinsic impedance parameters described above, both electric field intensity and magnetic field intensity for the EM wave travelling along the z-axis (fig. 2) can be expressed in the phasor form:

$$\overline{\mathbf{E}}_x(+z) = \overline{\mathbf{E}}_{x0} e^{-\alpha z} e^{-j\beta z} \tag{1.12}$$

$$\overline{\mathbf{H}}_y(+z) = \frac{1}{|\eta|} \overline{\mathbf{E}}_{x0} e^{-\alpha z} e^{-j\beta z} e^{-j\theta\eta} \tag{1.13}$$

$$\overline{\mathbf{E}}_x(-z) = \overline{\mathbf{E}}_{x0} e^{\alpha z} e^{j\beta z} \tag{1.14}$$

$$\overline{\mathbf{H}}_y(-z) = -\frac{1}{|\eta|} \overline{\mathbf{E}}_{x0} e^{\alpha z} e^{j\beta z} e^{-j\theta\eta} \tag{1.15}$$

Where $\mathbf{E}_{x0}$ indicates the amplitude of EM wave at z=0, while $\mathbf{E}_x(z)$ and $\mathbf{H}_y(z)$ denote electric field and magnetic field which propagate in the z-axis while oscillating in the direction of x-axis and y-axis respectively. $\mathbf{E}_x(+z)$ and $\mathbf{H}_y(+z)$ are forward moving waves, while $\mathbf{E}_x(-z)$ and $\mathbf{H}_y(-z)$ are the backward moving waves.

The quantities $e^{-\alpha z}$ and $e^{\alpha z}$ determine if, or how fast, the amplitude decays with distance into the medium; the quantities $e^{j\beta z}$ $e^{-j\theta\eta}$ and $^{e\text{-}j\beta z}$ $e^{-j\theta\eta}$ describe the other characteristics of the wave such as phase, wavelength and velocity.

1.5 – Energy and power

Microwaves carries electromagnetic energy as it travels through a medium. A measure of the microwave power across a unit area is the Poynting Vector (in W/m^2) defined as:

$$\overline{\mathbf{P}} = \overline{\mathbf{E}} \times \overline{\mathbf{H}} \tag{1.16}$$

It is an instantaneous power density vector in the direction of microwave propagation and is a function of time and location. The Poynting vector for a plane wave traveling in z-direction as shown in Fig. 2, can be expressed as **P**(z,t). Its time average value, a more commonly used value to indicate the changes in microwave power with distance, is calculated as:

$$\mathbf{P}_{ave}(z) = \frac{1}{T}\int_0^T \overline{\mathbf{P}}(z,t)dt \tag{1.17}$$

For time-harmonic waves and using equations 1.12 and 1.13, the magnitude of microwave power as a function z can be written in terms of electric field intensity:

$$\mathbf{P}_{ave}(z) = \frac{1}{2|\eta|} E^2{}_{x0} e^{-2\alpha z} \cos\theta_\eta \tag{1.18}$$

or simply:

$$\mathbf{P}_{ave}(z) = P_{ave}(0) e^{-2\alpha z} \tag{1.19}$$

where $P_{ave}(0)$ is the microwave power flux intensity (W/m^2) at z=0.

1.6 – Propagation of microwaves in different media

For convenience, the discussion of EM wave characteristic is made in connection with different media classified into four different general categories: (1) free space, (2) lossless dielectric, (3) lossy dielectric, and (4) good conductor. As will be seen later, categories 1,2,4 can all be considered as special cases of category 3.

1.6.1 – Free space

Free space is defined as a perfect vacuum, or, at microwave frequencies, air. The permittivity, the permeability and the conductivity of a free space have the following values:

$\mu_0 = 4\pi \cdot 10^{-7}$ H/m (1.20)

$\sigma_0 = 0$ S/m

The permittivity and permeability of all other media are given relative to the dielectric properties of free space:

$\varepsilon = \varepsilon_r \varepsilon_0$ (1.21)

$\mu = \mu_r \mu_0$ (1.22)

Where ε_r and μ_r are dimensionless numbers, referred to as relative permittivity and relative permeability respectively. For free space, $\varepsilon_r = 1$ and $\mu_r = 1$. Food materials are generally non-magnetic in nature, the relative permeability approximates a value of one.

Using the values provide by equations 1.14, the intrinsic impedance of a free space (η_0) can be calculated from equation 1.11:

$$\eta = \frac{\mu_0}{\varepsilon_0} = 120\pi \approx 377\Omega \tag{1.23}$$

The velocity U_P for the EM wave travelling in free space is calculated from equation 1.10c as:

$$U_P = \frac{2\pi f}{\beta} = \frac{2\pi f}{2\pi f\sqrt{\mu_0 \cdot \varepsilon_0}} = \frac{1}{\sqrt{\mu_0 \cdot \varepsilon_0}} \cong 3 \cdot 10^8 \, m/s \tag{1.24}$$

The above value is indeed the speed of light. Thus, often the more conventionally used symbol *c* is used, instead of U_P. Likewise, the wavelength in free space (and air) is calculated using equation 1.10d:

$$\lambda_0 = \frac{2\pi}{\beta} = \frac{2\pi}{2\pi f\sqrt{\mu_0 \cdot \varepsilon_0}} = \frac{1}{f \cdot \sqrt{\mu_0 \cdot \varepsilon_0}} = \frac{c}{f} \tag{1.25}$$

1.6.2 – Lossless dielectric media

In a lossless dielectric (e.g. plastics, glasses, and other electrical non-conductive materials) the conduction current (expressed as the second term on the right-hand side of equation 1.4). Thus conductivity can be assumed approximately zero ($\sigma=0$).

The parameters that determine wave propagation, impedance, and phase angles expressed in the general equations 1.9 and 1.11 can be simplified into:

$$\alpha = 0 \tag{1.26}$$

$$\beta = 2\pi f\sqrt{\mu_r \mu_0 \varepsilon_r \varepsilon_0} \tag{1.27}$$

$$\eta = \sqrt{\frac{\mu_r \mu_0}{\varepsilon_r \varepsilon_0}} = \sqrt{\frac{\mu}{\varepsilon}} \tag{1.28}$$

$$\theta_\eta = 0 \tag{1.29}$$

1.6.3 – Lossy dielectric media

A lossy dielectric is defined as a media in which the electric conductivity is not equal to zero yet it is not a good conductor. Setting $\sigma \neq 0$ in equation 1.9 leads to a non-zero attenuation constant ($\alpha \neq 0$). The general wave equations and the associated parameters expressed in equations 1.9 to 1.19 therefore apply to lossy dielectric. According to equations 1.12 and 1.13, the amplitude of electric and magnetic fields decreases exponentially with travel distance.

The changes in amplitudes are quantified by the attenuation constant (α). Microwave power was lost (i.e. converted to heat) according to equation 1.19:

$$\mathbf{P}_{ave}(z) = P_{ave}(0)e^{-2\alpha z} \tag{1.30}$$

This is illustrated in figure 3 as an EM wave enters into a lossy dielectric.

The larger the value of the attenuation constant (α), the more rapidly the EM wave loses its power along the path of transmission. The ability of EM to penetrate a lossy dielectric material is indicated by power penetration depth, commonly (in contrast to the half power depth) defined as the distance over which the EM power decreases 1/e of the original value. From this definition, one can derive the expression for the power penetration depth (d_p) using equation 1.19:

$$\mathbf{P}_{ave}(d_p) = P_{ave}(0)e^{-2\alpha d_p} = \frac{1}{e}P_{ave}(0) \tag{1.31}$$

Using the last two terms in the above equations yields:

$$d_p = \frac{1}{2\alpha} \tag{1.32}$$

Substituting in equation 1.10a yields:

$$d_p = \frac{1}{2\pi f\sqrt{2\mu\varepsilon\left[\sqrt{1+\left(\frac{\sigma}{\omega\varepsilon}\right)^2}-1\right]}} \tag{1.33}$$

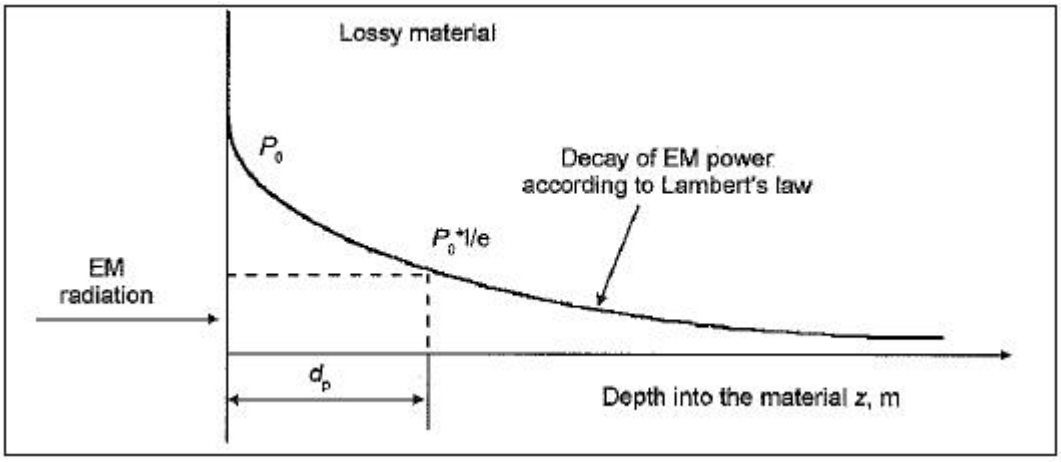

Fig. 3: Attenuation of EM waves in a lossy dielectric and definition of power penetration depth.

1.6.4 – Good conductor

Good conductors, such as metals, are characterized by extremely large electric conductivities (i.e. $\sigma_{copper}=6\cdot10^7$ S/m). Thus, setting $\sigma=\infty$ in equation 1.9 and 1.11 leads to $\sigma=\infty$, $\beta=\infty$, and $U_p=0$.

These values suggest that microwaves do not transmit in good conductors. In reality all metals are not perfect conductors and electric conductivity is not infinitely large. The electromagnetic wave does penetrate several micrometers, depending upon the electric conductivity of the materials. But for practical reasons, we consider all metals to be perfect electric conductors (PEC). Metals are used to confine microwave energy in a space (i.e. in a microwave cavity) or to guide microwave (i.e. in a waveguide) to a specific application location.

1.7 – Propagation of electromagnetic wave between two media

This section provides a brief description of the general characteristics of electromagnetic waves when travelling through two different yet adjacent media (e.g. from medium 1 to medium 2).

The wave travelling in medium 1 before encountering medium 2 is called the incident wave. At the interface between medium 1 and 2, a portion of the incident wave will enter medium 2 and be transmitted at a certain angle (θ_t) referred to as the angle of transmission (fig. 4a). This wave is called the transmitted wave. The rest of the incident wave will be reflected back to medium 1 at a certain angle called the reflection angle (θ_r). This wave is called the reflected wave. If the direction of the incident wave is perpendicular to the interface of the two media ($\theta_i=0$), the resulting angle of transmission and reflection will be equal to zero ($\theta_t=\theta_r=0$) (fig. 4b). This condition is called normal penetration of EM waves, since the direction of propagation is normal to the interface. In a more general case in which an incident wave travels at a certain angle to the interface between the two media ($\theta_i>0$), the angle of transmission and reflection will no longer be equal to zero. This condition is called oblique penetration of EM waves.

The portion of an incident wave being transmitted is quantified by the transmission coefficient (τ) defined as the ratio of the amplitude of the transmitted electric field over the amplitude of the incident electric field:

$$\tau = \frac{E_{x0(transmitted)}}{E_{x0(incident)}} \tag{1.34}$$

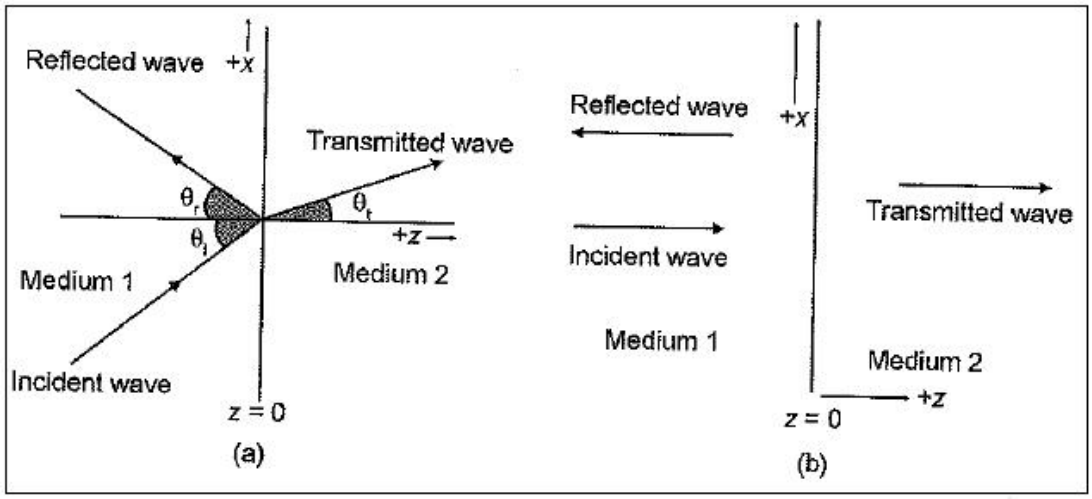

Fig. 4: Propagation of electromagnetic wave at the interface of two different media: (a) general case, and (b) normal penetration.

The portion of an incident wave being reflected is quantified by the reflection coefficient (ρ) defined as the ratio of the amplitude of the reflected electric field over the amplitude of the incident electric field:

$$\rho = \frac{E_{x0(reflected)}}{E_{x0(incident)}} \tag{1.35}$$

1.8 – Standing waves

Consider a simple condition where in transverse EM wave travels in the air in a direction normal to a good conducting surface, such as a metal wall. As known, the wave will be completely reflected back. To satisfy the boundary condition that the tangential electric field intensity at the metal wall is zero, the reflected wave is 180° out of phase with the incident wave at the reflection surface. The reflected wave and the incident wave, travelling with equal amplitude but in opposite directions, form a field pattern that appears to be stationary (referred to as a standing wave) with fixed locations of zero intensity, where the two waves are 180° out of phase, and maximum intensity, where the two waves are in phase. The locations for the maximum and zero intensity are adjacent to each other and separated by 1/4 wavelength with a zero intensity locations at the metal wall (fig. 5). The field intensity of the standing wave at the maximum is twice that of single travelling wave.

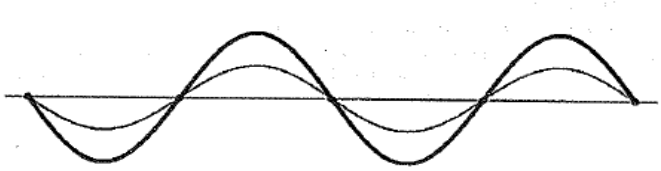

Fig. 5: Illustration of a standing wave oscillating with amplitude that changes with location in space. The right-hand minimum point is at the metal wall.

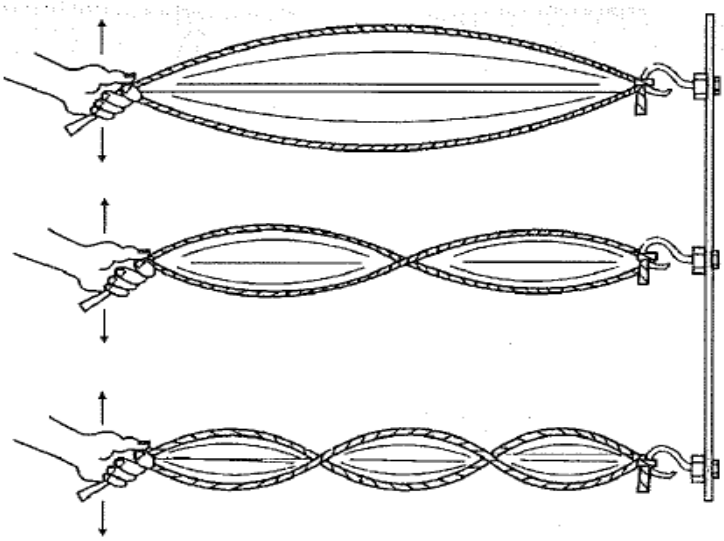

Fig. 6: Illustration of a standing wave with a flexible string; the location of nodes (minimum amplitude) and anti-nodes (maximum amplitude) are fixed in space, depending on wavelength.

An intuitive way to describe a standing wave is to image a flexible string with one end attached to a fixed wall (Fig. 6). Waves can be introduced by swinging the other end of the string. When the first full wave encounters the fixed points, it is reflected back in the opposite direction. Reflection happens because the wave from the string cannot travel beyond the wall. The point of the attachment causes a momentum change, shifting the phase angle by 180°.The first full wave now travelling backward encounters the second full wave travelling forward. The first and second wave interfere and form a standing wave pattern with node (minimum amplitude) and anti-node (maximum amplitude) at fixed locations. The standing waves in microwaves cavities create cold and hot spots, which is one of the main reasons for uneven heating.

Chapter 2

The microwave oven

2.1 - Magnetron

2.1.1 - Introduction

In the past it was felt that appropriate tubes (formed initially as a diode with cylindrical anode divided into two sectors was connected between the resonant system) in which the electrons were simultaneously controlled by the electric field between cathode and anode and a constant external magnetic field and axial, were able to keep the system under a resonant oscillation. This device could vary up to very high frequencies, limited only, by the inability to increase the frequency of the resonant circuit.

In this sense, the most important progress was made in England at the University of Birmingham in 1940, because the development of radar had requested a tube oscillator efficient and very powerful in the decimetre wave range. This progress is to use, as a resonant system, a series of cavities equal in number, being combined in the same anode tube, was obtained as the magnetron cavity.

The development of the idea implemented in England, which was, at that time, too busy by the war, was entrusted especially to laboratories and mainly American Bell Telephone Laboratories and the Radiation Laboratory, specially created in November 1940, for the study and design of radar at MIT in Cambridge, Massachusetts. The progress made at these laboratories were very rapid and impressive, at the end of the war were already available to more than fifty models of the cavity magnetron, for wavelengths between 1 and 50 cm.

2.1.2 - Motion of electrons in static electric and magnetic fields

Before examining the operation of the magnetron is necessary to consider briefly the motion of electrons under the action of electric and magnetic fields that initially considered to be static.

a) *Electric field.* An electron charge and mass m, subjected to an electric field **E** is urged by a force **F**, independent of the electron velocity **u**, such that:

$$\overline{\mathbf{F}} = e \times \overline{\mathbf{E}} \tag{2.1}$$

Since the electron charge is negative, the direction of the force, give strength and **E** is opposite to the conventional choice for the direction of the field.

b) *Magnetic field*. An electron subjected to a magnetic field induction **B** is urged by a force **F**, depends on the electron velocity **u**, given by:

$$\overline{\mathbf{F}} = e \times \left(\overline{\mathbf{u}} \wedge \overline{\mathbf{B}} \right) \tag{2.2}$$

The force is normal to the plane containing the vectors **u** and **B**, and its width is, as required by the vector product, equal to the product of two vectors of the modules for the sine of the angle formed by them ϑ.

Thus an electron moving parallel to the magnetic field ($\vartheta = 0$; $\sin\vartheta = 0$) is not subject to any

force, but instead an electron moving perpendicular to the field (ϑ =90°; sinϑ = 1) is motivated by the maximum force. Force **F** deflects the electron, and since this force is always orthogonal to the direction of **u,** also **F** changes constantly. If **B** and **u** are constant, the electron describes a circle of radius r can be determined. For that ϑ=90° e sinϑ =1 we have the fact that the centripetal force **F** is the centrifugal force balance mu^2 / r for which:

$$e\overline{\mathbf{u}} \wedge \overline{\mathbf{B}} = \frac{m\overline{\mathbf{u}}^2}{r} \tag{2.3}$$

Thus:

$$r = \frac{m\overline{\mathbf{u}}}{e\overline{\mathbf{B}}} \tag{2.4}$$

The time T_c taken to travel the circumference is given by:

$$T_c = \frac{2\pi r}{u} = \frac{2\pi m}{eB} \tag{2.5}$$

That is independent of both the radius, is the speed of the electron, then describes an electron faster, other conditions being equal, a circle, having to have a radius proportional to the velocity as shown in (2.4), will be largest in to employ the same time to cover it. It has the cyclic frequency:

$$f_c = \frac{1}{T_c} = \frac{eB}{2\pi m} \tag{2.6}$$

c)Electric and magnetic fields with agents. In this case the force being put on the electron is the vector sum of those due to the two fields individually so you can write:

$$\overline{\mathbf{F}} = e \times [\mathbf{E} + (\mathbf{u} \wedge \overline{\mathbf{B}})] \tag{2.7}$$

The study of the trajectories of electrons in this case is much more complex and can easily be developed only in the simplest cases.
Refer to the magnetron inserted in the schematic circuit of figure 1.

Assuming that the diameter of the anode is slightly larger than the diameter of the cathode, the cylindrical space between the two, which we call the space of interaction, can be approximated to the space between two flat surfaces such as those in figure 2.

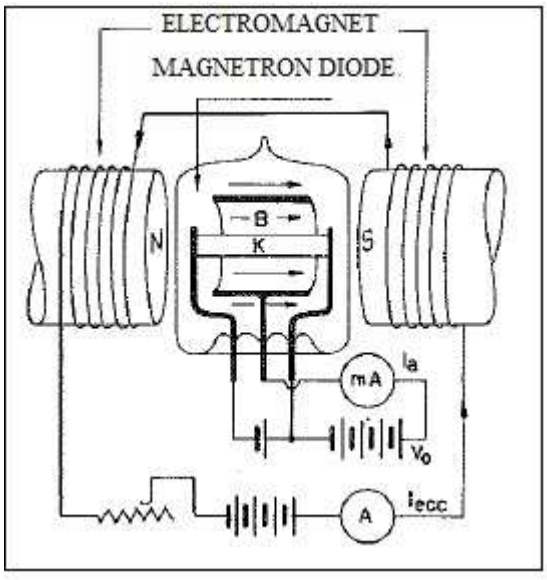

Fig. 1: Static supply diagram of magnetron

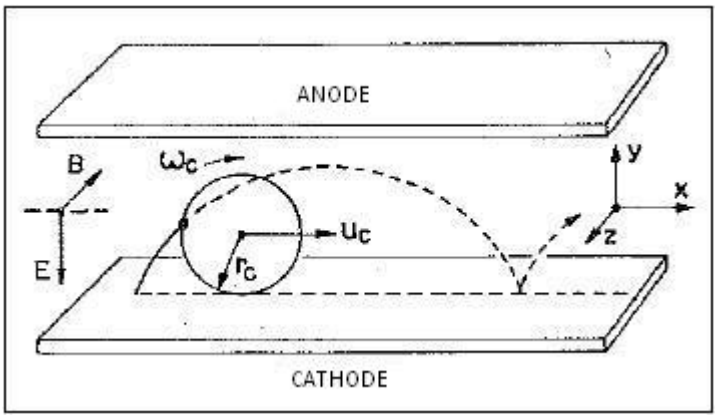

Fig 2: Cycloidal trajectories of an electron leaving the cathode with speed equal to zero, simultaneously subjected to a magnetic field and electric field, oriented as shown in the figure and supposing that the space of interaction between the cathode and anode is flat

Neglecting the space charge is shown that the outgoing electron from the cathode with zero velocity describes a cycloidal trajectory that can be imagined generated from the initial point of contact with the cathode of a circle which rolls with angular velocity ω_c given by $2\pi f_c$ and axial velocity $\mathbf{u_c}$ on the surface of the cathode in the x direction that is orthogonal to both **B** to **E**. The value of $\mathbf{u_c}$ (average speed of travel) is given by:

$$\overline{\mathbf{u}}_c = \frac{\overline{\mathbf{E}}}{\overline{\mathbf{B}}} \tag{2.8}$$

Since the rolling radius of the circle must satisfy the relation $r_c = u_c/\omega_c$ we have::

$$r_c = \frac{m\overline{\mathbf{E}}}{e\overline{\mathbf{B}}^2} \tag{2.9}$$

In the case of a cylindrical system (diode) instead of the floor, again neglecting the space charge, the trajectories of electrons can be considered approximately planetary, that is still obtained by rolling the circle in figure 2 on the cathode surface, which instead of being plane is cylindrical.

2.1.3 - Critical magnetic field

If $2r_c$ is greater than the distance between cathode and anode each electron emitted from the cathode, after a sudden planetary path, reaches the anode. The anodic current in this sense is independent of the value of **B** because all the electrons emitted from the cathode reach the anode and the diode is in saturation. **B** decreases with the increase of the radius r_c, and if this becomes less than half the distance between the cathode-anode electron, after reaching the summit of the epicycloid, returns to the cathode, then, assuming that the electron is not absorbed by the cathode, it starts a new cycle of the epicycloid. No electrons reach the anode and the anode current is zero. The transition between these two extremes is the case for that particular value of induction $\mathbf{B_c}$ that makes satisfied the relation:

$$2r_c = r_a - r_k = d \tag{2.10}$$

where:

- r_a = *radius of anode;*
- r_k = *cathode radius;*
- *d = distance between cathode and anode;*
- $\boldsymbol{B_c}$ = *critical value of magnetic induction.*

The critical induction $\mathbf{B_c}$ is obtained easily by substituting the above value of radius r_c for which we have:

$$B_c = \sqrt{\frac{2mE}{ed}} \tag{2.11}$$

Since it is supposed r_a just greater than r_k (almost electrodes plans) we may assume that the electric field is nearly uniform for which V = E ·d (anode voltage) for which we have:

$$B_c = \sqrt{\frac{2mV}{ed^2}} \tag{2.12}$$

We can then obtain the critical value V_c anode supply voltage corresponding to a given value of B:

$$V_c = \frac{eB^2d^2}{2m} \tag{2.13}$$

While for cylindrical electrodes:

$$V_c = \frac{eB^2r_a^{\,2}}{8m} \cdot \left(1 - \frac{r_k^{\,2}}{r_a^{\,2}}\right)^2 \tag{2.14}$$

So for values of V less than V_c the anode current is zero, while it cost for values of V above V_c.

2.1.4 - Cavity Magnetron

The magnetron allows the implementation of an oscillator adapted to the generation of waves centimeters. This can be achieved by exploiting the resonance between the average travel speed of the electrons u_c and velocity of a travelling wave obtained by extracting in the magnetron's anode a succession of cavity (travelling wave magnetron or cavity magnetron).

It includes:

1) a cylindrical cathode;

2) the anode mass with cavities;

3) the coaxial line or waveguide output, coupled to a cavity.

The anode and the output line are no continuous potential, that are connected to ground, the potential for a negative supply voltage V is applied to the cathode, so the two wires of the cathode must be isolated for maximum working voltages, they are surrounded two caps of glass (sometimes both covered by a single protective cover glass as well). A window glass welded to the metal must close the output line. The vacuum space is limited not only by these closures glass, a metal box attached to the cylindrical outer surface of the anode, but higher than it.

The magnetron must then be submitted to the magnetic field required for its operation, then it must be mounted between the pole of a magnet.

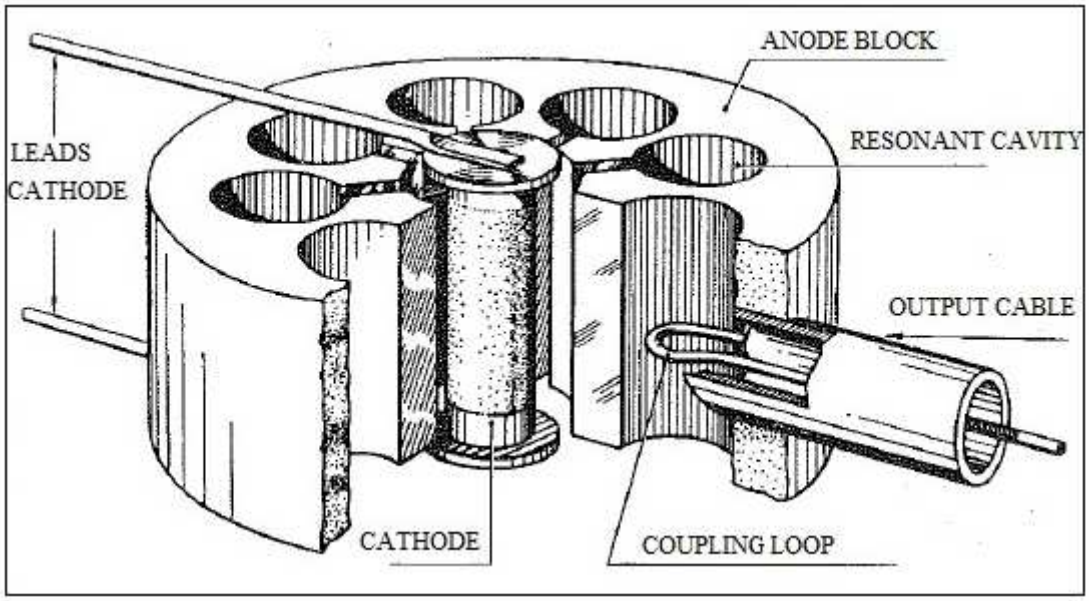

Fig. 3: Diagram of a magnetron cavity.

2.1.5 - Overview of operation

Suppose that the cavities obtained in the anode are all equal to each other (exception to this rule the anode to "rising sun") and they will then have the same resonance frequencies.

These cavities are coupled to each other because the electric and magnetic fields RF overflow, both in the space of interaction between the cathode and anode internal cylindrical surface, both in flat space above and below the anode block. So these cavities, when excited, oscillating in phase with each other certain conditions. You can have different "modes" of oscillation, each of which will determine, in the space of interaction, the overlap, the electric and magnetic fields continues, an RF field with special features along the periphery anodic cyclic. All this will give rise around the anode in the presence of a standing wave or progressive wave, and finally the combination of the two.

Considering then the RF field due to the oscillatory regime of the anodic cavity system, we must now understand how this system can be maintained by oscillatory reciprocal action between the electrons and that field; what is required to see how the electrons can give to this field part of purchased energy from continuous electric field to which they are subjected, thus transforming a part of the continuous anodic power supply in oscillatory RF power.

If the magnetic induction **B** is subjected to the magnetron is above the critical $\mathbf{B_c}$, it is seen that the electrons move cycloidal motion consists of a rotating component and a longitudinal; system of cavities gives rise to standing waves (or progressive) along the anode is synchronized with the travelling longitudinal speed of the electron $\mathbf{u_c}$. Then there are electrons that give energy to the RF field, ie useful, and others that absorb energy and thus are harmful.

2.1.6 - The oscillatory ignition

As soon as the battery is connected between the anode and the cathode (made of copper coated with strontium that releases electrons to the anode), the emitted electrons are deflected by the Lorentz force all, describing the trajectories that otherwise, in the absence of Magnetic field, would be radial. Along this trajectory, the electron approaches the slits of the anode resonant cavities, brushing.

Because each virtual slot produces a capacitor, whose plates are the same metal edges of the plaque marking each slot, when the electron approaches an edge of the slot, it becomes polarized as a normal armature of a capacitor. Then, the electron, continuing his cycloidal trajectory that will take him to fall back on the cathode, moves away from the edge of the slot, previously polarized, and near the other edge, biasing the latter.

Meanwhile, the board previously polarized, because of removal of the charge, it gradually loses its polarization becomes positive than the other. So, during the cycloidal trajectory, the electron polarizes the first one edge and then the other, creating a reversal of polarization in the condenser of each virtual anode slit.

If given the speed with which this electron deflected by the Lorentz force along the trajectory, we realize with very high speed is produced the changing polarization of the capacitors of each virtual slot. This change of electric field represents a starting point oscillating. That's right: the virtual condenser, with the initial electronic shift, becomes the seat of a variation of the voltage across its terminals, ie a variation of the electric field as a dielectric (or vacuum interstice of each slot), ie of an oscillation. This initial starting swing is enough to produce a perennial phenomenon of self-oscillation. In fact, the capacitor of each virtual slot is connected to a hollow anode which produces the inductive part of a resonant circuit. This means that, in the 8-cavity magnetron, there are eight LC resonant circuits which start to oscillate at their resonant frequency when the battery is connected to two electrodes of direct current of the tube. So, in the hollow anode is established an oscillation of the magnetic field, while an oscillation, between the slits, of the electric field which we call "radio-frequency electric field", or, simply, "RF field."

2.1.7 - The preservation of self-oscillation and the electronic clouds

Until the battery isn't disconnected between the anode and cathode, the self-oscillation will never cease. The maintenance regime of self-oscillatory phenomenon is due to the presence of RF electric field that, once triggered, will sustain themselves until the battery is disconnected and will not be interrupted, therefore, the emission of electrons from the cathode.

Because the RF electric field triggered is variable over time, the electrons emitted from the cathode can be continually "fired" at times and in areas of the space of interaction where the resulting electric field is accelerating or braking. The resulting electric field is said accelerator, when and where the RF has the same direction as the electrostatic field produced by the battery. In this case, the resulting electrical force is the sum of the electrostatic force and the instantaneous value of the electric force of the RF field. The resulting electric field is said braking, when the RF field is opposite to the static field. The electrons that come under the action of an accelerating electric field absorb energy from this; this energy is converted from electrical to mechanical and electron accelerates its motion considerably. The acceleration of the electron motion produces, by reflection on himself, an increase of the deflecting force, with the result that not only accelerate in speed, it is also subjected to an increase of the Lorentz force that will turn sharply to the right in the path . These electrons escaping under the action of a field accelerator, gaining energy and accelerating their motion, electric particles are particularly "dangerous". But, given the very high speed and strong deviation, describing a trajectory that makes short-range remain for a short time of interaction in the vacuum of space, and then will be absorbed by the cathode.

What, however, interesting to analyze in order to understand the operation of the magnetron is the leakage of electrons in time and in the spaces in which the electric field resulting braking: These charges are called useful electrons to underline that it is they are responsible for the proper functioning of device and the perpetual sustenance of its oscillations. These charges, ie those issued under the braking electric field, being held back in their normal motion, significantly decrease the speed and also trajectory changes. In fact, if the speed decreases, also decreases the deflecting force of Lorentz that the new trajectory becomes almost a straight line, directing the electron to the anode. The slowdown of the motion, in turn, causes that the useful charges, for navigating the new almost straight line towards the anode, take longer than he had spent under the action of the accelerating electric field or under the influence electrostatic field of a single battery. In addition, useful electrons, braking from the field, have given their kinetic energy and, now, they continue their slow motion for the mechanical inertia alone. Approaching, however, to the anode electrode can be charged, as, with new energy, ie the energy of the electrostatic field of the battery anode.

But the speed of their motion is still considerably weaker and, meanwhile, time passes, so the "hectic" RF electric field makes a full swing and back again to establish a field braking when they are still in the space of interaction . So, give again their mechanical energy that they had regained, approaching the anode. This trip will last them for several cycles of the oscillators to RF electric field, until they reach the anode. But other useful charges, behind them, refer the same path, forming the so-called "electronic clouds" (fig. 4).

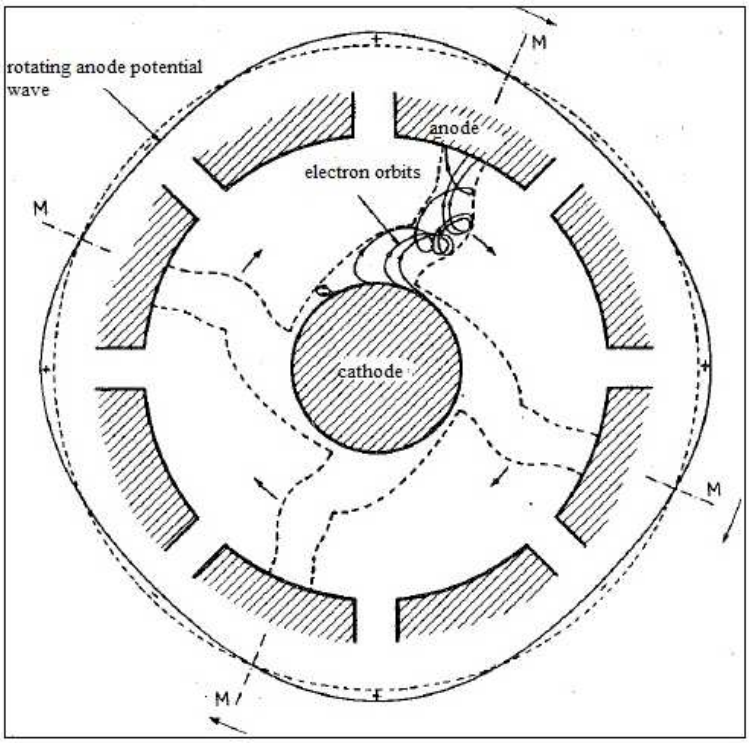

Fig. 4: Representation of the radial electron cloud (bounded by dashed lines) which is expressed in the interaction space. In one of the rays are marked 4 electrons orbits of which one returns on the cathode and 3 reaches the anode.

You can then take three points on the operation of the magnetron:

1. The outgoing electrons from the cathode under the accelerating field (electron dangerous) absorb energy from the RF field, but they, immediately after, disappear from the interaction space, falling on the cathode. The useful electrons, however, each time they are held back, give kinetic energy to the RF field, feeding the latter and avoiding, therefore, that breaks. The operation of the magnetrons is explained so well: the oscillations persist after ignition because the RF electric field absorbs energy from the useful electrons repeatedly. And it also absorbs in quantities greater than those that must give the electrons dangerous. In fact, they disappear quickly, while useful, with the continuous slowing down, are made to persist for a long time in the space of interaction and, for all this time, will literally "exploited" by the RF field to get to transfer as much energy as possible from electrostatic field of the underlying battery. You can say, therefore, that the useful electrons in their "slow and tormented" journey to the anode, act as a simple means of energy transfer; transfer that occurs from the oscillating electric field to the RF through the transformations: electricity (the battery) to mechanical energy (the kinetic energy of the useful electrons) to electricity (that absorbed from the RF field for support).

2. The useful electron's slow progress produces a thickening of them in various areas of interaction space that is the electronic clouds in the radial form. The number of rays is always equal to the number of cavities in the anode block because the edges of the anode are polarized electrically or with the positive or negative, and the clouds will be attracted only by the anode's edges which, at a given time, have taken positive electrical polarity. In the most common, with eight cavities anodic, the clouds are four electronic rays. In addition, the electron rays, during operation of the magnetron, move constantly around the cathode (which is, therefore, the central axis) at a rate called synchronous speed.

In this regard, if the number of cavities is N is then that the electron will complete the entire lap around the cathode in a time Ts (synchronous period) given by:

$$T_s = \frac{T \cdot N}{2} \tag{2.15}$$

where, indicating with ω_s synchronous angular velocity, is:

$$\omega_s = \frac{2\pi}{\frac{T \cdot N}{2}} = \frac{\omega}{\frac{N}{2}} \tag{2.16}$$

ie the angular velocity is equal to the synchronous pulse of resonant cavities divided by the number of pairs of cavities.

The above calculation is not the only possible synchronous speed. The electron is forced to cede power even if the continuous path between two slits is done in an odd number k (k = 1,3,5,7 ...) of half-waves, so in general we have:

$$\omega_s = \frac{\omega}{k \cdot \frac{N}{2}} \tag{2.17}$$

The denominator is the number of periods T and the electron takes to make a complete turn around the cathode.

The rotation of the electron rays is because the speed of oscillation of the RF electric field is greater than the average earnings of the electrons, ie the period of oscillation of the electric field is much smaller than the time it takes to help the offices along the route from cathode to anode. For this reason, the rotation of the polarity of the anode edge (rotation that follows, of course, the RF electric field), being more abrupt, forces the rotating electron rays at an angle.

2.2 - Waveguides

2.2.1 - Introduction

A waveguide is a hollow metallic channel, any section, usually rectangular or circular (fig. 1), containing air or other dielectric. Within this tube and with appropriate excitation electromagnetic wave can propagate.

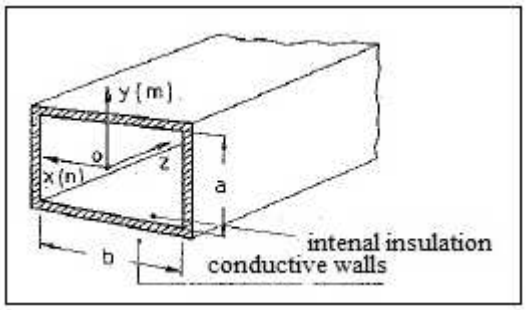

Fig. 1: Structure of a rectangular waveguide.

The transmission of electromagnetic waves by metallic tubes was studied as early as the late nineteenth century by Lord Rayleigh and other physicists without an experimental result. Later, during the Second World War, through the American scientific studies, was analyzed and solved the problem of radar and simultaneously developed the technique of the waveguides and resonant cavities.

2.2.2 - Transmission of the waveguide

The propagation within a waveguide is obtained by "trapping" the radio waves in a metal tube. It is necessary that the wave would fit within the tube, ie, that it has short wavelength, and may therefore change with respect to the structure that it has in free and indefinite space.

It can be said that the transmission in the guide occupies an intermediate position between that of the classical two-wire lines and propagation in free space; has in common with the first that is channelled in some way the flow of energy, with the second the electric and magnetic force lines' mutual concatenation.

It reminds one of the elementary properties of an electromagnetic wave propagating in free and indefinite space namely that if a wave meets a infinitely conductive surface, it is reflected with the known laws of optics, this is because they induce currents in the metal surface generate a second wave (reflected wave). The incident wave and the reflected give rise to a result field that, at points adjacent to the surface, the tangential electric and normal magnetic components that are zero. This condition is what determines the shape of the electromagnetic field near the metal walls.

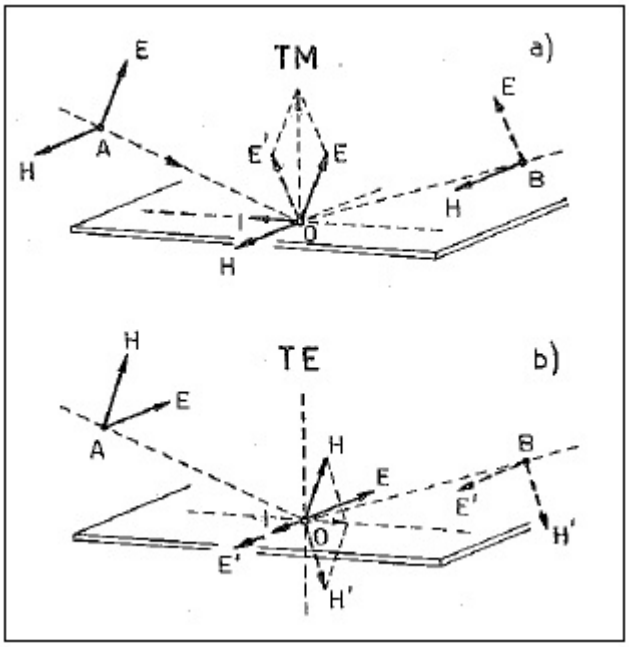

Fig. 2: Reflection of an electromagnetic wave on a flat surface.

Figure 2 shows an example of how this happens in situations where one of the two vectors, components of the incident wave, reaches tangentially the surface; in the first case (TM) is the magnetic field **H** to be tangential to the surface; in the second case (TE) is the electrical **E**.

As mentioned at the point of incidence O the electric resulting should be orthogonal to the surface or anything and the magnetic tangential to the surface. So in the first case the reflected wave is associated with the electric vector **E'** which, added to **E**, gives a component orthogonal to the surface. In the second case the reflected wave is always associated with the electric vector **E'**, but this time equal and opposite to **E**, so that the resulting electric field at O is zero; it will also be associated with the magnetic vector **H'** which, added to **H**, gives a field resulting magnetic tangential to the surface.

If the walls are not infinitely conductive things get complicated, but for the case of metals such as copper, brass, aluminium, etc.. the phenomenon is essentially unchanged.

In conclusion, a wave that propagates in a hollow metallic channel, which vanish, like seen, the tangential components of electric field and normal components of magnetic field, has the electric field lines normal to the walls and the magnetic field lines tangential.

2.2.3 - Propagation in rectangular waveguide

For easy understanding of the mechanism and characteristics of the propagation of a wave guided in a tube, it refers to the resulting interference of multiple plane elementary waves that propagate reflecting, like zigzag, on the walls.

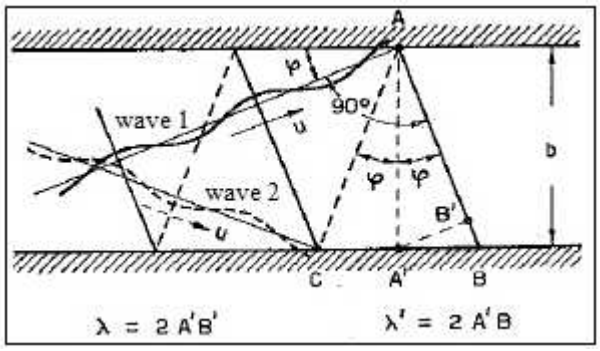

Fig. 3: Wave fronts, of the 2 components at every point of guide's wall, must be equal and opposite, for example maximum on A and C.

As already mentioned, on the conductive walls of the guide, the tangential component of the electric field must be zero. In order for this condition is satisfied, including the width *b* of the guide, φ angle and λ length of component waves, a relation must be verified that you can easily determine. Figure 3 consider. So that at point A, the tangential component of the electric field is zero, it is necessary that the wave 1 and wave 2, in A, present equal value and of opposite sign fields: for example, may have, a maximum positive value (wave front denoted by solid line) and the other a maximum negative (dashed wave front). The same must happen in C. The distance between these two wave fronts 1 (marked with solid line) is obviously equal to (or multiple) of length λ of the incident wave (*wavelength in free space*). It has therefore:

$$\lambda = 2A'B' = 2b\sin\varphi \tag{2.18}$$

The resulting combined field of the two component fields has its maximum at a distance λ' (wavelength in the guide) that is equal to 2A'B:

$$\lambda' = 2AB\sin\varphi = \frac{2b}{\cos\varphi}\sin\varphi = 2btg\varphi \tag{2.19}$$

considering these two reports it has:

$$\lambda' = \frac{\lambda}{\cos\varphi} = \frac{\lambda}{\sqrt{1-\sin^2\varphi}} = \frac{\lambda}{\sqrt{1-\left(\frac{\lambda}{2b}\right)^2}} \tag{2.20}$$

So we have that the wave length in guide λ' is therefore larger than the wave length λ of free space wave (or of individual components in the waveguide) and because the resulting wave frequency *f* coincides, obviously, with the component waves, also the velocity **u'** of the wave propagation in the waveguide is greater than that of free space. In fact we have: $\boldsymbol{u'} = \lambda' f = \lambda f/\cos\varphi$, ie:

$$u' = \frac{u}{\cos\varphi} = \frac{u}{\sqrt{1-\left(\frac{\lambda}{2b}\right)^2}} \tag{2.30}$$

This propagation speed of the resulting waves in the guide is called phase velocity.

Conversely, if we consider that each component wave runs the wave guide, like zigzag, with velocity **u**, the average velocity $\mathbf{u_{gr}}$ of each component, along the axis of the guide, will be less than **u** and will be called group velocity. So we have:

$$u_{gr} = u \cdot \cos\varphi = u \cdot \sqrt{1-\left(\frac{\lambda}{2b}\right)^2} \tag{2.31}$$

and then:

$$u = \sqrt{u_{gr} \cdot u'} \tag{2.32}$$

ie the speed of electromagnetic waves in free space ($3 \cdot 10^8$ m / s) is equal to the geometric average of the phase velocity and group velocity.

Finally, if we put $\varphi = 90°$ it has that $\cos\varphi = 0;\ \lambda' = \infty;\ u' = \infty;\ ugr = 0$;

so the value of λ_c (critical wavelength) of λ, for which the above conditions occur, is given by:

$$\lambda_c = 2b \tag{2.33}$$

For this wavelength and for all wavelengths larger, elementary waves do not propagate along the longer axis of the guide, but oscillate between a wall and the other, so the guide is no longer suitable for the transmission of electromagnetic energy.

The corresponding frequency to the critical wavelength is:

$$f_c = \frac{u}{\lambda_c} = \frac{u}{2b} \tag{2.34}$$

It is called the *cutoff frequency or critical frequency* for which the waveguide is only suitable for the transmission of waves with higher frequency to it.

2.2.4 - "Modes" of propagation

The first observation that can be done, valid in all cases of guided waves, is that it is not possible wave propagation within the guide without the electromagnetic field present a longitudinal component, unless, there is at inside a second conductor, but then you cannot speak of waveguide but of cable (coaxial cable).

The "mode" of the propagation in which the longitudinal component (to the direction of propagation) is magnetic and the transverse component is electric, denoted by TE (transverse electric mode), the mode in which the longitudinal component is electric and the transverse magnetic is denoted by TM (transverse magnetic mode).

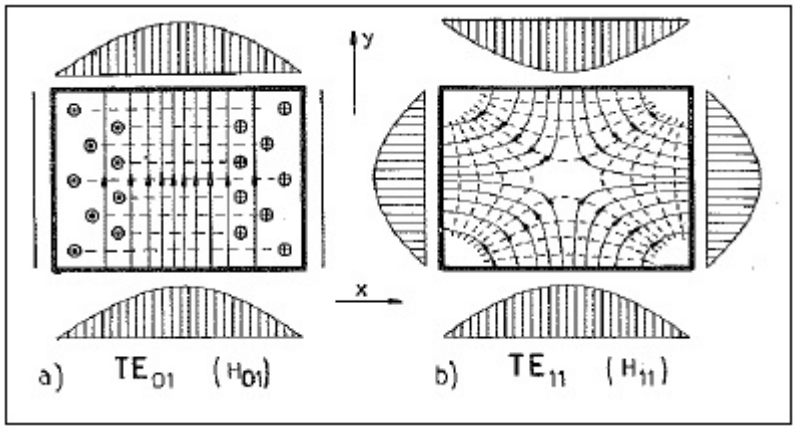

Fig. 4: Field configuration in cross-section of a rectangular waveguide: a) TE01 mode; b) TE11 mode. The solid lines represent the forces' lines of the electric field coplanar with the plane of the drawing; dashed lines are the projections of the forces' lines of the magnetic field.

In the example of figure 4a, along the walls, in the y direction, the field is zero while in the x direction, the field has variable intensity according to a half-sine; the configuration of the field, in this case, will be identified by the initials TE_{01}.

But in the case of figure 4b, the field along the walls, while being always normal to them, as it must be, has variable intensity according to a half-sine in both the direction, the y-direction and the x-direction; so this configuration will be identified by the initials TE_{11}.

In the situation of figure 5a is imagined to have a larger section of the guide, or to double the size of the guide along the x direction, and leave unchanged the dimension along y; then we obtain two configurations, of figure 4a, in phase opposition ie zero field along y, while the electric field along x, at this time, has variable intensity according to a full sine. The overall configuration will be characterized by the initials TE_{02}.

If doubling the size of the guide along x and y too long, obtains the TE_{22} mode (note that the field along the walls must always be normal to them) (fig. 5b).

In general you can get any "mode" characterized by the initials TE_{mn} where m is the number of half-sine that varies the intensity of the electric field in the y direction (side a) and n according to the x direction (side b).

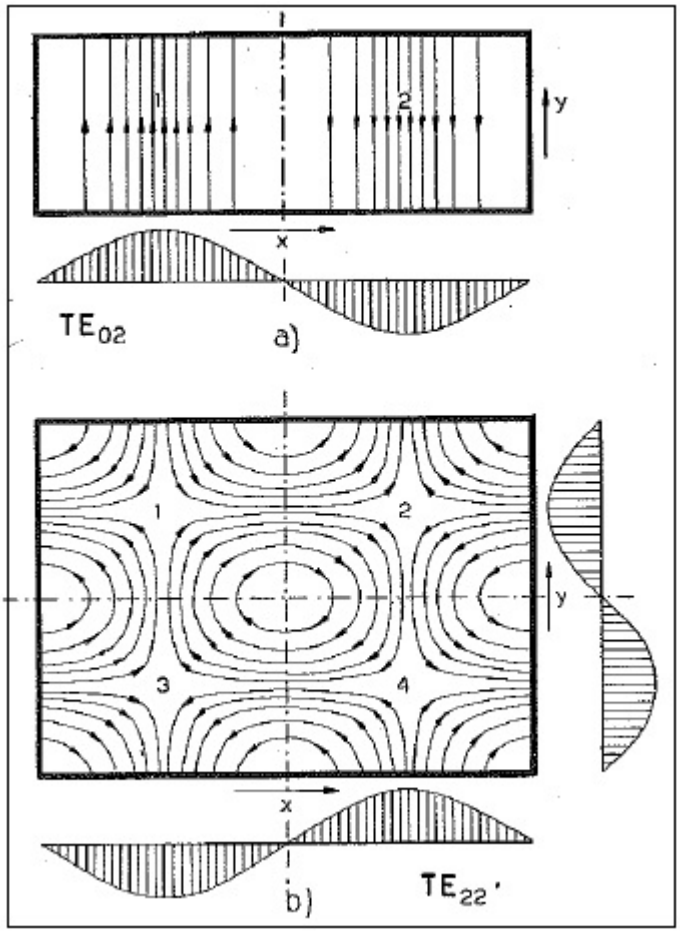

Fig. 5: Field configuration for “harmonic modes”.

Of course, instead of thinking of the larger section of the waveguide, all the different modes listed above, can be obtained by imagining to reduce, conveniently, the length of the exciters waves that increasing the frequency. These modes of excitation are called "harmonic modes" while TE_{01} and TE_{11} modes you say "fundamental modes."

In addition to the field configurations of the type TE, there are configurations of type TM in which we find the magnetic field lines, closed on themselves, coplanar with the x-y cross section of the guide; in longitudinal section, however, we find the strength lines of the electric field, ending on the walls (fig. 6).

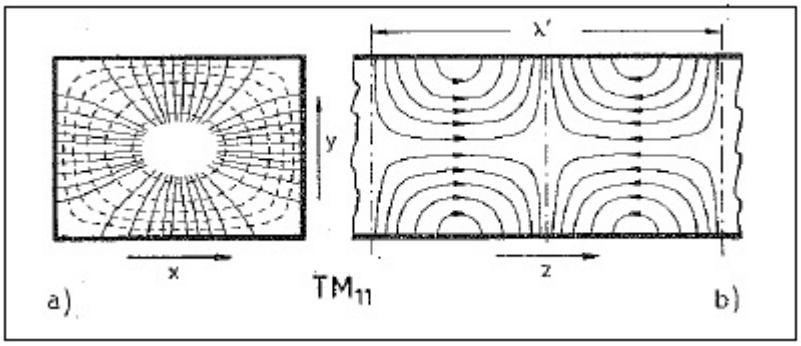

Fig. 6: Field configuration in cross-section a) and in longitudinal-section b) of a rectangular waveguide with TM11 excitation. Dash lines represent the lines of magnetic field coplanar with the transversal plane; solid lines are the projections of the lines of the electric field.

2.2.5 - Losses in the waveguide

The transmission of electromagnetic energy along a guide in the frequency range above the critical one, is not without losses. This calculation is rather complex. The losses refer to those found in the dielectric contained in the guide, those due to the resistivity of the conductor forming the walls of the guide and those due to discontinuities in the guide.

If the dielectric is formed by dry air, as often happens, the former are generally negligible compared to the other.

For rectangular guides with copper walls ($\rho = 0{,}0175\ \Omega \cdot mm^2/m$) a $_{mn}$ attenuation in decibels per meter due to the resistivity of the walls is given by following expressions:

TE mode:

$$a_{0n} = 0{,}1475 \cdot 10^{-3} \cdot \sqrt{\frac{n}{b^3}} \cdot \frac{\frac{p}{2} + v^2}{\sqrt{v - v^3}}; \qquad \text{[Db/m]} \qquad (2.35)$$

$$a_{mn} = 0{,}1475 \cdot 10^{-3} \cdot \frac{\sqrt[4]{m^2 \cdot p^2 + n^2}}{\sqrt{b^3 \cdot v}} \cdot \left(p \cdot \frac{m^2 \cdot p + n^2}{m^2 \cdot p^2 + n^2} \cdot \sqrt{1 - v^2} + \frac{(1+p) \cdot v^2}{\sqrt{1 - v^2}} \right); \qquad \text{[Db/m]}$$

with m and n different from zero.

TM mode:

$$a_{mn} = 0{,}1475 \cdot 10^{-3} \cdot \frac{\sqrt[4]{m^2 \cdot p^2 + n^2}}{\sqrt{b^3 \cdot (v - v^3)}} \cdot \left(\frac{m^2 \cdot p + n^2}{m^2 \cdot p^2 + n^2} \right); \qquad \text{[Db/m]} \qquad (2.37)$$

where:

- m and n are the number of half-sine that varies the electric field in the y direction and x, respectively;
- b is the side of the guide in the x direction;
- p = b / a is the ratio between the sides of the guide;
- $v = f_c / f = \lambda / \lambda_c$ is the ratio of the cutoff frequency and the agent.

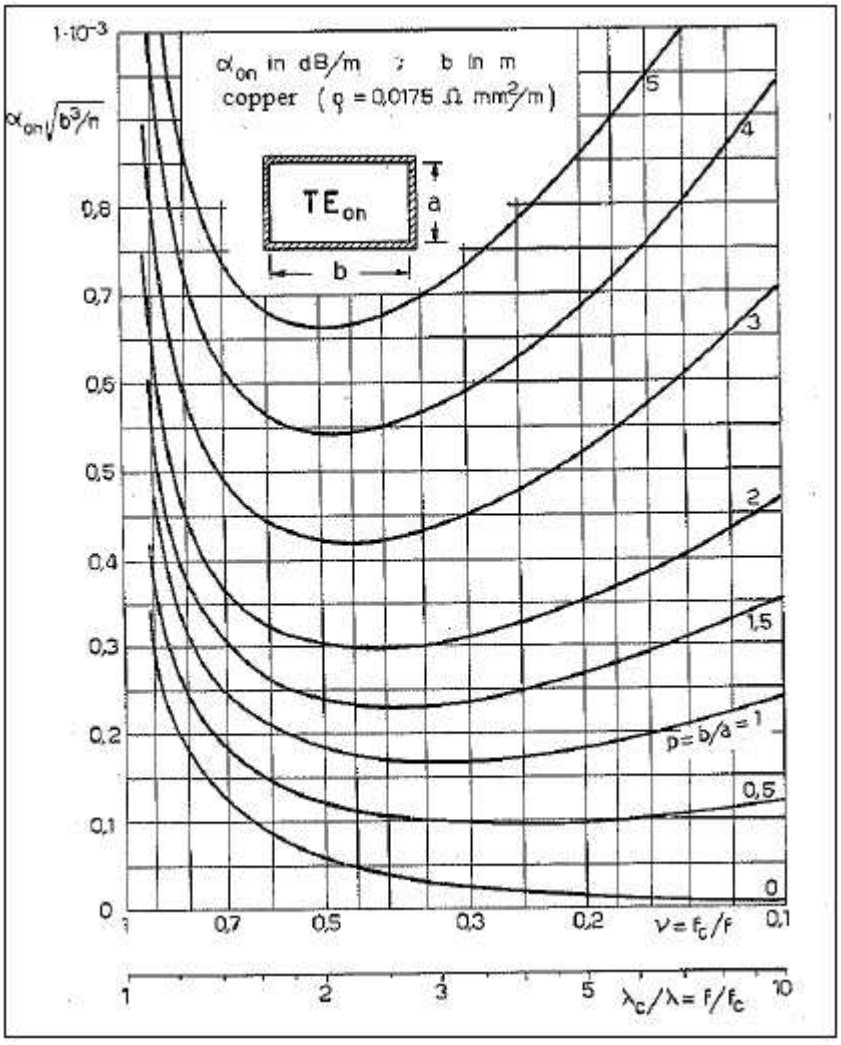

Fig. 7: Attenuation in a copper rectangular waveguide filled with dry air or empty. Mode of wave propagation: TM_{0n}. With decreasing of p=b/a and equal to b, the guide's section increases and thus the attenuation decreases; for p=0 it has a=∞ so wave propagates from 2 plane parallel conducting and undefined walls to distance b.

2.3 - Resonant cavities

2.3.1 - Introduction

Any box or conducting internal cavity walls, if properly excited, limits a space that is home to electromagnetic oscillations.

The shape of the field depends on the interference between the direct waves produced by the exciter source and those reflected from the walls; for particular frequencies, in the box, standing waves occur for which, for these frequencies, the cavity resonates.

The form used to represent the resonant cavity is toroidal; the centre creates a real capacitor and the metal frame that is built around armature, can be thought as the union of many metal tight coils, which are connected in parallel, that representing the inductor (fig. 1).

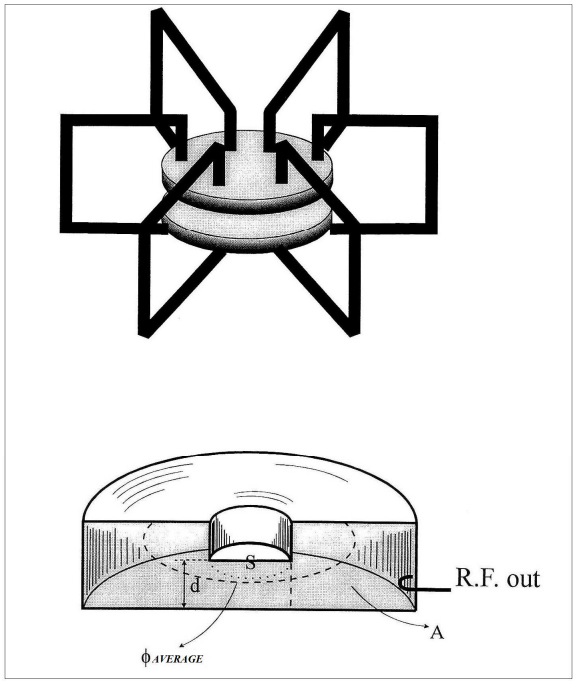

Fig. 1: Parametric representation of a cavity.

While between the two planar surfaces, namely the armature, it produces a capacitive effect with its electric field, in the surrounding duct the magnetic flux flows.

Therefore, the resonant cavity is equivalent to a parallel LC circuit but, unlike a circuit composed of inductor and capacitor, in which the electrical parameters of inductance and capacity are concentrated in the respective components, in cavities, these electrical parameters, are distributed uniformly in all parts of space which forms the structure itself.

By varying the spacing between two planar surfaces at the centre of the cavity, it also changes the capacitance of the resonant circuit which is equivalent to the cavity, modifying, therefore, the resonant frequency:

$$f_0 = \sqrt{\frac{d \cdot \phi}{A \cdot S}} \cdot \frac{1}{2\pi \cdot \sqrt{\varepsilon_0 \cdot \mu_0}} \tag{2.38}$$

where:

- d is the distance between the plates;
- $\phi = 2\pi r_{ave}$ is the average circumference of the toroid;
- A is the section of the torus;
- S is the surface of the armature.

The resonance frequency, therefore, depends on the size of the cavity.

In choosing the appropriate form to be assigned to the cavity, we must keep in mind the following criteria:

- The coefficient of resonance or quality of the resonator Q increases with the ratio of the volume and the inner surface of the cavity;
- Forms should be selected which lead to a field configuration with a precise orientation (sphere not suitable) and that minimizes spurious oscillations.

When the wavelength decreases to values comparable with the size of the circuit (fig. 2b), the radiated energy becomes important, therefore, the coefficient of resonance is low; to improve it not just reduce the ohmic resistance in series with the circuit (fig. 2c), but above all should be removed the radiation energy. For this reason we come to the toroidal resonator (fig. 2d).

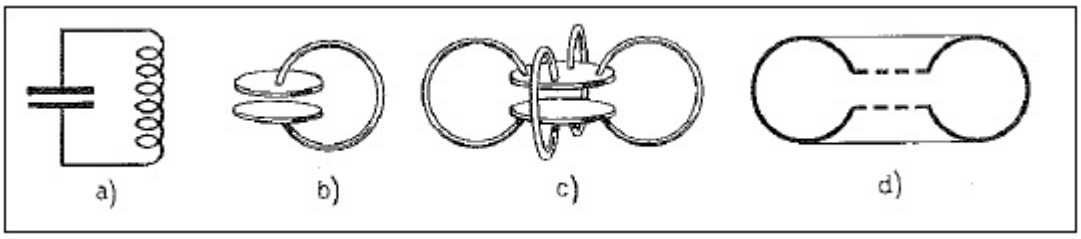

Fig. 2: Derivation of a resonant cavity for subsequent transformation of a concentrated constant circuit.

2.3.2 - Quality coefficient

If the cavity is completely closed, ie if there are no energy losses due to irradiation, the only remaining losses are due to the electrical resistivity of which formed the walls of the cavity and the dielectric loss angle, which is internal; if it is vacuum or dry air, the dielectric losses are zero or negligible compared to those due to the resistivity of the walls.

It is called the coefficient of resonance or quality Q of the cavity, the ratio:

$$Q = 2\pi \cdot \frac{Stored\ energy}{Energy\ lost\ in\ a\ period} \tag{2.39}$$

Knowing that the depth of penetration is given by:

$$\delta = \sqrt{\frac{2\rho}{\omega\mu}} = \sqrt{\frac{\rho_{rame}}{\pi\mu_0}} = \sqrt{\frac{\rho_r}{f \cdot \mu_r}} = 6.7 \cdot \sqrt{\frac{\rho_r}{f \cdot \mu_r}} \quad [Cm] \tag{2.40}$$

where:

- ρ_r is the resistivity of the conductor relative to copper and therefore equal to 1;
- μ_r is the permeability of the conductor relative to copper and also equal to 1.

So we have:

$$\delta = \frac{6.7}{\sqrt{f}} \tag{2.41}$$

Generally, remaining valid the hypothesis that the dielectric losses are negligible, and that $\rho_r = 1$ and $\mu_r = 1$, the expression of the quality coefficient becomes:

$$Q = \frac{2}{\delta} \cdot \frac{\int_V H^2 dV}{\int_S H^2 dS} \tag{2.42}$$

where the integral in the numerator should be extended to the whole volume V of the cavity and the integral in the denominator should be extended to the entire inner surface of the cavity.

The amount:

$$Q \cdot \frac{\delta}{\lambda} = \frac{2}{\lambda} \cdot \frac{\int_V H^2 dV}{\int_S H^2 dS} \tag{2.43}$$

is said to *form factor of the resonator*. So it appears that with increasing frequency f, ie with decreasing wavelength λ, the form factor of a fixed cavities increases.

2.3.3 - Dielectric losses heating in the resonant cavity

The dielectric loss heating is based on the heat that is manifested in the mass of a dielectric material subjected to the action of a high frequency alternating electric field.

This is due, in real dielectrics, to the polarization processes related to the movement of microscopic distances of electric charges "related" to the structure of the material and the direct passage of the conduction currents that occur for the presence of "free" charges that move over macroscopic distances under the influence of the field.

The dielectric materials are mostly characterized by low electrical conductivity and low thermal conductivity, thus preventing the possibility of use of certain types of heating; this is the reason for the widespread use of dielectric heating for industrial processes, but now also in the home , which requires a rapid heating and heating evenly distributed in the mass of the body.

2.3.4 - Polarization processes

A dielectric material, therefore, differs from a conductor for the polarization properties under the action of an electric field.

The process of polarization manifests itself in different ways, at different frequencies.

Here is that there are different types of polarization such as electronic and ionic. These polarizations are defined elastic or characterized by an elastic deformation of the electron orbits in the presence of applied electric field; as a result the atom behaves as a dipole oriented to the external field. Only thy differ in the frequency of elastic oscillations that in the first case is of the order of 10^{14} - 10^{16} Hz and in the second case of 10^{11} Hz.

Differs from these the dipolar polarization or to orientation that is manifested in that substances called "polar" into where, even in the absence of external field, the molecules are dipoles. These are disorderly oriented in the absence of the field due to thermal agitation while under the influence of the field tend to rotate around its axis and take the orientation of the field. The orientation, however, is hampered by the movements of thermal agitation that you have the so-called relaxation polarization.

2.3.5 - Power transformed into heat in the material to be heated

In a dielectric material provided with the vector fields **E** (electric field) and **D** (electric flux density) the electrostatic energy density per unit volume is given by:

$$W = \frac{\overline{E} \cdot \overline{D}}{2} \qquad [J/m3] \qquad (2.44)$$

with:

$$\overline{D} = \varepsilon_0 \overline{E} + \overline{P} = (1 + \frac{\overline{P}}{\varepsilon_0 \cdot \overline{E}})\varepsilon_0 \overline{E} = (1 + \alpha)\varepsilon_0 \varepsilon \overline{E} \qquad (2.45)$$

It is said dielectric polarization vector :

$$\overline{P} = \alpha \varepsilon_0 \overline{E} \qquad (2.46)$$

with:

- ε_0=8.86 · 10^{-12} dielectric constant of vacuum [F/m] ;
- α is the dimensionless coefficient of proportionality said dielectric susceptibility of the material.

From the first Maxwell equation in the presence of **E** and **D** we have:

$$rot\overline{H} = \sigma \cdot \overline{E} + \frac{\partial \overline{D}}{\partial t} \tag{2.47}$$

with:

- H is the magnetic field strength;
- σ is the electrical conductivity media;
- G is the density of conduction current;
- $\frac{\partial D}{\partial t}$ is the electric current density.

In the case of sinusoidal, we have:

$$rot\overline{H} = \sigma \cdot \overline{E} + j\omega\varepsilon_0\varepsilon\overline{E} \tag{2.48}$$

Where the term on the right of the equals sign is the total current density sum of the conduction current density and displacement.

Since, as mentioned above, under the action of the electric field, the polarization process of the related charges is not instantaneous, in an alternative field the polarization vector results out of phase delayed among the carrier field strength. Also D results out of phase delayed than E by an angle δ_p characteristic of active power in the process of polarization of the dielectric.

Therefore, the diagram of figure 3 shows that the total current density can be represented or conduction current:

$$\overline{G_t} = \left(\sigma + j\omega\varepsilon_0\dot{\varepsilon}\right)\overline{E} = \dot{\sigma}_t\overline{E} \tag{2.49}$$

with:

- $\dot{\varepsilon} = \varepsilon' - j\varepsilon''$ (2.50)
- $\dot{\sigma}_t = \left(\sigma + \omega\varepsilon_0\varepsilon''\right) + j\omega\varepsilon_0\varepsilon'$ (2.51)

the latter called complex equivalent electrical conductivity of the dielectric.

Or as displacement current:

$$\overline{G_t} = j\omega\varepsilon_0\left(\dot{\varepsilon} - j\frac{\sigma}{\omega\varepsilon_0}\right)\overline{E} = j\omega\varepsilon_0\varepsilon'\left(1 - jtg\delta\right)\overline{E} \tag{2.52}$$

with:

- tgδ is the tangent of the total dielectric loss angle.

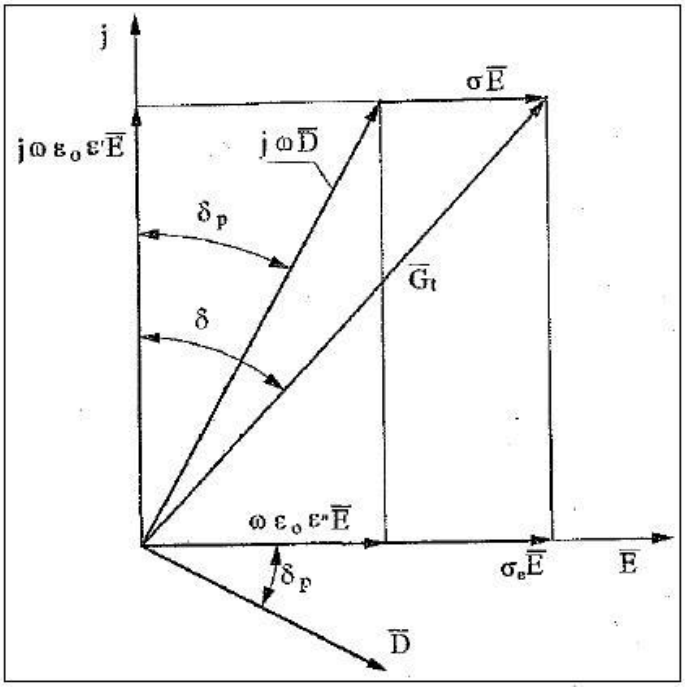

Fig. 3: phasor diagram of a dielectric material subjected to an alternating electric field.

The diagram shows that the angle of total loss δ is greater than δ_p since the former takes into account both the thermal energy that is put into play by the conduction currents and even the energy due to the polarization of the alternative electric field.

By the relations given above we have:

$$\dot{\sigma}_t = j\omega\varepsilon_0\varepsilon'(1-tg\delta)$$
$$tg\delta = \frac{\varepsilon''}{\varepsilon'} + \frac{\sigma}{\omega\varepsilon_0\varepsilon'} = tg\delta_p + \frac{\sigma}{\omega\varepsilon_0\varepsilon'} \qquad (2.53)$$

Therefore the parameters ε' and tgδ completely characterize the properties of a dielectric subjected to an alternating electric field, and is commonly referred to them in practice.

The complex power per unit volume in the dielectric, calculated using the known relationship:

$$p + jq = \bar{E} \cdot \bar{\bar{G}}_t = \bar{\bar{\sigma}}_t \cdot \bar{E}^2 \qquad (2.54)$$

According to the previous report of σ_t:

$$p + jq = (\sigma + \omega\varepsilon_0\varepsilon'' - j\omega\varepsilon_0\varepsilon')E^2 = \omega E^2\varepsilon_0\varepsilon'(tg\delta - j) \qquad (2.55)$$

Where the real part is the power [in W/m^3] converted into heat in the material that results therefore proportional to the frequency, the square of the electric field and the product ε'· tgδ also called *loss*

factor, which in turn depends on the temperature, the frequency and moisture content in the same material.

Conventionally heating systems, in the frequency range between 1 and 100 MHz, are called to dielectric losses (or radio frequency), while those at higher frequencies are classified as microwaves heating. This corresponds to the fact that in the first case, the wavelength is typically much larger than the size of the object to be heated and the need for use of frequency generators of very different for dielectric losses and microwave heating.

In practice, given the greater bandwidth, dielectric losses in the frequency most commonly used when no other factors make it inappropriate, is that of 27.12 MHz; in the microwave range, for the availability of industrial power generators, the two frequencies in use are those of 915 and 2450 MHz.

Chapter 3

Microwave heating distribution and uniformity

3.1 - Introduction

During microwave heating several interacting variables related to food, packaging and the microwave oven itself will influence how the food will be heated.

Microwave heating of foods has sometimes been connected with uneven heating, due-to so called “hot and cold spots” which may be present in the food product after heating.

The microwave heating profile in foods is determined by the thermo-physical properties of the food item (dielectric properties, but also thermal properties) as well as of the distribution of the absorbed microwave power in the food. The latter is, in turn, determined by several factors: the electric field inside the microwave cavity, the dielectric properties (complex permittivity) of the food item but also by the microwave frequency.

Heating uniformity is, however, also to a great extent influenced by size, geometry, position and composition of food as well as package during heating.

3.2 – Dielectric and thermal properties

The macroscopic interaction between an electromagnetic field and a material is expressed by the permittivity ε″ and the permeability μ of the material. The permittivity describes the electrical properties, while the permeability describes the magnetic properties of the material. However, since foods are non-magnetic, the magnetic part of the power contribution will not give rise to heating.

The permittivity designates how a material will interact with microwaves by expressing to what extent and how the material will absorb microwave energy and convert it into heat, how strong the reflection and the transmission phenomena will be, as well as how much the microwave wavelength will be reduced in the material.

The permittivity is a complex quantity. Thus it consists of both a real part (the real permittivity ε′) and an imaginary part (the dielectric loss factor ε″).Basically, the permittivity describes the ability of a material to absorb, transmit and reflect electromagnetic energy.

The absorbed microwave power is related to the permittivity and to the electric field by the following equation (see chapter 2.3.5):

$$P = 2\pi f \varepsilon_0 \varepsilon'' |E^2|$$

where P is the power which is absorbed in a given volume of the food material (W/m^3), f is the frequency in Hz, E is the electrical field strength in V/m inside the food, ε_0 is the permittivity in free space ($8.854 \cdot 10^{-12}$ F/m), and ε″ is the relative dielectric loss factor.

The complex permittivity, or as commonly said the dielectric properties, of a food material varies with the composition of the food, but also with the temperature and the frequency. Since water is generally a major constituent in most foods, its permittivity will play a major role in determining the dielectric properties of the food. Knowledge of the dielectric properties of foods is useful when developing

foods and constructing ovens, as well as when selecting packaging material. Today, oven construction, packaging design and product development of microwavable foods are to a large extent made based upon microwave simulations which predict the heating pattern for a given scenario.

3.3 – Heating phenomena which influence heating performance and uniformity

The influence of geometry parameters on the microwave heating distribution was describe by Ohlsson and Risman (1978) for spheres and cylinders. In this sections selective heating effects are described, related to the composition and shape of the food material its self. For simplicity, we consider the microwave field to be evenly distributed and of a given field strength at the food surface.

3.3.1 – Concentration effects

A slab with sharp corners and edges which is microwave heated will show field and energy concentration there, which cause selective heating, especially at the corners. Briefly described, a sharp edge or corner will act as an antenna and attract more energy than surrounding areas.

Consider microwave heating as electromagnetic waves which may be reflected, absorbed or refracted, it can be seen that part of the energy is reflected at the food surface, and part of the energy is refracted.

For cylindrical or spherical geometries, such concentration effects can cause concentration of energy to the centre of the food, depending, however, on both the food diameter and the dielectric properties. This centre overheating effect occurs for diameters of approximately one to three times the penetration depth in the material. For cylinders, concentration effects occur when the electrical field is parallel to the cylinder axis. The effect will be stronger for food with high permittivity values. At 2450 MHz centre heating usually happens at diameters between 25 mm and 55 mm.

Microwave heating performance are thus affected by several possible heating phenomena. Among these are edge overheating effect, run-away heating in frozen foods.

3.3.2 – Run-away heating phenomenon

Pure ice has much lower dielectric properties than thawed foods. Most of the water in frozen foods is found as ice crystals within the food item. The reason for the fact that frozen foods absorb microwave energy at all is that approximately one-tenth of the water remains unfrozen as a strong salt solution inside the food (Ohlsson and Bengtsson, 2001). Since the regions that are thawed in the very beginning of a microwave thawing process will have much higher loss factor ε'', as compared with still frozen regions, they will heat very rapidly. This phenomenon is called thermal run-away heating (Buffler, 1993). Particularly in foods with high salt content, the surface may at high temperatures act as a shield during microwave heating. This is because the penetration depth will be lower for salty foods. Run-away heating may thus occur for high-salt foods, especially in the surface regions.

3.3.3 – Edge and corner overheating

The so-called edge (or corner) overheating effect is often noted especially when frozen foods are heated or thawed. Edges and corners have a tendency to heat or thaw first, which intuitively could be understood by the fact that the amplitudes of the electromagnetic fields are concentrated at such areas of the food, due to scattering phenomena.

Edge overheating is strongly influenced by the polarization and incident angle of the incident field, the angle and curvature of the edges, the permittivity of the heated food materials, and the presence of other scatterers close to the edge (Sundberg, 1998a). For food loads heated at 2450 MHz, both loss mechanisms due to ionic conduction as well as dielectric relaxation are present.

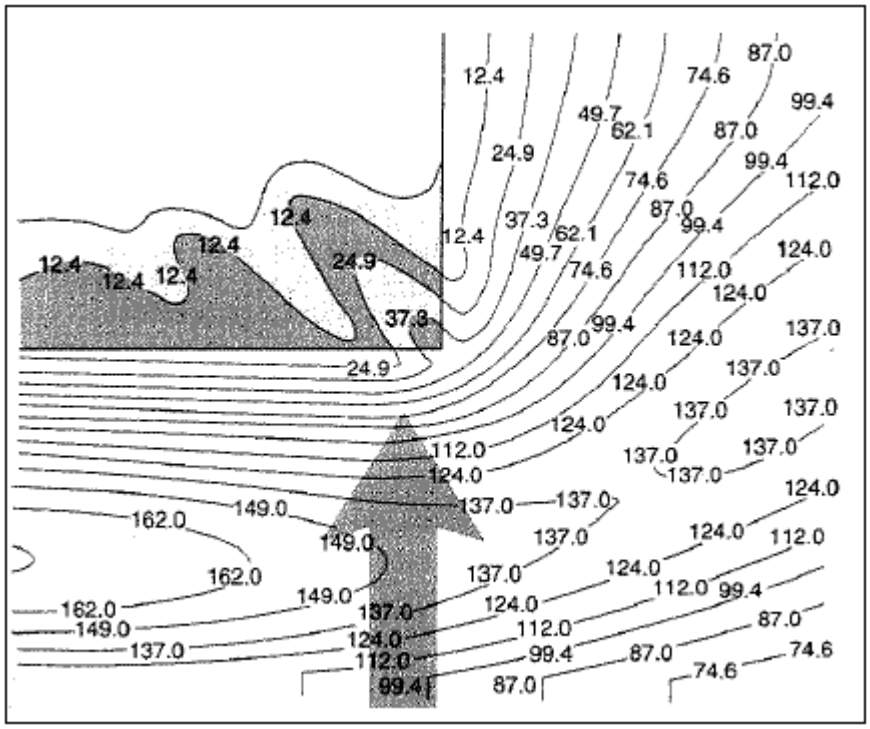

Fig. 1: The phenomenon behind edge overheating. The electromagnetic fields are concentrated at the corners of the food, due to the scattering phenomena.

3.3.4 – Centre overheating

For foods which are spherically or cylindrically shaped, i.e. foods with convex surfaces, refraction and reflection phenomena will result in concentration of the microwave power distribution to the geometrical centre for certain diameters (Ohlsson and Rismann, 1978). This phenomenon is called centre overheating. It is influenced by different factors, mainly the geometries, size and complex permittivity values of the foods.

Chapter 4

Experimental tests

4.1 - Introduction

The experimental phase consists of a series of laboratory tests, with three different microwave ovens, using same loads, and making a number of temperature measurements by two methods: the first using a thermocouple and then detecting the temperatures in a number of points within the sample; the second using an infrared camera, so through an optical detection in different sections of the load.

The aim is to evaluate, in the same test conditions, the temperature distribution, the efficiency, and compare the results obtained with those acquired using the simulation code COMSOL Multi-physics that will be analyzed in the next chapter.

4.2 – Microwave ovens

- *MWO 1(see Appendix A):*

Cavity dimension H×W×D: 180×295×290 mm

Wave guide: 1

Max power: 800 W

- *MWO 2(see Appendix B):*

Cavity dimension H×W×D: 170×290×290 mm

Wave guide: 2

Max power: 700 W

- *MWO 3(see Appendix C):*

Cavity dimension H×W×D: 225×345×340 mm

Wave guide: 2

Max power: 950 W

4.3 – Equipment for temperature measuring

- *Power analyzer:*

The power analyzer is multi-function device that measure precisely continuous current, alternative current, the intensity of DC or AC and power in Watts.

Today, power analyzers have many features such as, insulated current input, measurement of harmonics, current measurement, power measurement, etc.).

Fig. 1: Power analyzer.

- *Thermocouple:*

A thermocouple is a device consisting of two different conductors (usually metal alloys) that produce a voltage proportional to a temperature difference between either end of the pair of conductors.

Fig. 2: Thermocouple with a stick attached for an accurate measurement.

- *Infrared camera:*

The infrared camera is a particular camera, sensitive to infrared radiation, capable of obtaining images or filming thermographic.

Starting from the detected radiation will therefore be obtained by the temperature maps of the exposed surfaces are often used for scientific or military. The cameras are divided into non-radiometric and radiometric. The first to measure the absolute temperature value of each point in the image. The image, in fact, is built on a matrix of a number of pixels for a certain number of rows. The electronics of the instrument "reads" easily the energy stored by each pixel and generates an image, in black and white or false colour, the object observed.

With infrared cameras can measure the temperature in each point of the image but you have to insert the instrument (or in the processing software in post processing) two parameters, temperature and emissivity which could achieve the correct temperature.

Fig. 3: Infrared camera: the camera detects the radiation that are transmitted and processed in the instrument display.

4.4 – Agar-gel samples

Agar-gel samples were prepared by dissolving 2% of certain quantity of water. The agar-water solution was heated at 90°C until agar powder was totally dissolved and the gel solution was clear. It was then poured into several glasses with the same amount each one; finally it was cooled to room temperature into solid samples with the shape of a truncated cone. So the dimensions were: high of 50 mm. the bottom diameter of 55 mm and the upper diameter of 45 mm (see fig.4 and 5).

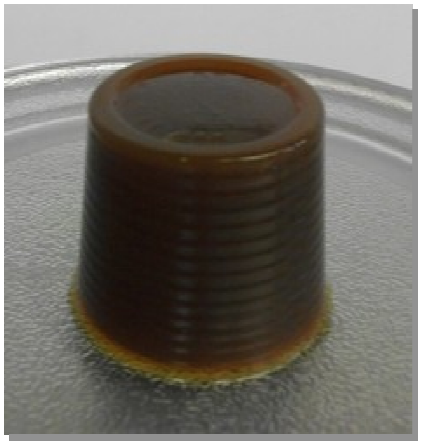

Fig. 4: Agar-gel sample.

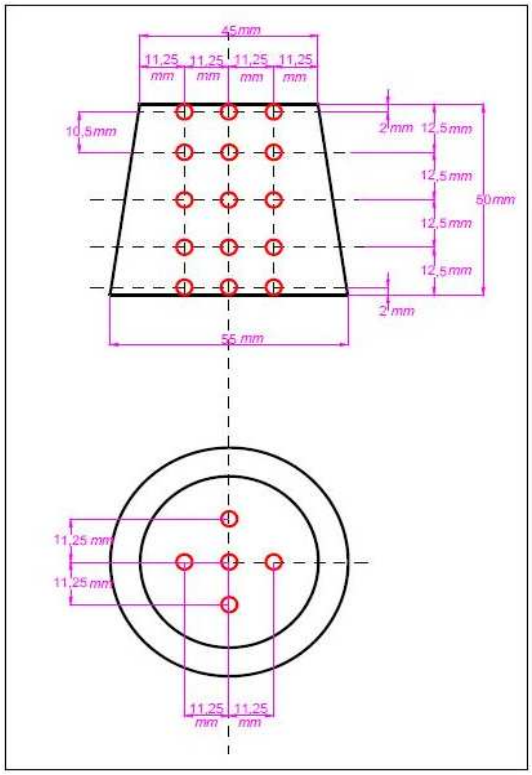

Fig. 5: Dimensions of the agar-gel sample.

Property	Value
Specific heat capacity, C_p (kJ/kg·°C)	4.2[a]
Thermal conductivity, k (W/m·°C)	0.60[a]
Density, ρ (kg/m^3)	1070[a]
Dielectric constant, ε'	73.6[a]
Dielectric loss, ε''	11.5[a]
Average surface heat transfer coefficient (h)	41.7[b]

[a] *Data from Barringer et al. (1995)*

[b] *Data from Yang and Gunasekaran (2001)*

Table 1: Dielectric, physical, and thermal properties of 2 % agar-gel.

4.5 - Tests with agar-gel sample (using thermocouples)

The test consists of heating, multiple samples of a water solution of agar, having the consistency of a gel (fig. 4), within the cavity of the 3 different microwave ovens.

The proof is divided into several phases, which are repeated for each oven, in which you go to make measurements of temperature, using a thermocouple in various parts of the material in the shape of a truncated cone; all this after placing each individual sample in the center of the turntable, and warmed it up to the maximum power of each oven for a time of 30 seconds each (in reality, then this time will vary for MWO 2 and 3, because of, otherwise, the dissolution of the gelatin solution).

Assuming we split our sample into 5 floors or the top surface, the half-plane in the middle, the bottom surface and two half-planes intermediate to these three mentioned, we proceeded with the measurement of temperature in different positions as in figure 6.

The different phases have been imposed for a measurement as accurate as possible and obtained within 10-15 seconds by the exit of the sample from the oven.

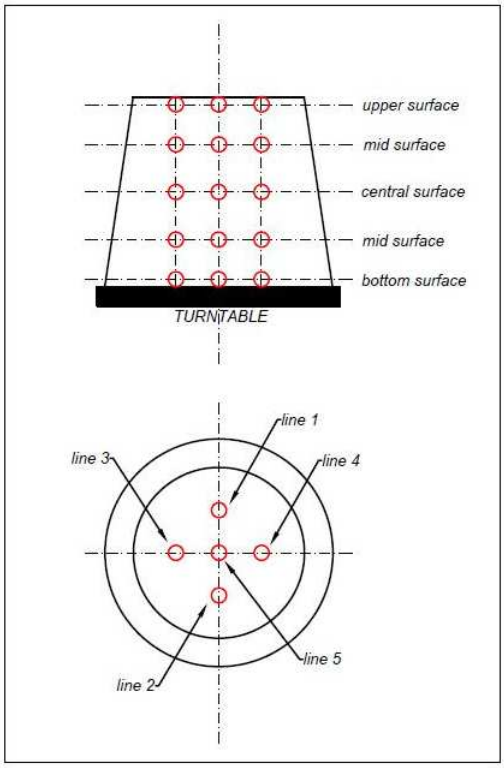

Fig. 6: Temperature measurement locations (upper surface = 0.2 cm; first mid surface = 1.25 cm; central surface = 2.5 cm; second mid surface 3.75 cm; bottom surface = 4.8 cm).

4.5.1 - Efficiency calculations

Here are the measurements and calculations in the various cases relating to the transferred power and the efficiency in different types of testing:

4.5.2 - First test with MWO 1:

- Mass of agar-gel = 0.093 kg
- $t_{HEATING}$= 30 s
- $\vartheta_{INITIAL\text{-}AGAR}$= 19°C
- ϑ_{ROOM}= 18°C
- ϑ_{PLATE} = 18° C
- $\vartheta_{OVEN\ INSIDE}$ = 16°C

Measurements:

Depth [cm]	Line 1[°C]	Line 2[°C]	Line 3[°C]	Line 4[°C]	Line 5[°C]
0,2	42	55	58	45	38
1,25	59	50	58	57	64
2,50	57	49	46	46	68
3,75	65	61	54	49	68
4,8	52	45	45	39	50

Depth [cm]	Line 1[°C]	Line 2[°C]	Line 3[°C]	Line 4[°C]	Line 5[°C]
0,2	47	42	42	43	46
1,25	61	60	61	54	68
2,50	49	57	54	46	74
3,75	56	56	64	56	76
4,8	46	43	50	41	42

Depth [cm]	Line 1[°C]	Line 2[°C]	Line 3[°C]	Line 4[°C]	Line 5[°C]
0,2	36	41	52	45	40
1,25	50	53	61	58	71
2,50	56	68	56	50	68
3,75	55	76	60	49	68
4,8	52	52	48	43	48

Depth [cm]	Line 1[°C]	Line 2[°C]	Line 3[°C]	Line 4[°C]	Line 5[°C]
0,2	38	37	50	45	41
1,25	55	53	60	54	57
2,50	49	48	50	50	74
3,75	60	58	59	48	77
4,8	42	44	46	41	54

Once the temperatures obtained, to estimate the power absorbed by the sample and performance, we need to find a final average temperature that takes into account all the measurement values:

$$\vartheta_{average} = \frac{\sum_{1}^{100} \vartheta_{measurement}}{n} = 54°C$$

Average energy supplied:

$$W_{\sup plied} = \frac{\sum W_{\sup plied}}{n_{proofs}} = 9.4Wh$$

Average power absorbed by agar-gel:

$$Q_{absorbed} = \frac{m \cdot c \cdot (\vartheta_{average} - \vartheta_{IN-AGAR})}{t} =$$

$$= \frac{0.093 \cdot 4200 \cdot (54 - 19)}{30} = 455.7W$$

Average power provided and system efficiency:

$$Q_{\text{sup } plied} = \frac{W_{\text{sup } plied}}{t} = 9.4 \cdot \frac{3600}{30} = 1128W$$

$$\eta_{system} = \frac{Q_{absorbed}}{Q_{\text{sup } plied}} = \frac{455.7}{1128} = 0.40$$

Considering that magnetron absorbs 400 W of totals 1200 W, we take 2/3 of the supplied power, or 800 W, this is the useful power, and recalculates the efficiency interested only the cavity:

$$\eta_{cavity} = \frac{Q_{absorbed}}{Q_{useful}} = \frac{455.7}{800} = 0.57$$

The following is the graph of temperature as a function of the depth of the sample:

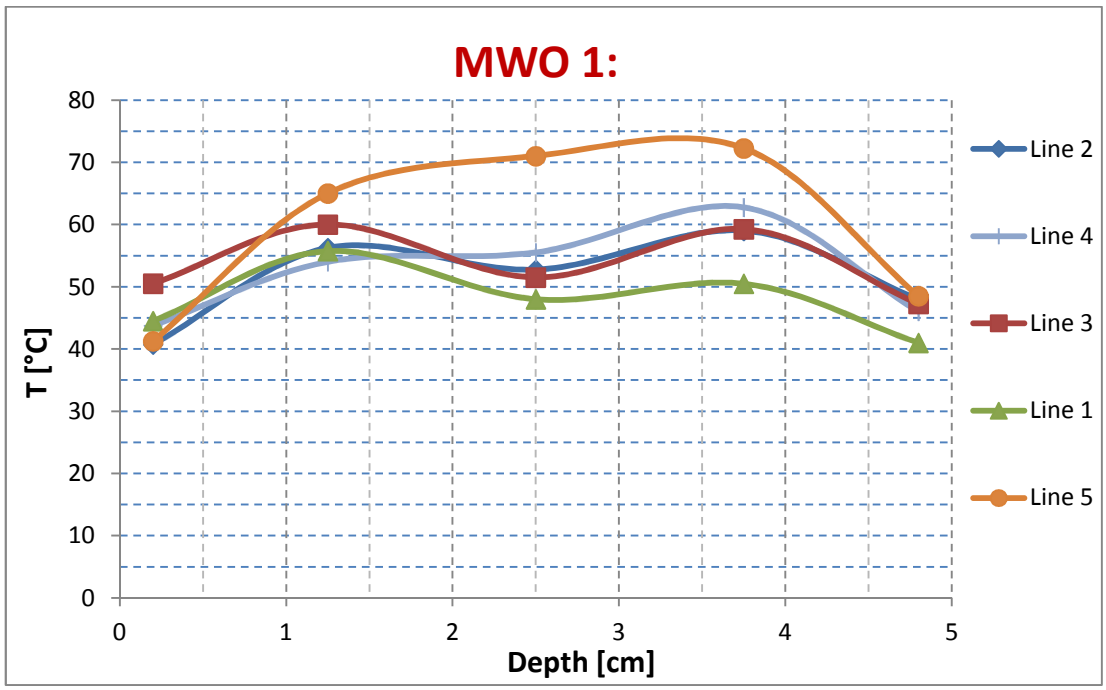

The efficiency obtained in the cavity, so without considering the power "held by the magnetron", is 57 %; can be reached also after heating of 30 seconds at maximum power of 800 W, a hot spot of 77°C at a depth of 3.75 cm into the agar's proof along the line 5, or the central one. The cold spot rather low is 36°C at a depth of 0.2 cm, and near the upper surface, along the line 1. As can be seen from the chart temperature/depth, line 5(average of all the lines 5 measured), which is the line affected by the measures along the central axis of the sample, is the one who suffers most heating, because it reaches to the depths of 1.25 cm, 2.5 cm, and 3.75 cm, respectively, the temperatures of 65°C, 71°C and 74°C. These measurements are reliable, not only for the values obtained, but also for characterizing the fact that more warming in the central part of the piece, take us back to the center phenomenon of overheating effect (see chapter 3.3.4); because Ohlsson and Rismann in the 1978 have studied that cylindrical and spherical loads, undergo more intense warming in the central part just as in our case.

4.4.2 - Second test with MWO 2:

- Mass of agar-gel = 0.093 kg
- $t_{HEATING}$= 20 s
- $\vartheta_{INITIAL\text{-}AGAR}$= 19°C
- ϑ_{ROOM}= 18°C
- ϑ_{PLATE} = 18° C
- $\vartheta_{OVEN\ INSIDE}$ = 16°C

Measurements:

Depth [cm]	Line 1[°C]	Line 2[°C]	Line 3[°C]	Line 4[°C]	Line 5[°C]
0,2	23	21	22	25	23
1,25	27	28	27	28	33
2,50	30	28	26	26	45
3,75	49	47	35	38	34
4,8	59	55	48	44	31

Depth [cm]	Line 1[°C]	Line 2[°C]	Line 3[°C]	Line 4[°C]	Line 5[°C]
0,2	24	24	26	23	27
1,25	30	30	29	30	29
2,50	30	30	28	31	43
3,75	41	45	39	40	38
4,8	55	50	35	48	31

Depth [cm]	Line 1[°C]	Line 2[°C]	Line 3[°C]	Line 4[°C]	Line 5[°C]
0,2	25	23	23	23	26
1,25	28	28	28	25	28
2,50	30	28	27	29	47
3,75	49	49	39	37	40
4,8	45	49	40	40	30

Depth [cm]	Line 1[°C]	Line 2[°C]	Line 3[°C]	Line 4[°C]	Line 5[°C]
0,2	25	24	25	26	27
1,25	33	27	30	32	32
2,50	33	31	32	30	40
3,75	47	43	39	39	36
4,8	50	59	34	38	35

Once the temperatures obtained, to estimate the power absorbed by the sample and performance, we need to find a final average temperature that takes into account all the measurement values:

$$\vartheta_{average} = \frac{\sum_{1}^{100} \vartheta_{measurement}}{t} = 34°C$$

Average energy supplied:

$$W_{\sup plied} = \frac{\sum W_{\sup plied}}{n_{proofs}} = 5.5Wh$$

Average power absorbed by agar-gel:

$$Q_{absorbed} = \frac{m \cdot c \cdot (\vartheta_{average} - \vartheta_{IN-AGAR})}{t} =$$

$$= \frac{0.093 \cdot 4200 \cdot (34 - 19)}{20} = 292.95W$$

Average power provided and system efficiency:

$$Q_{\sup plied} = \frac{W_{\sup plied}}{t} = 5.5 \cdot \frac{3600}{20} = 990W$$

$$\eta_{system} = \frac{Q_{absorbed}}{Q_{\sup plied}} = \frac{292.95}{990} = 0.30$$

Considering the useful power is 700W, the efficiency is recalculated as:

$$\eta_{cavity} = \frac{Q_{absorbed}}{Q_{useful}} = \frac{292.95}{700} = 0.42$$

The following is the graph of temperature as a function of the depth of the sample:

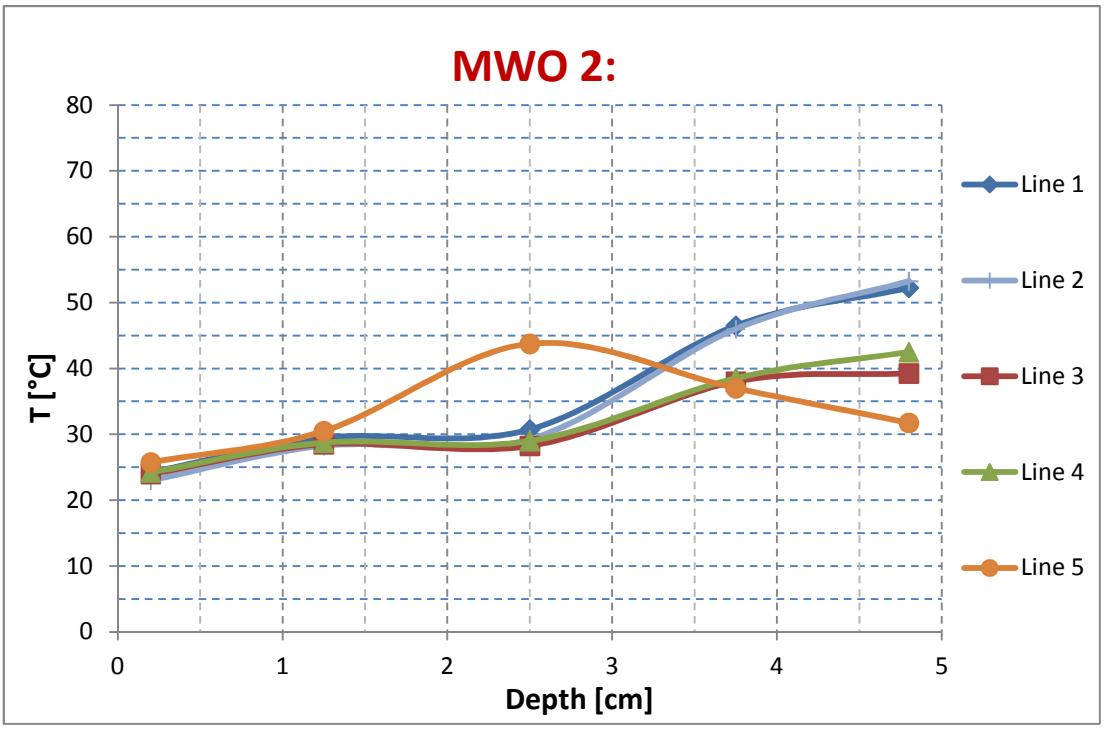

The efficiency obtained in the cavity, so without considering the power "held by the magnetron", ever is 42 %. So in this case we can say that the line who suffers most heating is line 1 unlike the other case where the hottest line was the central. There is therefore that the lower part of the piece, the ends, will heat up more; in fact, in the piece, at the depth of 4.8 cm the temperature reaches 59°C. There is also a hot spot at the center of the load, so at a depth of 2.5cm, where it achieves 47°C. This leads us to retrieve again the centre overheating effect and the edge effect with predominance with the lower part.

4.4.3 - Third test with MWO 3:

- Mass of agar-gel = 0.093 kg
- $t_{HEATING}$= 20s
- $\vartheta_{INITIAL\text{-}AGAR}$= 19°C
- ϑ_{ROOM}= 18°C
- ϑ_{PLATE} = 18° C
- $\vartheta_{OVEN\ INSIDE}$ = 16°C

Measurements:

Depth [cm]	Line 1[°C]	Line 2[°C]	Line 3[°C]	Line 4[°C]	Line 5[°C]
0,2	33	30	35	33	39
1,25	50	41	45	45	49
2,50	54	43	40	49	47
3,75	57	56	38	53	52
4,8	43	47	34	44	33

Depth [cm]	Line 1[°C]	Line 2[°C]	Line 3[°C]	Line 4[°C]	Line 5[°C]
0,2	38	34	31	30	37
1,25	45	46	42	38	51
2,50	41	43	39	45	52
3,75	56	50	49	53	67
4,8	46	34	36	41	46

Depth [cm]	Line 1[°C]	Line 2[°C]	Line 3[°C]	Line 4[°C]	Line 5[°C]
0,2	30	35	30	30	32
1,25	44	38	34	43	42
2,50	53	49	41	44	54
3,75	59	48	54	51	58
4,8	46	40	48	32	58

Depth [cm]	Line 1[°C]	Line 2[°C]	Line 3[°C]	Line 4[°C]	Line 5[°C]
0,2	37	30	33	30	32
1,25	43	44	40	40	46
2,50	44	44	41	41	50
3,75	60	55	58	49	55
4,8	39	45	40	43	61

Once the temperatures obtained, to estimate the power absorbed by the sample and performance, we need to find a final average temperature that takes into account all the measurement values:

$$\vartheta_{average} = \frac{\sum_{1}^{100} \vartheta_{measurement}}{t} = 44°C$$

Average energy supplied:

$$W_{\sup plied} = \frac{\sum W_{\sup plied}}{n_{proofs}} = 8.8Wh$$

Average power absorbed by agar-gel:

$$Q_{absorbed} = \frac{m \cdot c \cdot (\vartheta_{average} - \vartheta_{IN-AGAR})}{t} =$$

$$= \frac{0.093 \cdot 4200 \cdot (44 - 19)}{20} = 488.25W$$

Average power provided and system efficiency:

$$Q_{\sup plied} = \frac{W_{\sup plied}}{t} = 8.8 \cdot \frac{3600}{20} = 1584W$$

$$\eta_{system} = \frac{Q_{absorbed}}{Q_{\sup plied}} = \frac{488.25}{1584} = 0.31$$

Considering the useful power is 950W, the efficiency is recalculated as:

$$\eta_{cavity} = \frac{Q_{absorbed}}{Q_{useful}} = \frac{488.25}{950} = 0.52$$

The following is the graph of temperature as a function of the depth of the sample:

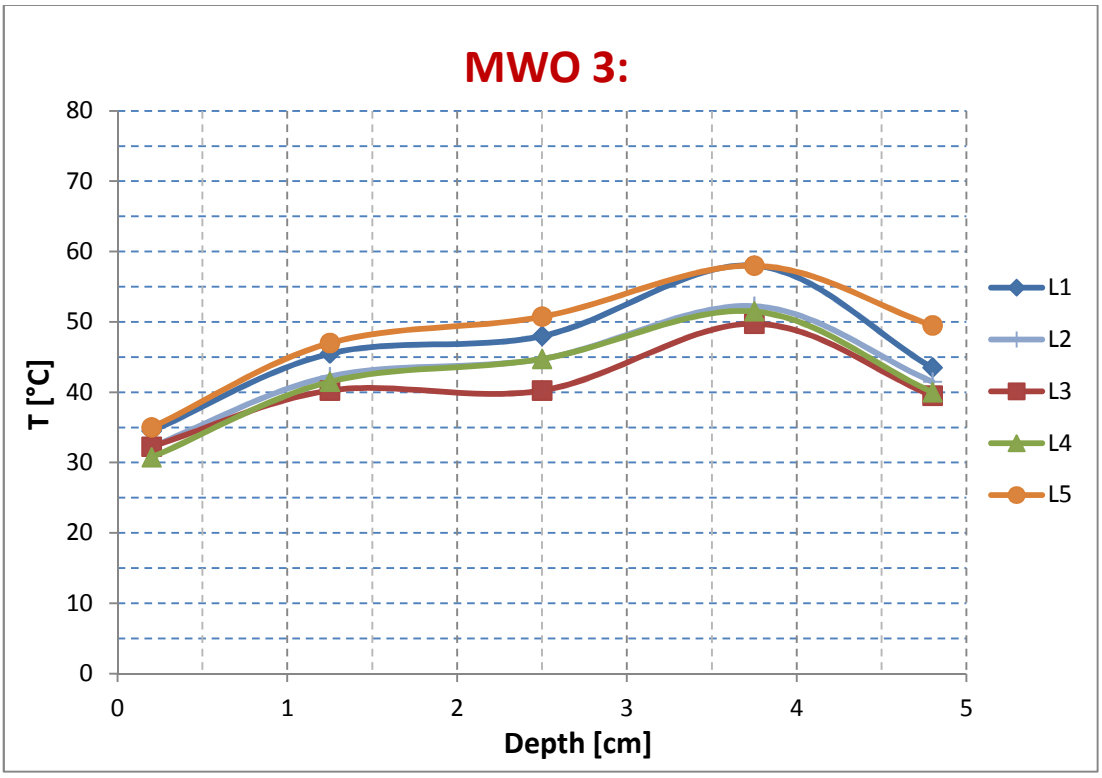

In this case the efficiency obtained in the cavity, so without considering the power "held by the magnetron" ever, is 52 %, can be reached also after heating of 20 seconds at maximum power of 950 W, a hot spot of 67° C, at a depth of 3.75 cm again, into the agar's proof along the line 5, or the central one. The cold spot rather low is 30° C at a depth of 0.2 cm, and near the upper surface, along the line 1. Looking at the chart temperature/depth, line 5, is the one who suffers most heating again (centre overheating effect). Furthermore, it can be seen that a good heating uniformity in the piece as there is no significant ΔT and a certain symmetry, respectively, between lines 1 and 2 and lines 3 and 4; also graphically you can see how the lines are too close together and sometimes overlapping too.

4.4 – Test with agar-gel samples (using infrared camera)

This chapter presents the measures taken with an infrared camera to have, first, a comparison with the measurements by thermocouple; the sections made, also, allow us to make a comparison , after, between the real temperature distribution and that obtained by the numerical model COMSOL Multi-physics.

The following case consists in heating of the samples with the same modalities already described for the previous case with the thermocouple. The only difference lies in the detection of temperatures. In this case in fact, two tests were carried out for each oven, which correspond to two surveys with the IR camera: a section along the axis of 3-5-4 and the other along the axis 1-5-2. Once detected the temperature distribution, having previously set also the correct epsilon on the machine, it was possible, by means of a program, to obtain the temperatures along the different lines. The tables in the various cases were extracted from the program called Piced. The temperature measurements were associated with the scale in pixels, with a suitable approximation, the corresponding pixel values were normalized and converted to a centimetre scale (of which we give some values). Later they were given the values in a graph for a comparison with measurements made using a thermocouple.

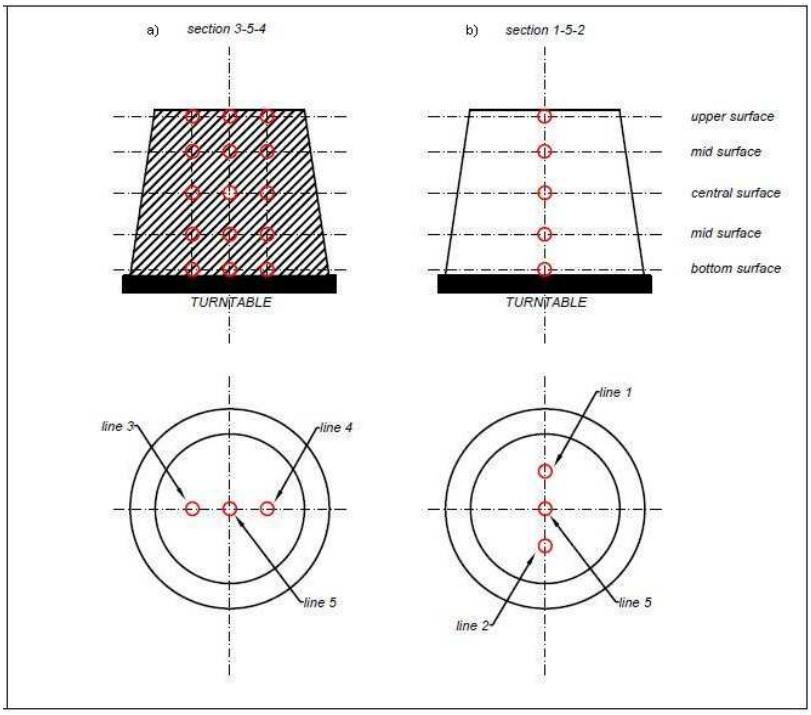

Fig. 7: Temperature measurement locations by different section: a) section 3-5-4; b) section 1-5-2 (upper surface = 0.2 cm; first mid surface = 1.25 cm; central surface = 2.5 cm; second mid surface 3.75 cm; bottom surface = 4.8 cm).

4.5.1 - Efficiency calculation

Here are the measurements and calculations in the various cases relating to the transferred power and the efficiency in different types of testing.

4.5.2 – First test with MWO 1:

Here are the temperature detected by the infrared camera through the section 1-5-2 and 3-5-4 of the load as measured by the thermocouple; the temperatures* extracted correspond to the points of the lines shown in figure 7:

Depth [cm]	Pxl	Line 5 [°C]	Line 1 [°C]	Line 2 [°C]
0,22625	1,81	42,79	57,53	54,54
1,24375	9,95	65,39	54,73	54,78
2,54375	20,35	78,66	42,18	40,18
3,73	29,84	76,48	51,35	58,35
4,80375	38,43	56,63	35,43	41,37
5,08625	40,69	28,47	1,83	3,45

Depth [cm]	Pxl	Line 3 [°C]	Line 4 [°C]
0,217948718	1,36	50,35	46,68
1,232371795	7,69	62,57	59,14
2,246794872	14,02	57,31	64,64
3,767628205	23,51	61,75	63,99
4,782051282	29,84	56,44	62,91
5	31,2	45,48	57,13

* for simplicity, have been reported in the tables of each tests, only the values corresponding to the discretization points (fig. 7), but for the realization of graphics and for the evaluation of the efficiency, reference is made to all values extracted from the program.

Considering a range of temperature measured for a certain numbers of volume in different position of the load, here is the average temperature estimates:

$$\vartheta_{average} = \frac{\sum_{i}^{n} \vartheta_{measurement}}{n} = 56°C$$

Average power absorbed by agar-gel:

$$Q_{absorbed} = \frac{m \cdot c \cdot (\vartheta_{average} - \vartheta_{IN-AGAR})}{t} =$$

$$= \frac{0.093 \cdot 4200 \cdot (56 - 19)}{30} = 481.7W$$

Considering the useful power is 800W, the efficiency is recalculated as:

$$\eta_{cavity} = \frac{Q_{absorbed}}{Q_{useful}} = \frac{481.7}{800} = 0.60$$

This is the temperature distribution of the section 1-5-2 and 3-5-4 of the load where you can see that the trend is similar to a "X" and the central part has got the two hot spots (white points at 81.2 °C). By using the program it was possible to extract the temperature values of the central line, the line 5, and the laterals. (figure 8-9).

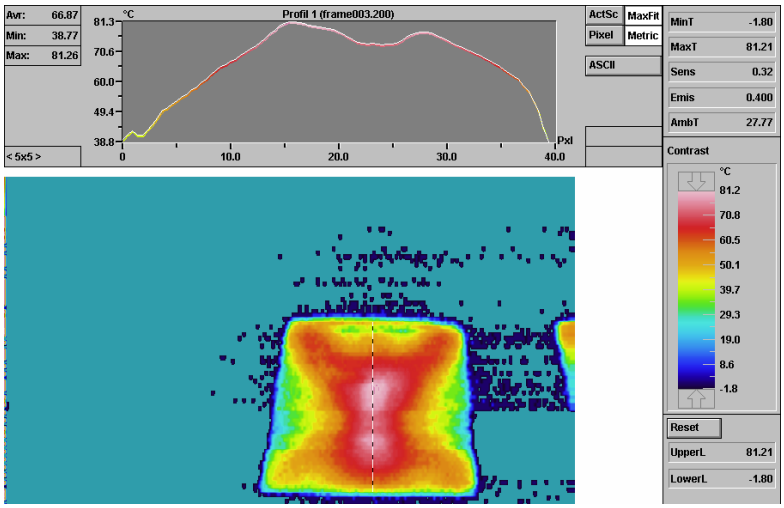

Fig. 8: Section 1-5-2 of the load: temperature distribution and graphic of the central line or line 5.

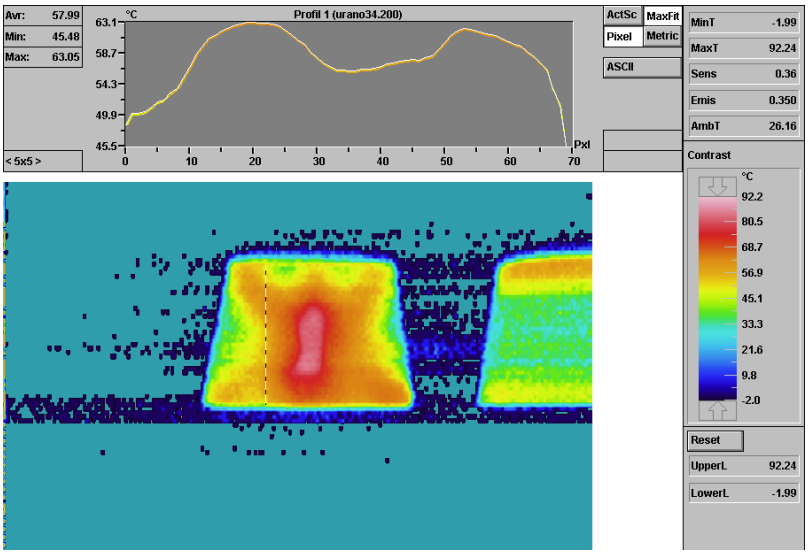

Fig. 9: Section 3-5-4 of the load: temperature distribution and graphic of the lateral line, in this case line 3.

The following is the graph of temperature as a function of the depth of the sample:

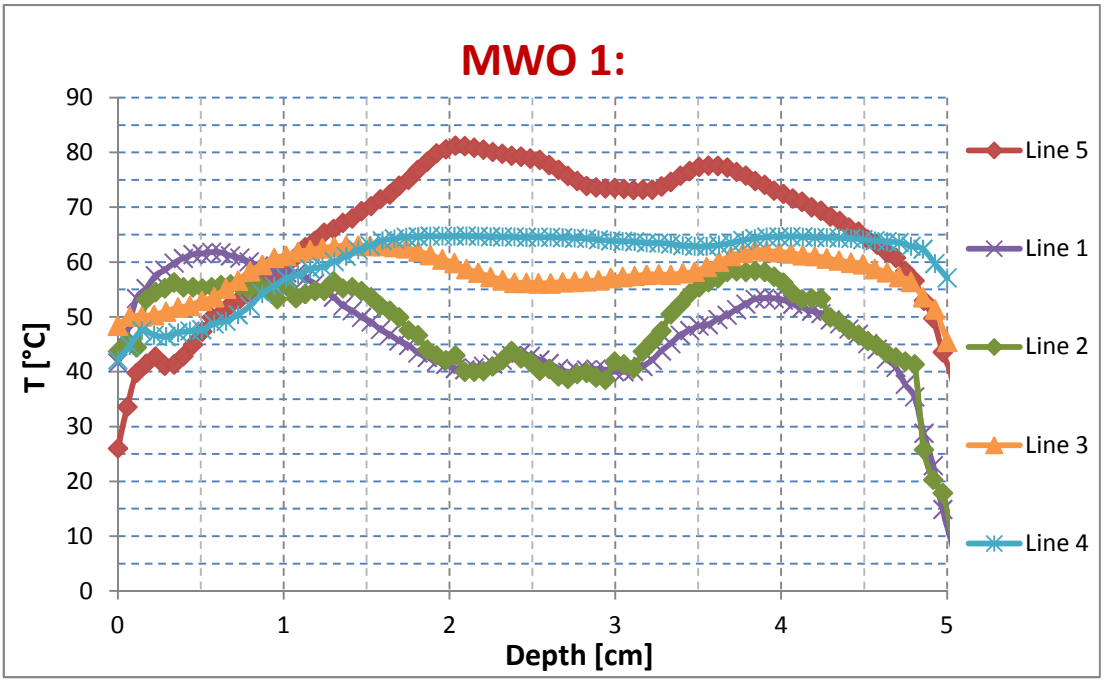

The efficiency obtained in the cavity, so without considering the power "held by the magnetron", is 60 %; as stated above, there are two hot spots of about 80°C into the agar's proof along the line 5; also in this case, as the test with the thermocouple, line 5 is the one who suffers most heating .

From the graph we can also note a certain symmetry between the side lines, respectively, for sections made but not total; this means that there is not much uniformity of heating in the sample that suffers the greater warming in the middle (centre overheating effect) and in the ends (edge effect). Having said this, even if the temperature is not the same, must be noticed that in this case the piece is heated decidedly for almost the whole section view.

4.5.4 – Second test with MWO 2

Depth [cm]	Pxl	Line 3 [°C]	Line 4 [°C]	Line 1 [°C]	Line 2 [°C]	Line 5 [°C]
0,234968901	1,36	14,07	10,41	0	2,04	5,53
1,249136144	7,23	21,61	21,92	22,5	19,92	28,68
2,5	14,47	26,53	30,56	30,26	25,85	42,44
3,749136144	21,7	45,75	52,64	49,15	41,67	47,46
4,842778162	28,03	28,8	39	29,25	28,55	23,74
5	28,94	7,6	12,97	2,26	8,85	0

Also in this case, considering a range of temperature measured for a certain numbers of volume in different position of the load, here is the average temperature estimates:

$$\vartheta_{average} = \frac{\sum_{i}^{n} \vartheta_{measurement}}{n} = 33°C$$

Average power absorbed by agar-gel:

$$Q_{absorbed} = \frac{m \cdot c \cdot (\vartheta_{average} - \vartheta_{IN-AGAR})}{t} =$$

$$= \frac{0.093 \cdot 4200 \cdot (33-19)}{20} = 273.4W$$

Considering the useful power is 800W, the efficiency is recalculated as:

$$\eta_{cavity} = \frac{Q_{absorbed}}{Q_{useful}} = \frac{273.4}{700} = 0.39$$

At this time the temperature distribution of the sections 1-5-2 and 3-5-4 of the load, shows that there are two hot spots on the bottom corners of the sample and an another heated just above the center point. The hottest points, at the bottom edges, reach 70°C, but in the lateral measurement line, drawn with the program, are not detected them because they are too close to the edge. So the temperature noticed, at the depth between 3.75 cm and 4.8 cm, is about 53°C (fig. 10). With regard to the center line, the hottest point detected is located just above the center of the workpiece, at a depth intermediate between 1.25 cm and 2.5 cm, and it's about 45°C.

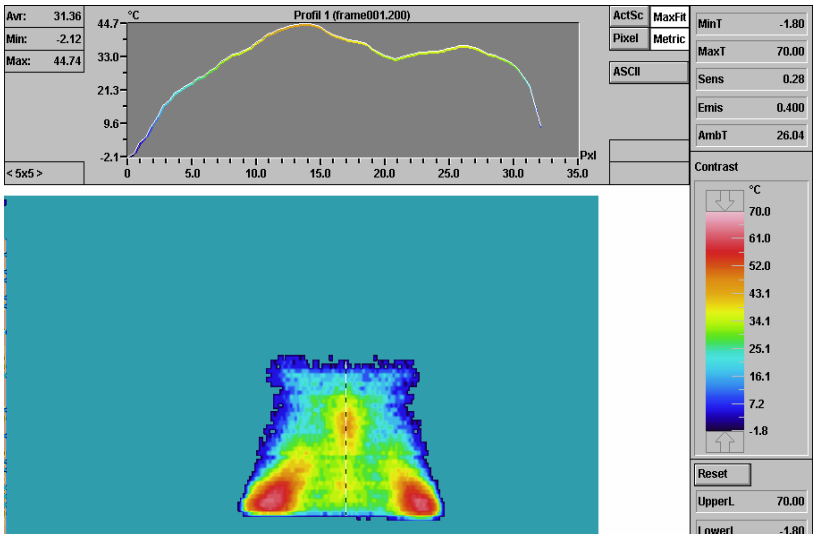

Fig. 10: Section 1-5-2 of the load: temperature distribution and graphic of the central line.

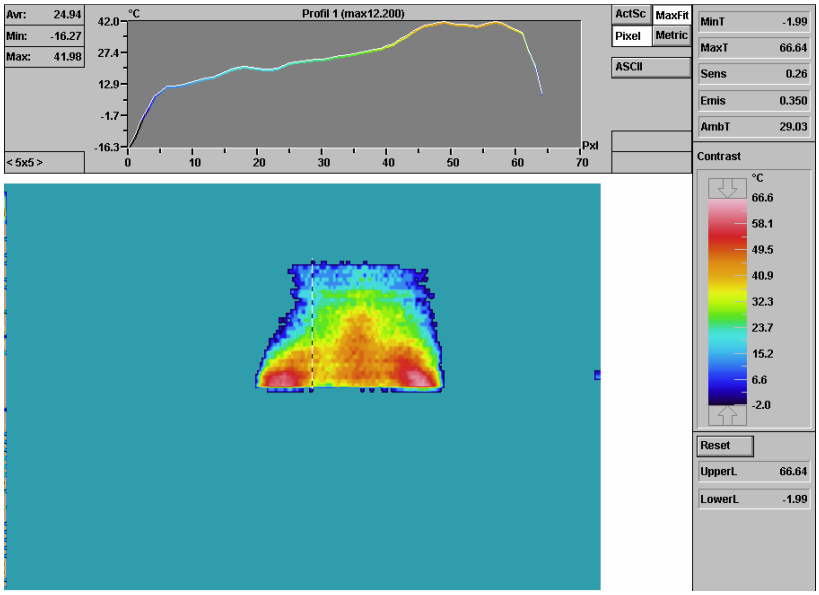

Fig. 11: Section 3-5-4 of the load: temperature distribution and graphic of the lateral line

The following is the graph of temperature as a function of the depth of the sample:

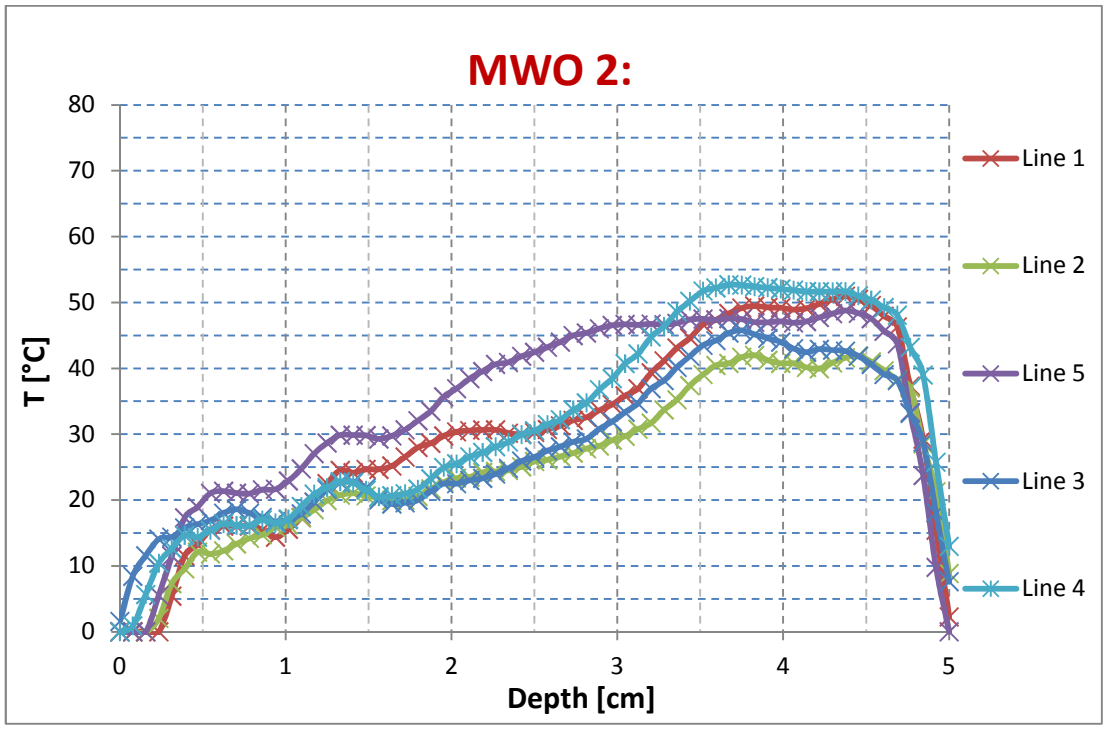

The efficiency obtained in the cavity, so without considering the power "held by the magnetron", ever is 39 %. So in this case we can say that the line who suffers most heating is line 4 at a depth of 3.75 cm with 53°C. There is therefore, as the case with the thermocouple, that the lower part of the piece, the ends, will heat up more and also the central part (violet line).This considerations lead us to retrieve again the centre overheating effect and the edge effect with predominance with the lower part.

The fact that the heating is more practically only in the lower part of the piece, leads us to affirm that this oven is probably more suited to a low load, a few centimeters in height, like a steak for example.

4.5.3 – Third test with MWO 3:

Depth [cm]	Pxl	Line 3 [°C]	Line 4 [°C]	Line 1 [°C]	Line 2 [°C]	Line 5 [°C]
0,234968901	1,36	29,37	32,05	35,48	28,39	27,28
1,249136144	7,23	43,6	51,12	41,85	44,98	50,55
2,5	14,47	41,14	48,52	51,39	45,13	66,12
3,749136144	21,7	60,03	63,24	55,99	63,04	67,4
4,842778162	28,03	48,08	47,78	34,15	53,6	41,37
5	28,94	43,33	40,68	27,3	49,59	36,93

Also in this case, considering a range of temperature measured for a certain numbers of volume in different position of the load, here is the average temperature estimates:

$$\vartheta_{average} = \frac{\sum_{i}^{n} \vartheta_{measurement}}{n} = 48°C$$

Average power absorbed by agar-gel:

$$Q_{absorbed} = \frac{m \cdot c \cdot (\vartheta_{average} - \vartheta_{IN-AGAR})}{t} =$$

$$= \frac{0.093 \cdot 4200 \cdot (48-19)}{20} = 566.3W$$

Considering the useful power is 800W, the efficiency is recalculated as:

$$\eta_{cavity} = \frac{Q_{absorbed}}{Q_{useful}} = \frac{566.3}{950} = 0.59$$

Also in this case, the temperature distribution of the sections 1-5-2 and 3-5-4 of the load shows that the trend is similar to a “X”; the most heated parts are the red parts where the load reach a temperature between 58°C and 70°C (small white spot) in particular in the bottom of the sample, at the edges and just below the central part. Figure 12 shows that the hot spot, regarding the central line, is at a depth between 2.5 cm and 3.75 cm and it’s among 52°C and 63°C. Figure 13 represent the temperature graph of the lateral line, in this case line 3 that is very similar to the symmetrical line 4; the hot zone is at a depth between 3.75 cm and 4.8 cm, and indicate a temperature among 55°C and 65°C. Note also, nearby the central part of the piece, to the outside, a fairly cold zone, where the temperature remains around 30°C.

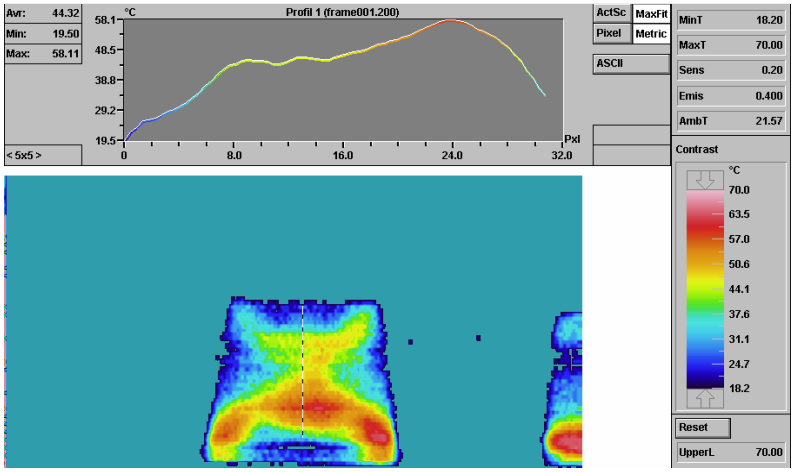

Fig. 12: Section 1-5-2 of the load: temperature distribution and graphic of the central line.

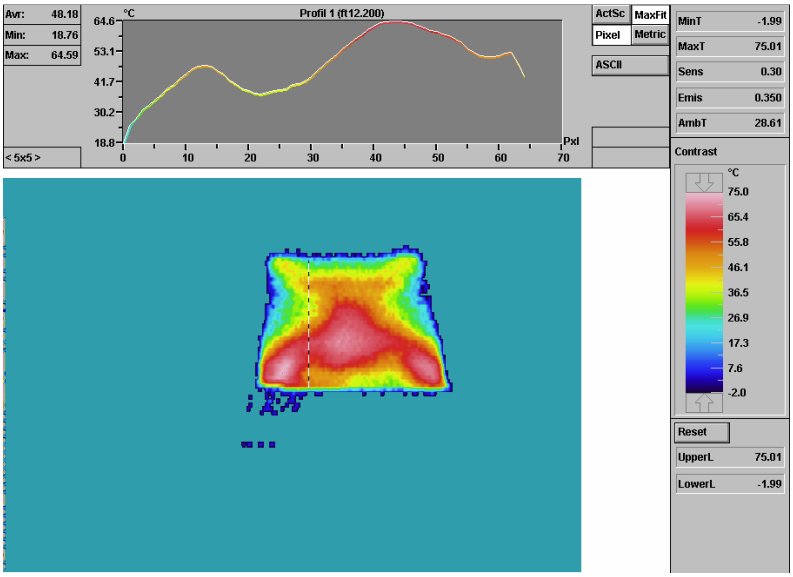

Fig. 13: Section 3-5-4 of the load: temperature distribution and graphic of the lateral line.

The following is the graph of temperature as a function of the depth of the sample:

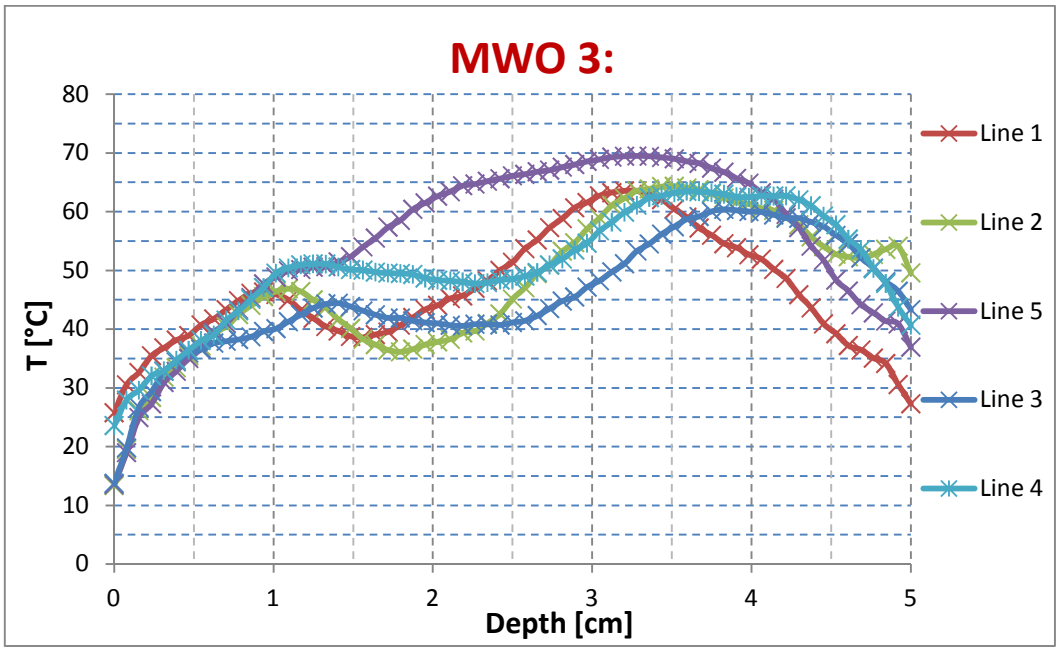

In this case the efficiency obtained in the cavity, so without considering the power "held by the magnetron" ever, is 59 %.

Looking at the chart temperature/depth, line 5, is the one who suffers most heating again (centre overheating effect). Furthermore, as seen for the case with the thermocouple, it can be noticed that a good heating uniformity in the piece.

4.5 – Comparison of experimental results

The following shows the comparison between the results from the thermocouple and that by the infrared camera.

- MWO 1:

The two lines 5 (IR= infrared camera; Tc= thermocouple) and the two lines 1 are overlapping and very similar. A little less for line 2, for the central points where there is a temperature's gap of about 10°C; this can be explained by the fact that the lines for the measurements made with the thermocouple are based on an average of many more values than those made with the infrared camera so the margin of the deviation is acceptable.

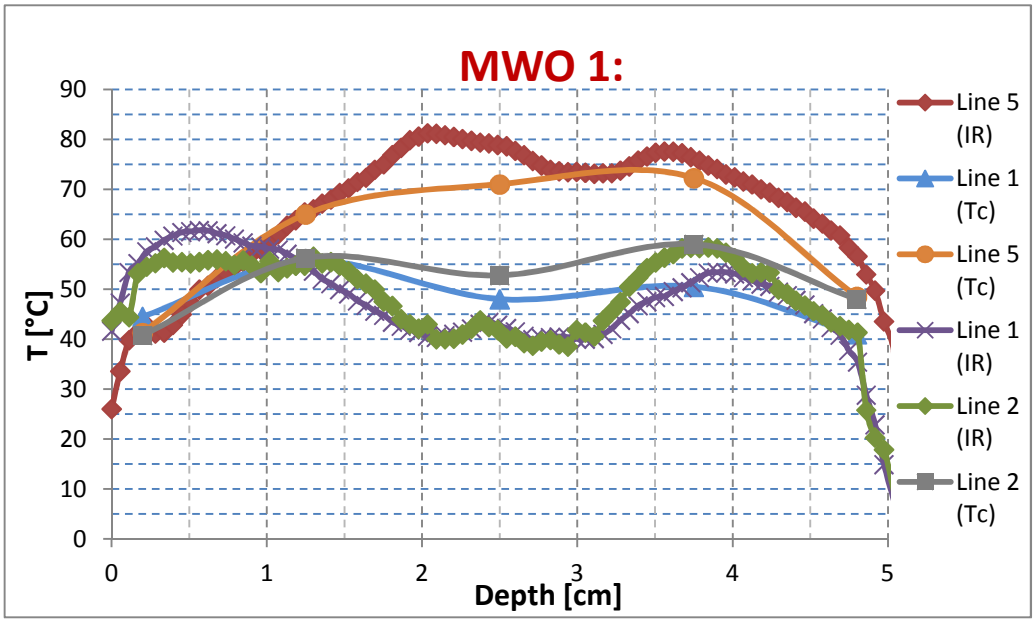

The two lines 3 (lines red and blue) are also very similar while lines 4 deviate still in the central part.

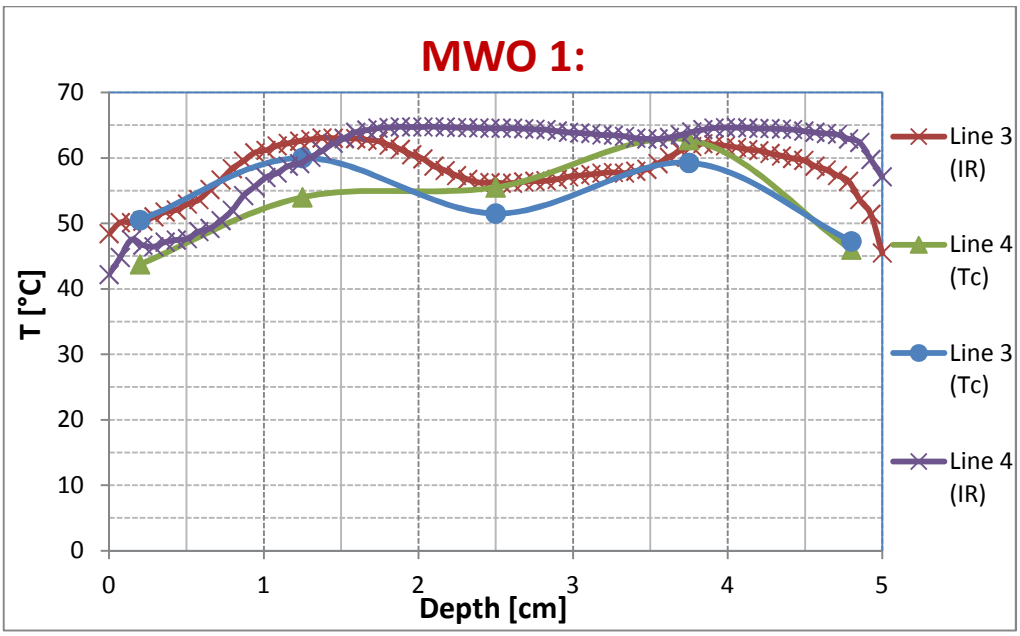

- MWO 2:

Lines 1 match virtually except for the initial values. Lines 2 differs lightly but this can be always explained by the fact that was talk before for the case of MWO 1.

Lines 5 are overlapped up to the central point after which deviate.

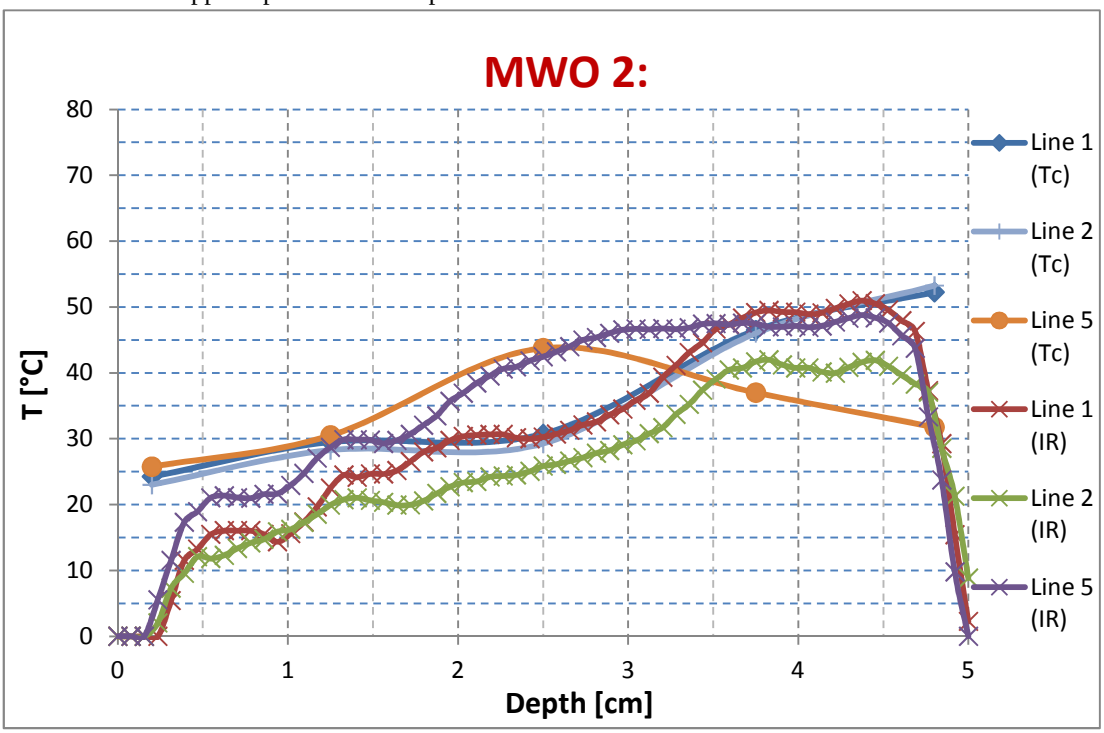

The trend for the other two side lines 3 and 4 is always the same; upper zone and cold as one approaches the plate, the sample is heated more.

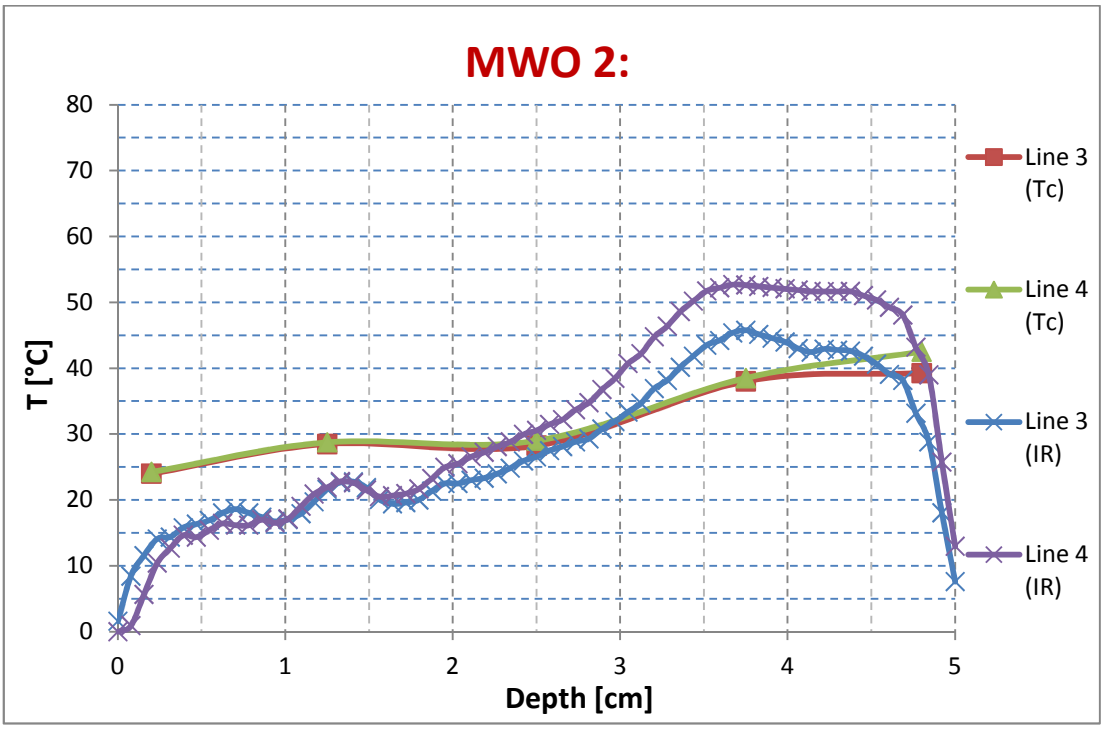

- MWO 3:

The side lines 1 and 2 are similar enough so that almost all points of discretization for the measurements with the thermocouple, coincide with those of the camera. The trend between point and point then varies but this is because the "T_c curves" are an interpolation of these points.

Lines 5 deviates a lot with a detection of the camera which shows a greater heating especially in the center of the piece.

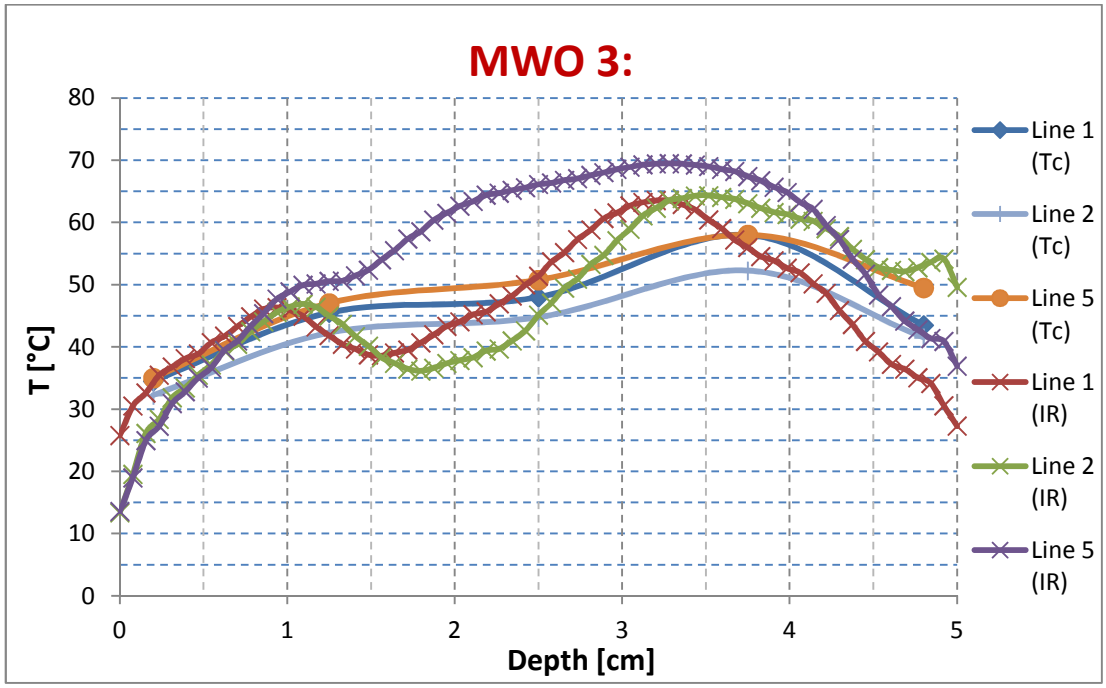

Lines 3 matching except for the final part while lines 4 are more distant.

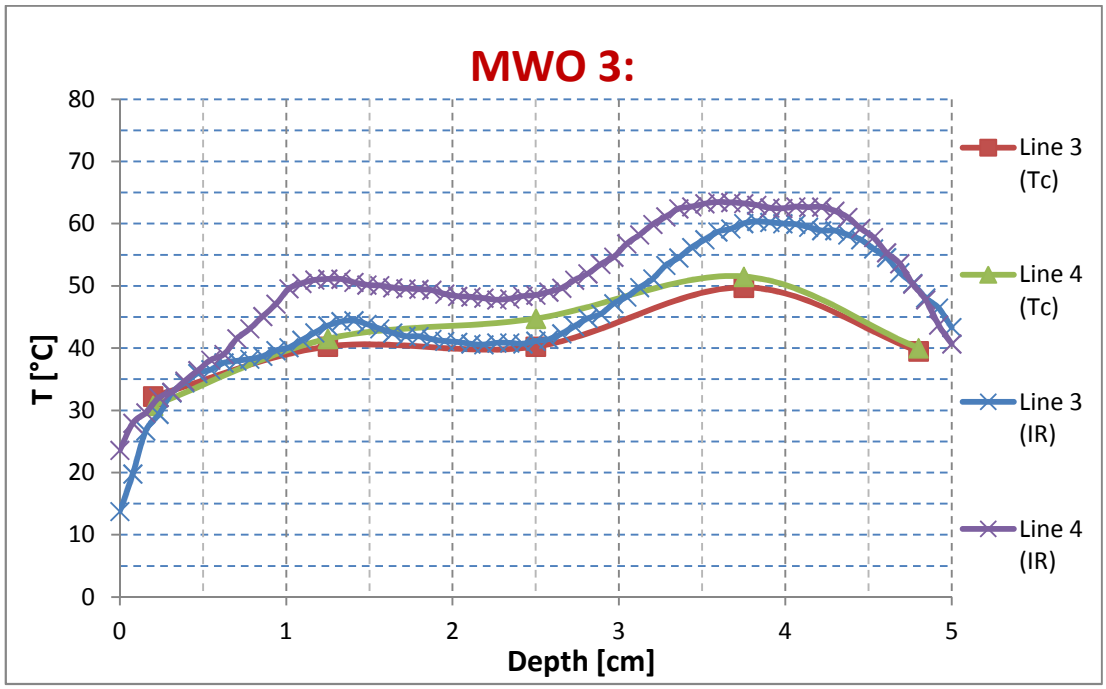

- Conclusions:

Depth[cm]	Line 1-2 [°C]	Line 5 [°C]
0,2	16-25	16-25
1,25	16-30	25-40
2,5	16-30	35-50
3,75	35-60	30-45
4,8	35-60	25-35

Table 1: Margin of error in the measurement with the thermocouple than on the infrared camera

The table above shows the temperature ranges about the hypothetical measurements detected for the case of MWO 2, looking at the images of the thermographic.

In fact, referring to the colour scale set on the thermographs, it can be noted that the values of temperature, at the depth used in the tests, vary in a range large enough in the neighborhood of the measuring point; ie the accuracy given by the camera in the reading point is greater than that obtained by thermocouple where the measurement error of the operator may have led to read a value more or less real. So this is to demonstrate that on the thermocouple temperature readings there is a margin of error due to the accuracy of the measure that may have influenced the results. Therefore can be any disagreement between the tests with the thermocouple and the ones with the infrared camera.

Furthermore, measurements with the infrared camera are related to each pixel of the frame, then normalized, and then the curves in the graphs is certainly more accurate, or better, reflects the reality more than the single interpolated points in the curves refer to measurements with the thermocouple; so in the last case you do not know the exact trend of the curves between the discretization points.

By contrast, the measurements made with the thermocouple are a large number for which the values reported in the graphs are based on an average. As the infrared camera surveys are only reported through the load in question, so it is more than probable that the values refer to measurements with the thermocouple are levelled compared to those taken by the infrared camera.

Ultimately it may be said that the ovens MWO 1 and 3 carry to a heating, of the load in question, much higher and with greater uniformity respect to the MWO 2. The latter, as already seen, it tends to heat up almost exclusively the lower part of the piece, and this leads us to affirm that this oven is probably more suited to a low load, a few centimeters in height, like a steak for example with respect to a load of 5 cm of height, as in our case.

Chapter 5

Numerical Models

5.1 – Introduction of Finite Element Method (FEM)

The Finite Element Method (FEM) is a numerical approach likely to find approximate solutions to problems described by partial differential equations by reducing them to a system of algebraic equations. The aim is to approximate the true pattern of unknown function with that of some special functions to known trends that generally are polynomial.

The main feature is the discretization of the continuous domain of the continuous domain of the departure in a discrete domain, by using mesh, trough of simple shape elements like triangles and quadrilaterals for 2D domains, and hexahedral and tetrahedral for 3D.

This step involves reducing the number of degrees of freedom, that are infinite in the continuous medium, considering only a few points, nodes, of the structure, that are therefore finite.

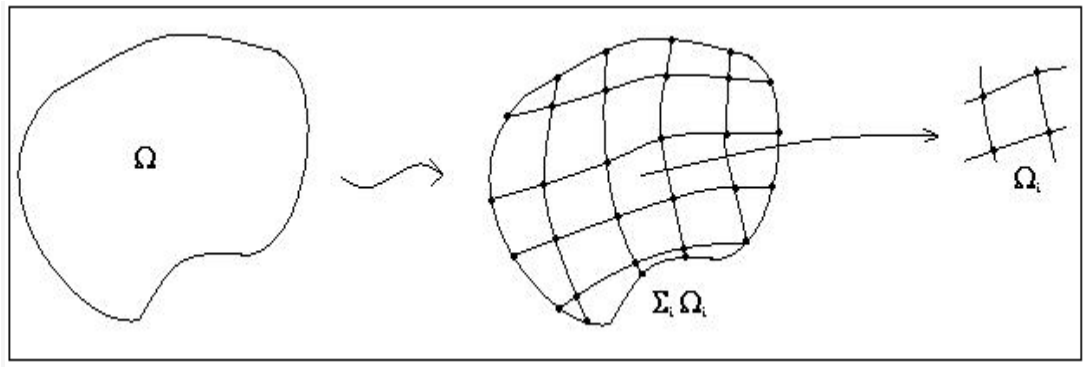

Fig. 1: Divided in subdomains.

Another characteristic is the description of the boundary conditions that define the interface between the subdomains of the model and their surroundings. Together with the initial conditions are necessary for a correct definition and resolution of the model.

5.2 – Software: COMSOL Multi-physics

COMSOL Multi-physics is a software package for modeling and simulate any type of physical process describable by PDE (partial differential equations), resolving them through appropriate solvers. The strength of COMSOL, compared to other software, is the presence of numerous modules corresponding to various physical phenomena that can be combined. The module on phenomena in radio frequency, RF, is based on the classic Maxwell's equations and enables to model and simulate electromagnetic waves. Examples of applications can successfully simulate and design include waveguides, antennas and transmission lines as well as multi-physic applications such as microwave heating devices.

The following are the main steps for the elaboration of one of these problems using the software COMSOL Multi-physics.

Modelling Instruction

Model Wizard

1) Go to the **Model Wizard** window.

2) In **Add physic** tree, select **Heat Transfer>Electromagnetic Heating>Microwave Heating.**

3) In the **Studies** tree, select **Preset Studies>Frequency-Transient.**

Global definition

First, define a set of parameter for creating the geometry.

1) In the **Model Builder** window, right click **Global Definitions** and choose **Parameters**.

2) Go to the **Settings** window for Parameters.

3) Locate the **Parameters** section. In the **Parameters** table, enter the data like the example.

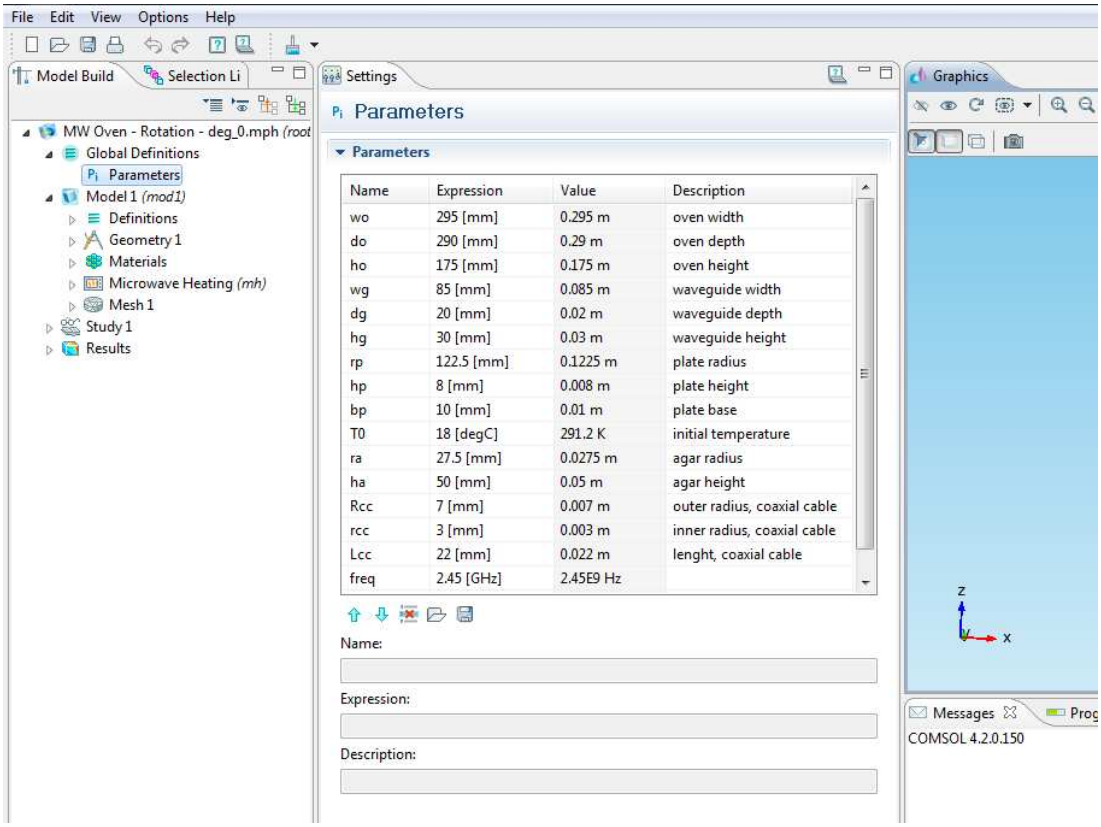

Fig. 2: Parameters table.

Geometry

1) In the **Model Builder** window, right click **Model 1>Geometry 1**

3) Chose **block** to create the oven cavity or the waveguide;

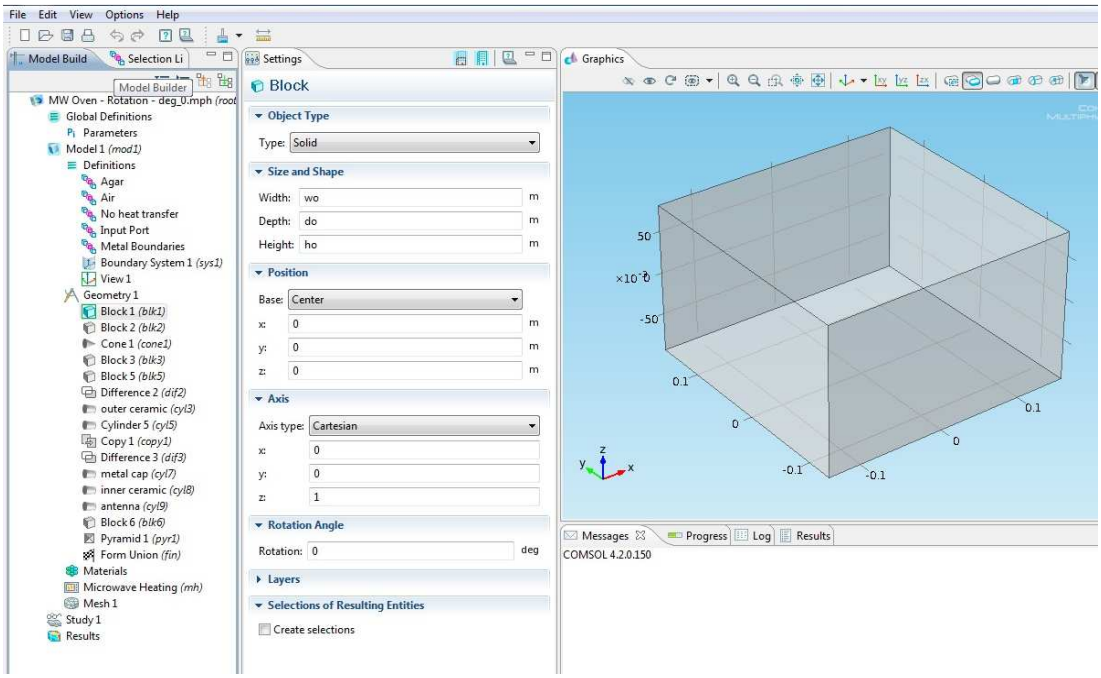

Fig. 3: Block that simulate the oven cavity.

2) Chose **cylinder** to create the turntable;

3) Finally you chose the shape of the load according to the treated case.

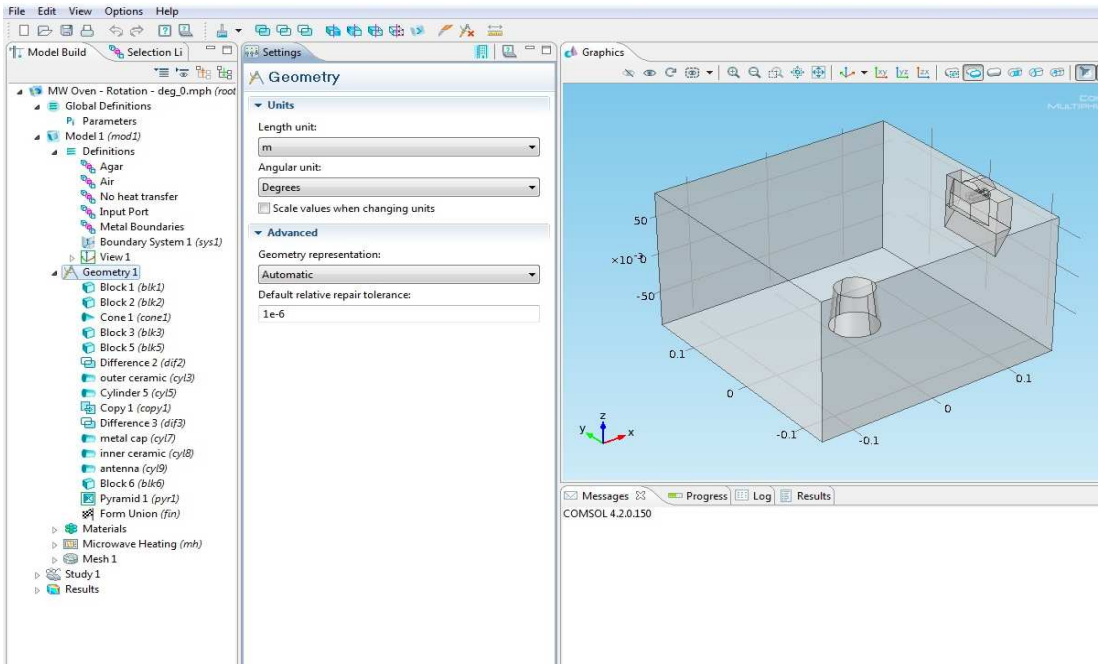

Fig. 4: Finally geometry of the microwave oven.

Definitions

Create the following selections definitions in order to make Domain and Boundary selections easier as you walk through these model instructions.

1) In the **Model Builder** window, right click **Model 1>Definitions** and chose **Selections>Explicit**.

2) Right click **Explicit 1** and chose **Rename**.

3) Go to the **Rename Explicit** dialog box and type the name of the load, for example Agar, in the **New name** edit field.

4) Then select the Domain interesting the load.

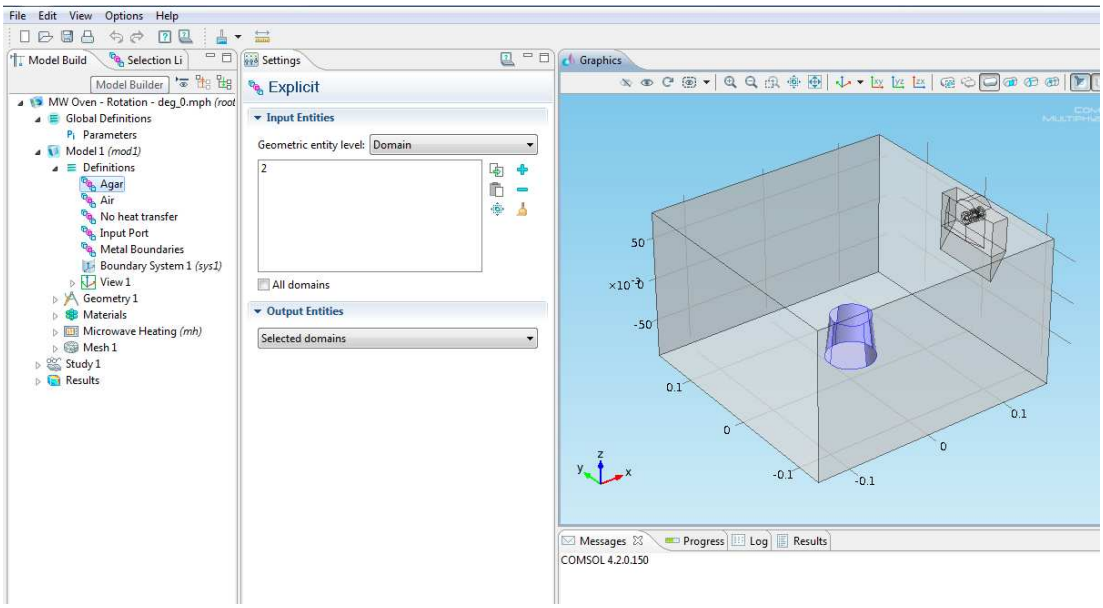

Fig. 5: Definition of the explicit: in particular, in this case, about the load.

Now you have to do the same operations to define the other features like the plate, the air, the port boundary, the metal boundaries etc..

Materials

Next, define the materials. You can already find some defined materials in the Material Library like Air or Copper for example.

1) In the **Model Builder** window right click **Model 1>Materials** and chose **Open Material Browser**.

2) Locate the **Materials** section, select **Built In>Air** (for example) and then right click and choose **Add Material to Model**.

3) After this in the **Model Builder** window, click **Air**, go to **Settings** window for **Material** and locate the **Geometry Entity Selection**. From the **Selection** list, select **Air**.

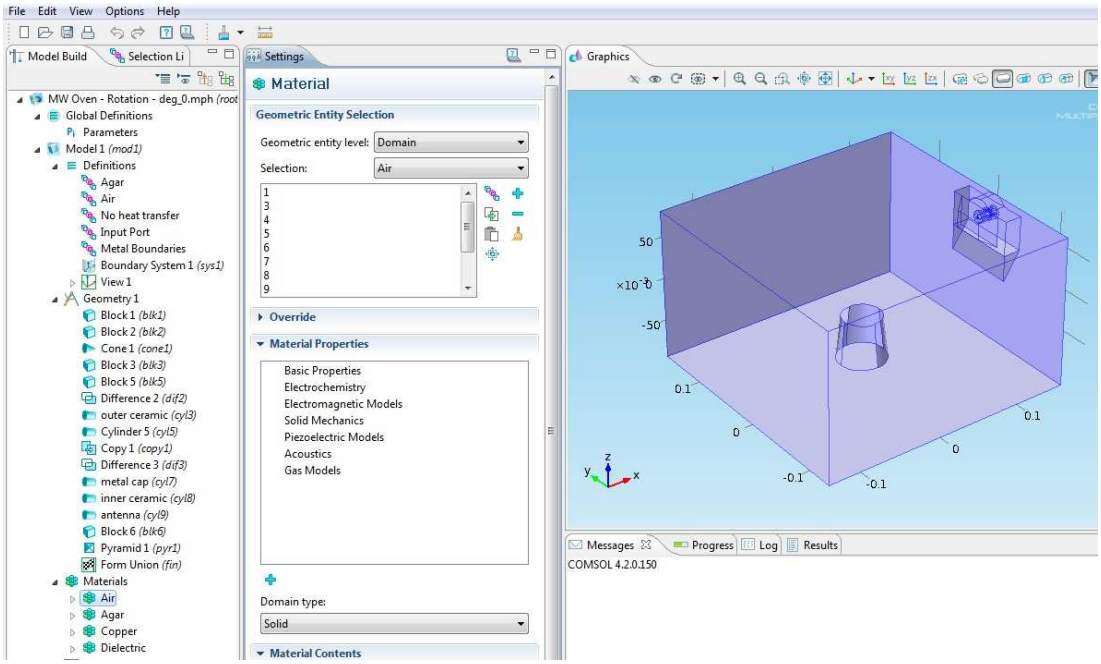

Fig. 6: Setting the material like air.

4) For a new material, in the **Model Builder** window, right click **Materials** and at this time chose **Material**. Right click **Material 2**, chose **Rename** and type the name of the load, like Agar, in the **New name** edit field.

5) Go to **Settings** window for Material and locate the **Geometry Entity Selection** section. From the **Selection** list, select Agar. Locate the **Material Contents** section and in the **Material Contents** table enter the features of the load like the electric conductivity, the relative permittivity or relative permeability etc..

Do the same operations to define the other materials like the copper for the metal boundaries or the glass for the plate etc..

Microwave Heating

It's now time to set up the physic. In this section you have to fix the Domain and Boundary conditions selecting the defined features above on Definitions.

1) In the **Model Builder** window, right click **Microwave Heating** and chose boundary condition **Electromagnetic Wave >Port**.

2) Locate the **Boundary Selection** section and from the **Selection** list select **Port Boundary**. Locate the **Port Properties** and in P_{in} edit field type the value of the power. Also specific the E_0 vector and the propagation constant for the first propagating mode β. If the type of port is coaxial, like in our case, only edit in P_{in} the value of the power.

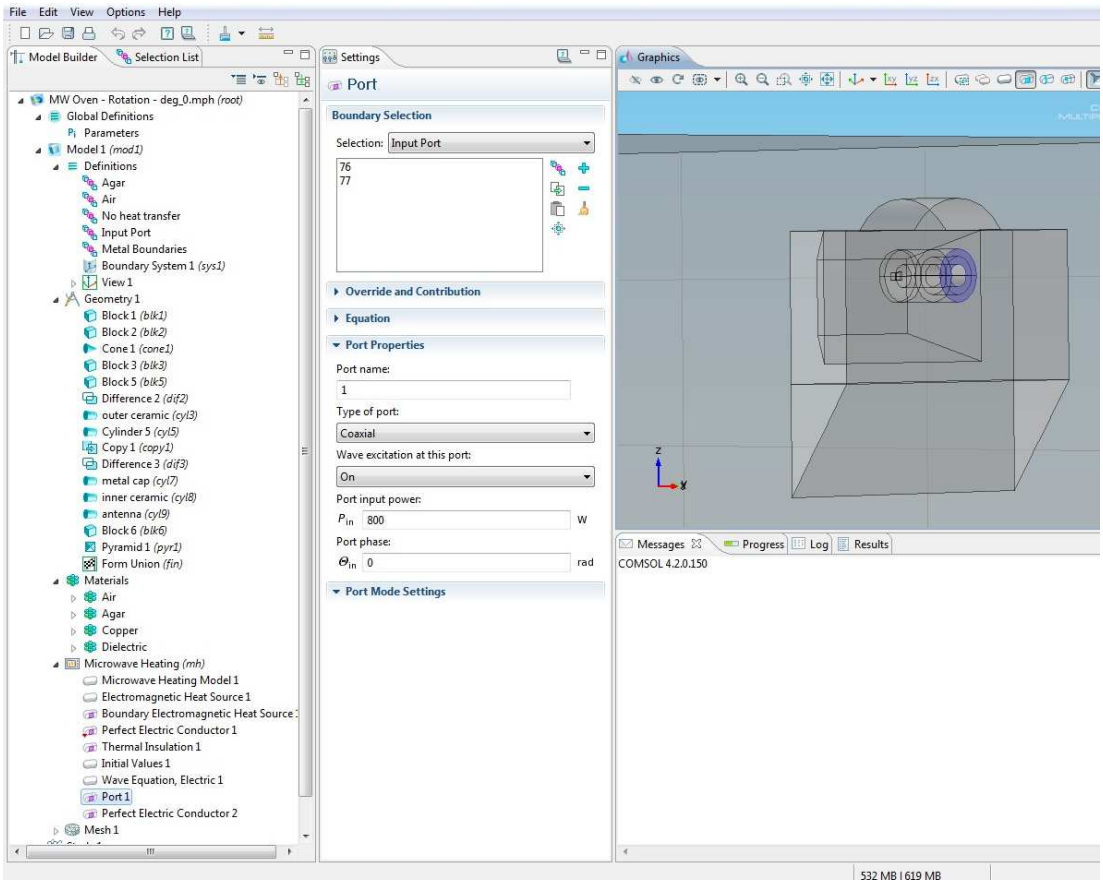

Fig. 7: Fixing the boundary condition, for example, about the port.

Next set up the remaining boundary conditions like the Perfect electric conductor and the Initial Values like the initial temperature of the load.

Mesh

In order to ensure convergence and get an accurate result, the mesh in this model is required to everywhere resolve the wavelength.

1) In the **Model Builder** window, right click **Model 1>Mesh 1** and chose **Free Tetrahedral**. Right click **Free Tetrahedral** 1 and chose **Size**. From **Geometry Entity Level** list select **Domain**. From the **Selection** list select Agar .

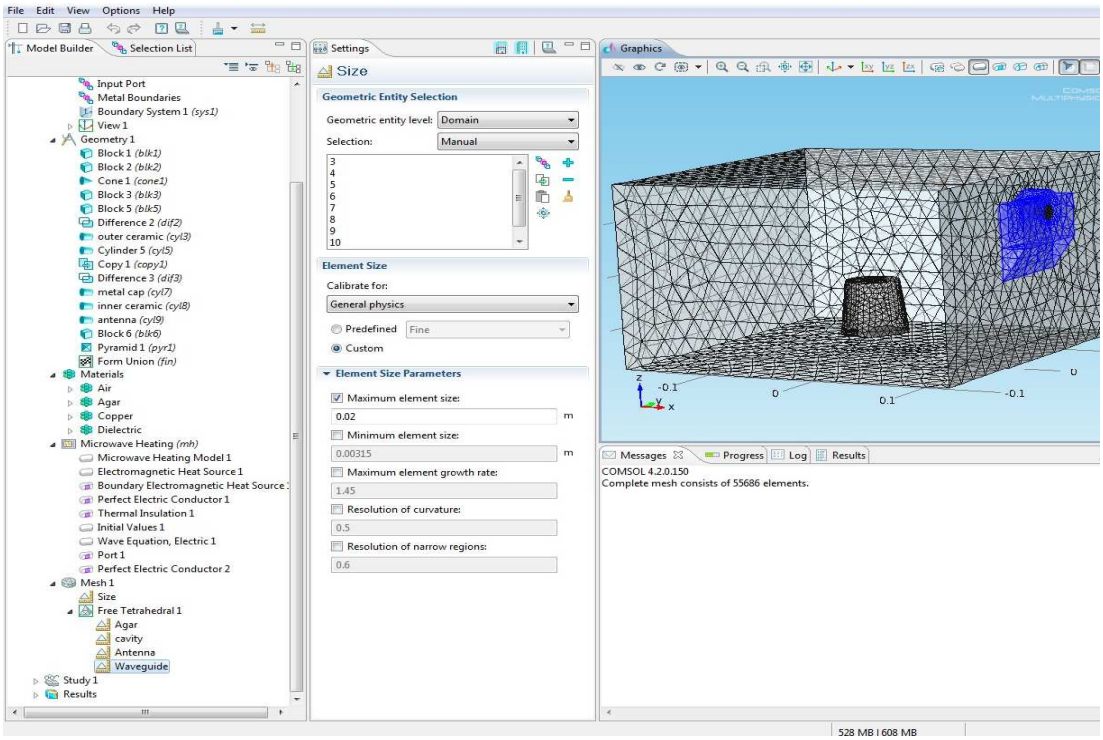

Fig. 8: Chose the appropriate mesh that can be predefined or customized according to the requirement.

2) Locate the **Element Size** section. From **Predefined** list select the type of accuracy like finer or extremely finer for a better result. Finally click the **Build All** button to check the mesh.

Study

1) In the **Model Builder** window, click **Study 1>Step 1**: **Frequency-Transient**. Go to **Settings** window and locate the study **Settings** section. In the **Times** edit field, type the range related to your case for example (0,1,30). This will give you output at every second from t=0 to t=30 s.

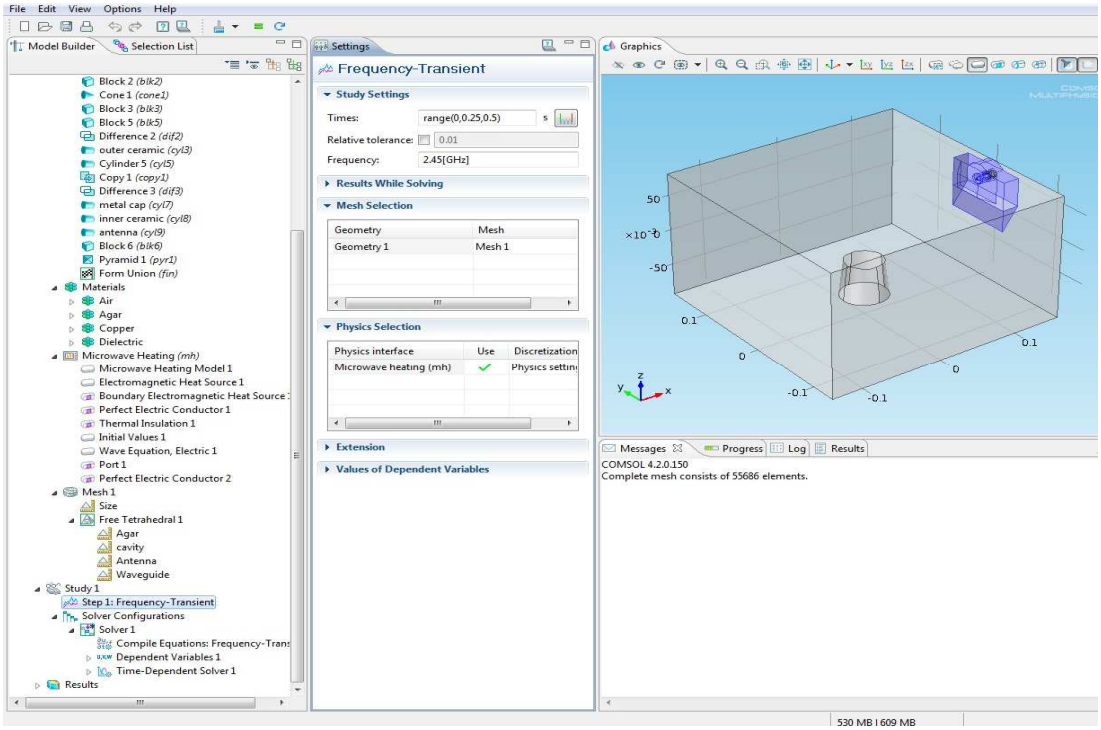

Fig. 9: The final step regarding the study settings to start the analysis.

2) In the **Frequency** edit field, type 2.45 GHz.

3) Finally in the **Model Builder** window, right click **Study 1** and chose **Compute** to starting the process.

Results

The Graphics window shows the temperature distribution on the surface of your load, for example the Agar sample, after the time you had set, like 30 sec in the case above.

Now you can do the considerations of the case and compare the results obtained with the software, with the experimental ones

5.3 – Simulation Results

First of all was set the problem using the software COMSOL Multi-physics or, as in the example explained before, it is built geometry of the oven in question, with the real dimensions previously measured (including the cavity, the waveguide, and antenna of the magnetron). Subsequently were placed the boundary conditions, ie, was considered the condition of perfect electric conductor (PEC) for metal and copper and air as the remaining domain; as regards the antenna was done with the configuration of the type figure 10. That is, is taken into account in the final part of the magnetron (the one that enters in the guide) maintaining a configuration as can be approximated to the real one (coaxial cable). In fact there is a hollow internally, that is none other than the final part of the coil which picks up the high-frequency wave; while externally there is a metal cap and a ceramic cap, from which radiates the field.

The last condition is that relating to the definition of the port so that simulates the effect of the field. This has been applied on the outer face relative to the coaxial cable in the direction orthogonal, therefore, to the input waveguide. The final part includes the study of the problem or, in our case, has been done before a frequency domain to analyze the distribution of the field at different frequencies (in the range of use ie 2.4-2.5 GHz) and then the real study with a frequency transient. All this, of course, with the Microwave Heating module that combines the study of the electromagnetic to the heat transfer.

To validate then, as accurately as possible, the test results obtained experimentally, was simulated, the time taken to perform the measurement that corresponds to an initial cooling. This means to make a study, with the duration of 10-15 seconds, by means of a heat transfer in solid with a so-called convective cooling; then set the value of coefficient of heat exchange, 7 $W/m^2 \cdot K$, and the ambient temperature, we have proceeded with a time dependent study.

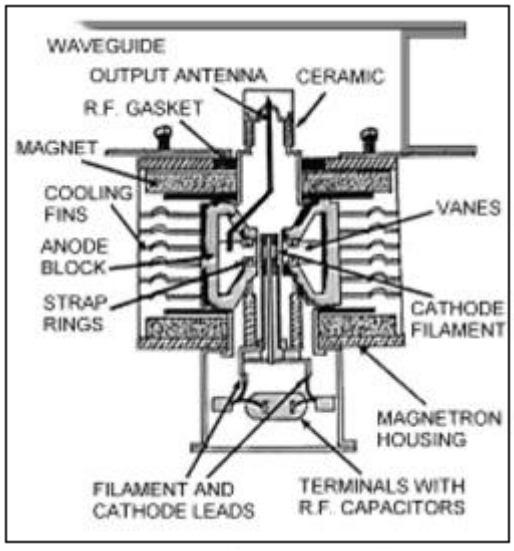

Fig. 10: Configuration of the antenna of magnetron.

After setting the problem using the software, was carried out with the execution of the instructions of the code, using the Matlab language, it could, by interfacing with COMSOL, to make the rotation of the turntable, not covered by the same.

The block diagram below represent the instructions used by the code for the simulation, and eventual validation, of the experimental tests. First have been inserted the inputs of the program: simulation time, the speed of rotation of the plate and the angle step. Starting from an initial temperature of the load it was set to a cycle that update the angle of rotation relative to the number of simulations per revolution, of the plate, for the overall duration, ie by the number of revolutions to be simulated. Everything through the description of the known mathematical laws of rotation. Then ultimately there is the heating from the initial temperature to that relating to the next step until the end of the process. This means COMSOL interfaced with live links of Matlab so the same software fetches updates with its new temperature rotated by the angle in question, and proceeds with the next step of heating.

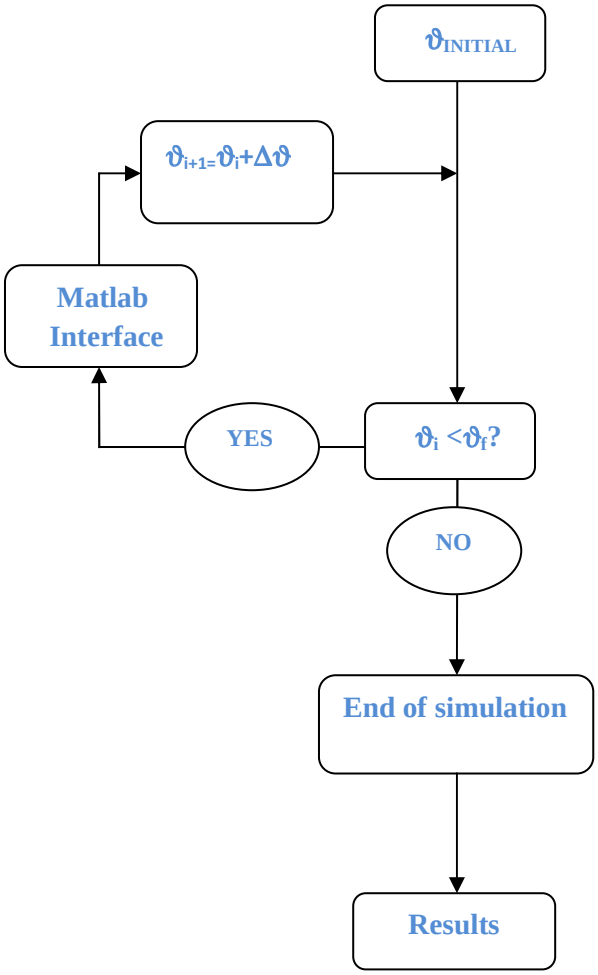

The following are the result obtained by the numerical model COMSOL Multi-physics interfaced with Matlab for the validation of the experimental test of each MWO.

- MWO 1:

COMSOL Multi-physics is a good software because it can carry out different studies in an individual problem. For which, before performing the final study (the so-called frequency-transient), an analysis was made in the frequency domain; ie it was investigated the different behavior of the load at different frequencies. In particular as regards the distribution of the field and the power absorbed by the load. So we proceeded to a parametric sweep in the frequency range between 2.4 GHz and 2.5 GHz with a certain step (fig. 24).

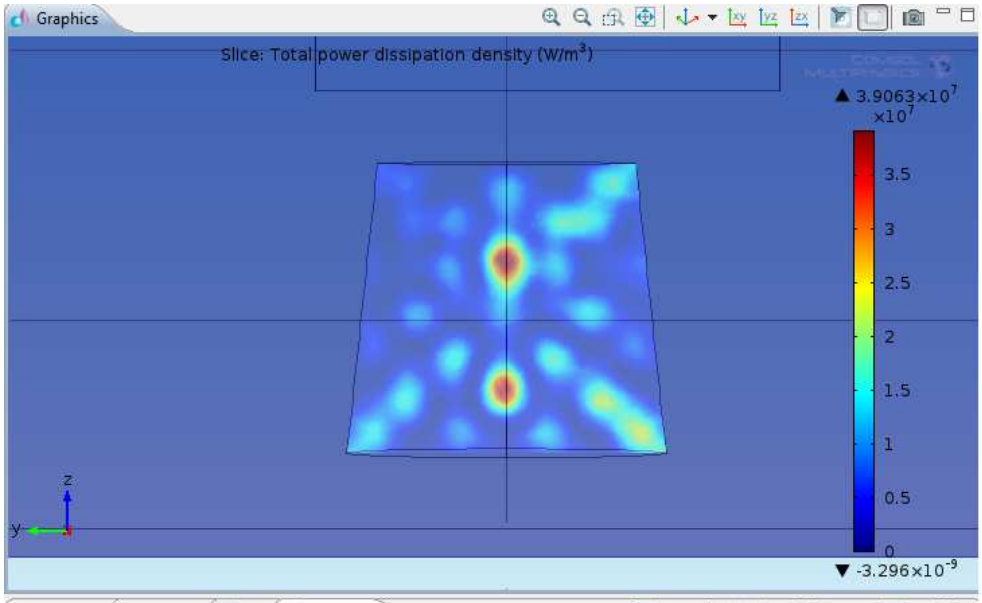

Messages | Progress | Log | Results

freq	Total power dissipation density (W)
2.405e9	161.44773
2.41e9	170.55838
2.415e9	184.29102
2.42e9	205.47029
2.425e9	237.20359
2.43e9	282.75296
2.435e9	343.14558
2.44e9	397.76879
2.445e9	416.91729
2.45e9	463.36462
2.455e9	457.37281
2.46e9	413.55392
2.465e9	360.93988
2.47e9	312.57289
2.475e9	277.07257
2.48e9	254.08602
2.485e9	242.05841
2.49e9	239.58123
2.495e9	245.39557
2.5e9	258.83742

Fig. 11: Frequency domain study for MWO 1: field distribution and values of power absorbed for different frequencies.

The result obtained are reported in the graph below; so for a frequency step of 5 MHz it have different power absorbed and so different efficiency. Moreover also the field's distribution varies for different frequency. So for this case is chosen to set the frequency of 2.45 GHz which corresponds to a power absorbed by the load equal to 463 W, that is the value that is closest to the experimental test. In fact this value corresponds to an efficiency of:

$$\eta_{cavity} = \frac{Q_{absorbed}}{Q_{useful}} = \frac{463}{800} = 0.57$$

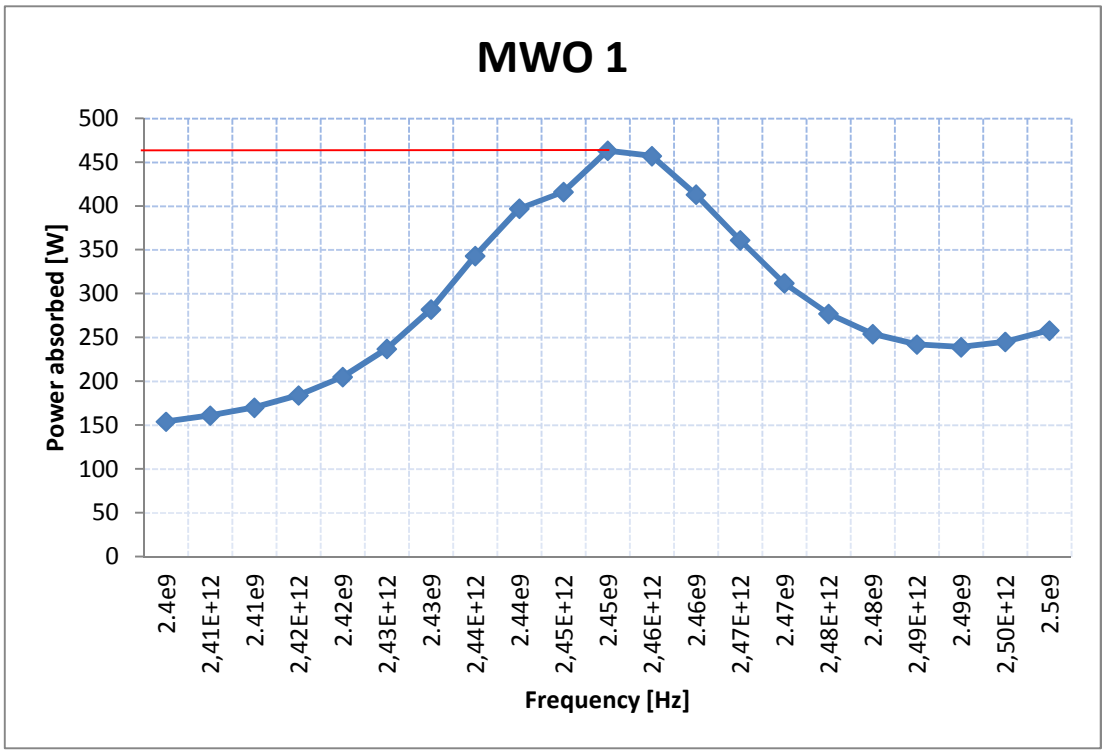

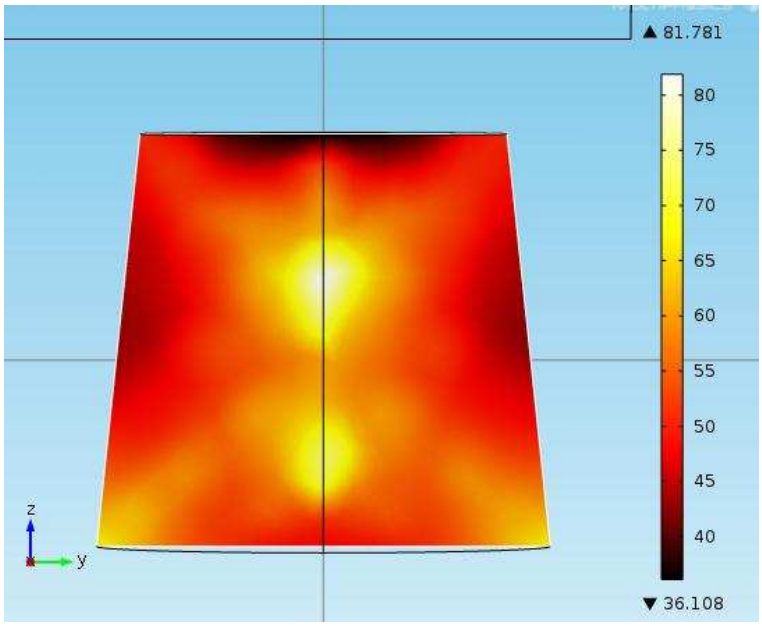

Fig. 12: Temperature distribution of section 1-5-2 of the load after 30 seconds for MWO 1.

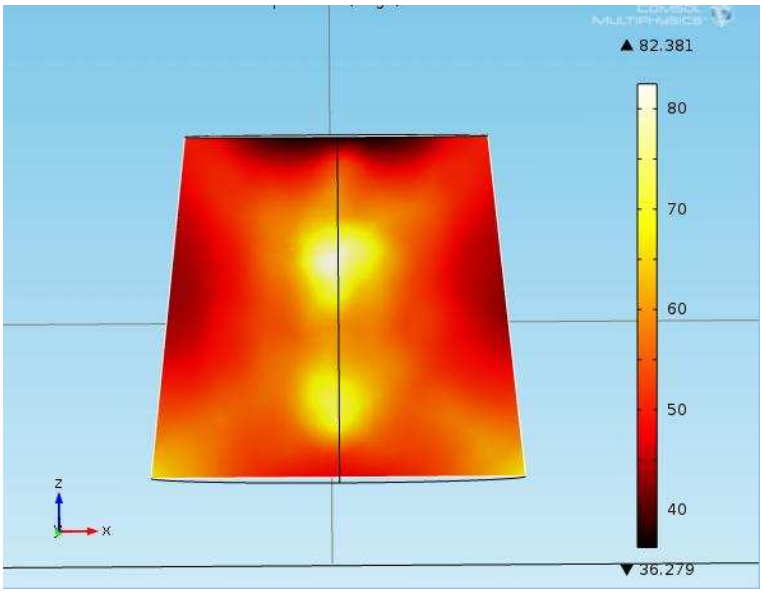

Fig. 13: Temperature distribution of section 3-5-4 of the load after 30 seconds for MWO 1.

The images above show the section 1-5-2 and 3-5-4 of the heated load, after 30 seconds of heating, for MWO 1. The two sections are very close each other and the temperature distribution is similar to a "X"; in fact the most heated parts are the edges and two points along the center line. The first get a temperature between 50°C and 60°C while the hot spots reach a peak of 80°C.

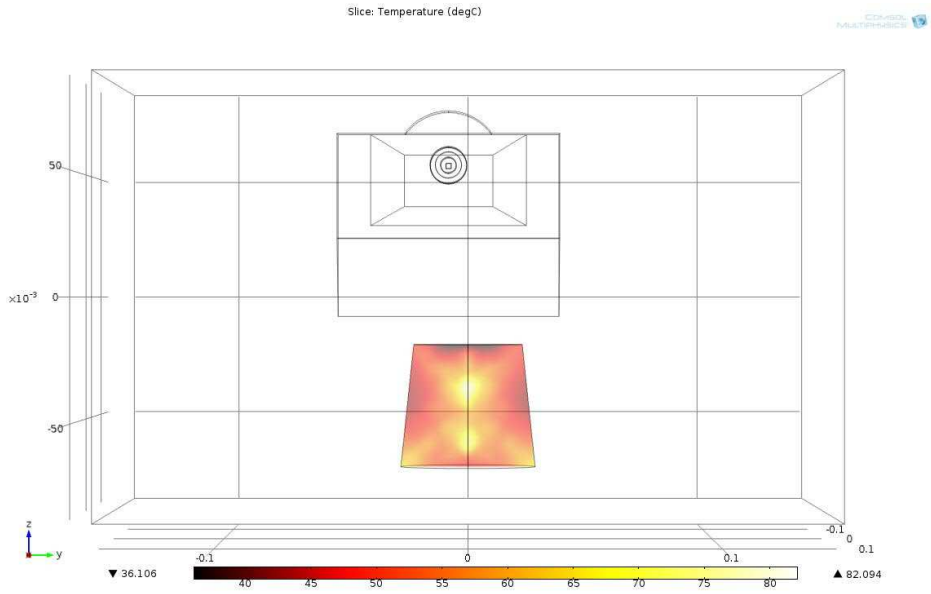

Fig. 14: Lateral view of MWO 1 with the heated load.

Finally has been simulated, the time taken to perform the measurement. Then through a heat transfer in solid was possible to simulate, with a convective cooling, for the duration relative to the measure, that is 15 seconds, the initial cooling of the workpiece.

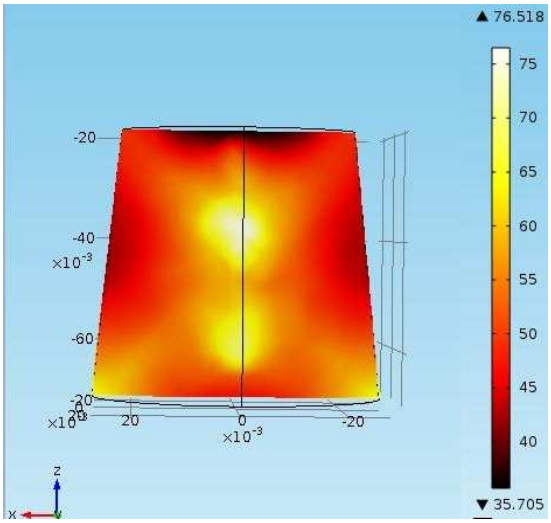

Fig. 15: Final temperature distribution of section 1-5-2.

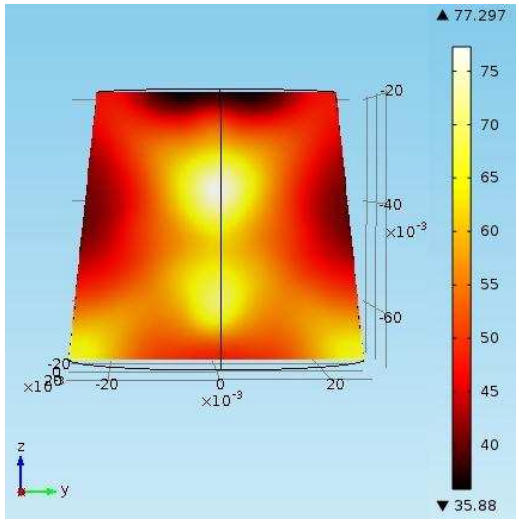

Fig. 16: Final temperature distribution of section 3-5-4.

Then compared to the end of heating, with the simulation inherent cooling we have that the distribution of temperature change a little, or better, conforms slightly; also as can be seen from the temperature detection in the figure 15-16, always relating to the two sections, there is a decrease in the order of 5-6°C, in fact the two peaks are 76°C and 77°C against 81°C and 82°C comparative to the end of the heating.

The following is the graph of temperature as a function of the depth of the sample with the data extract, after the study, from the software:

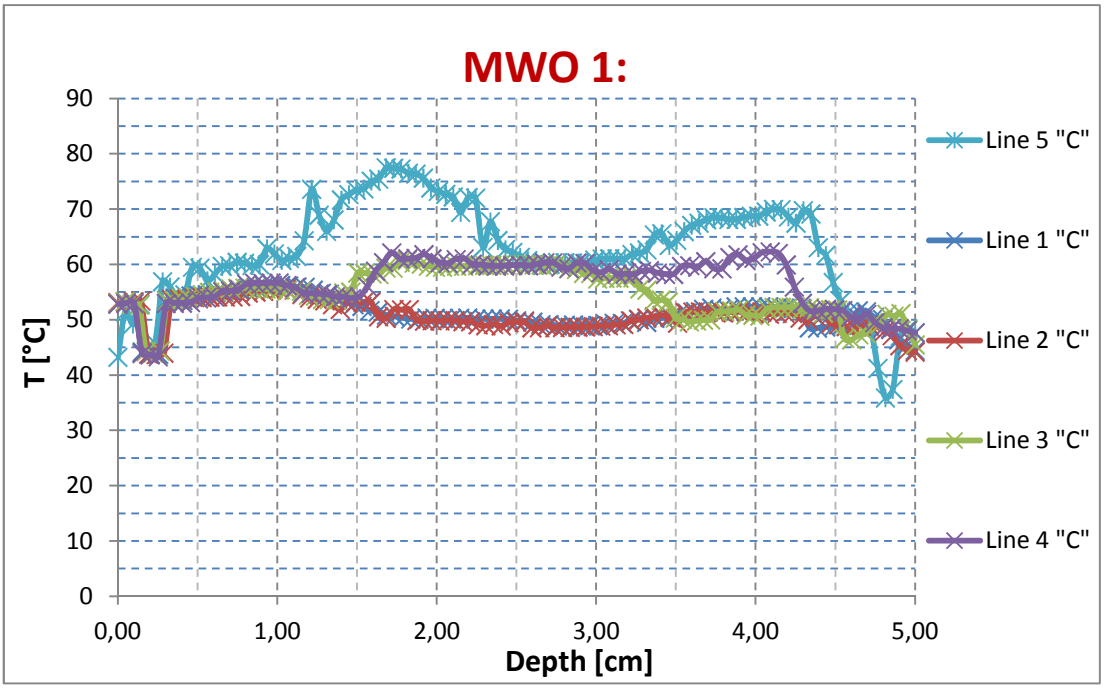

As can be seen from the graph line 5 is the one where it has the greater heating of the piece; in particular are noticed the two hot spots, one in the neighborhood of 2 cm in depth (of about 80°C) and the other around the 4 cm in depth (where it reaches about 70°C). It also denotes a neat symmetry of values respectively between the lines of the relevant sections, ie the lines 1-2 and lines 3-4.

- MWO 3:

Also in this case, before studying the final process, an analysis was made to know the distribution of the preliminary field, with the corresponding value at different frequencies and the power absorbed in the respective cases.

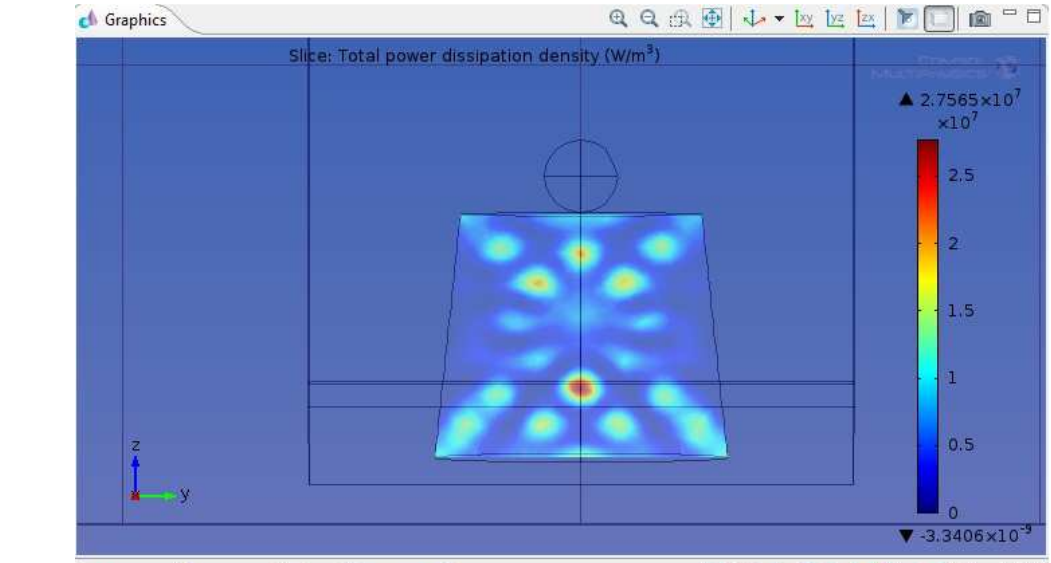

Messages | Progress | Log | Results

freq	Total power dissipation density (W)
2.426e9	261.10687
2.4265e9	302.89026
2.427e9	348.43482
2.4275e9	396.45655
2.428e9	445.29524
2.4285e9	493.42436
2.429e9	540.02669
2.4295e9	585.06002
2.43e9	628.80459
2.4305e9	671.33809
2.431e9	712.24619
2.4315e9	750.58496
2.432e9	785.00839
2.4325e9	813.99832
2.433e9	836.15947
2.4335e9	850.52872
2.434e9	856.80828
2.4345e9	855.3361
2.435e9	849.04354
2.4355e9	837.38678
2.436e9	821.72482
2.4365e9	804.14772

Fig. 17: Frequency domain study for MWO 3: field distribution and values of power absorbed for different frequencies.

The result obtained in the frequency domain for this case are in the graph below; so for a frequency step of 0.5 MHz, for a better precision, it have, also at this time, different power absorbed and so different efficiency too. Therefore it was set the frequency of 2.4285 GHz which corresponds to a power absorbed by the load equal to 493 W, that is the value that is closest to the experimental test. So the efficiency results:

$$\eta_{cavity} = \frac{Q_{absorbed}}{Q_{useful}} = \frac{493}{950} = 0.52$$

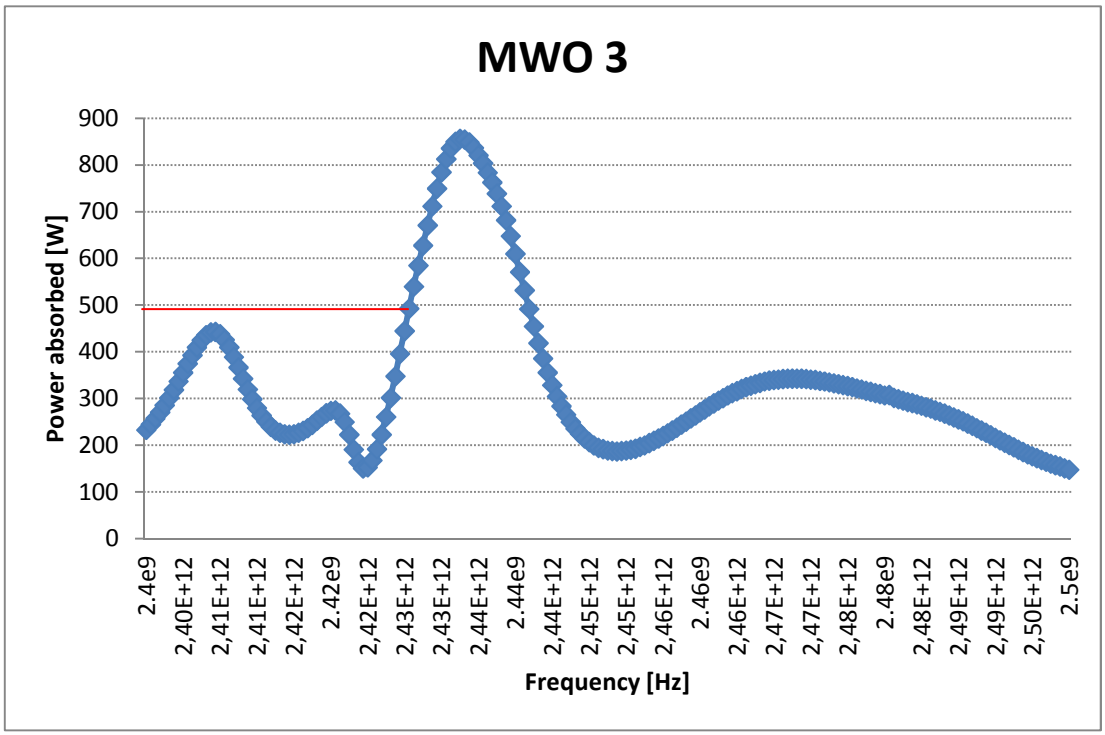

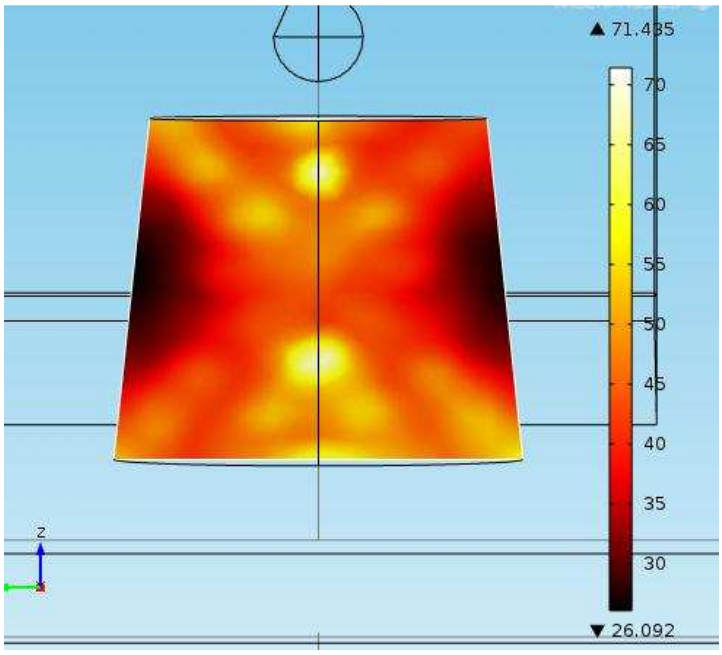

Fig. 18: Temperature distribution of section 1-5-2 of the load after 20 seconds for MWO 3.

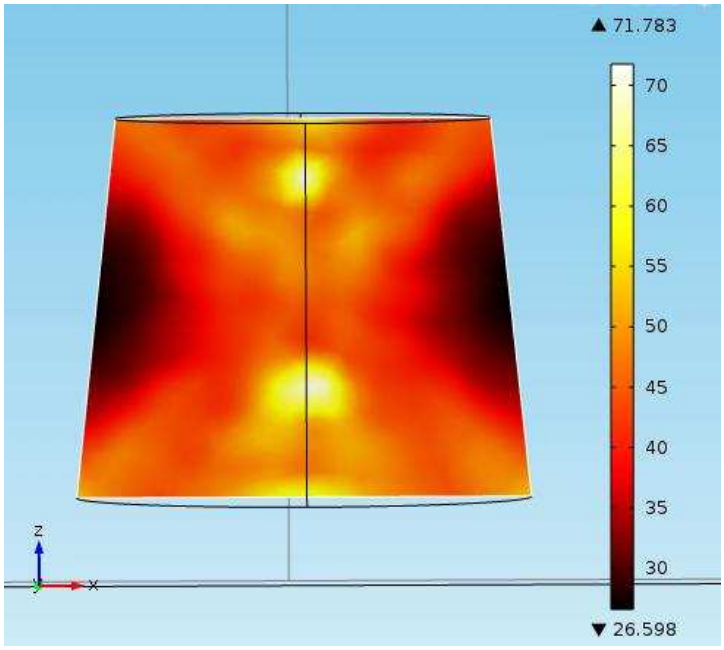

Fig. 19: Temperature distribution of section 3-5-4 of the load after 20 seconds for MWO 3.

For MWO 3 we have a similar temperature distribution of MWO 1 that represent again a “X”; a hot spot on the top and once on the bottom are the most heated points where it reaches 70°C.

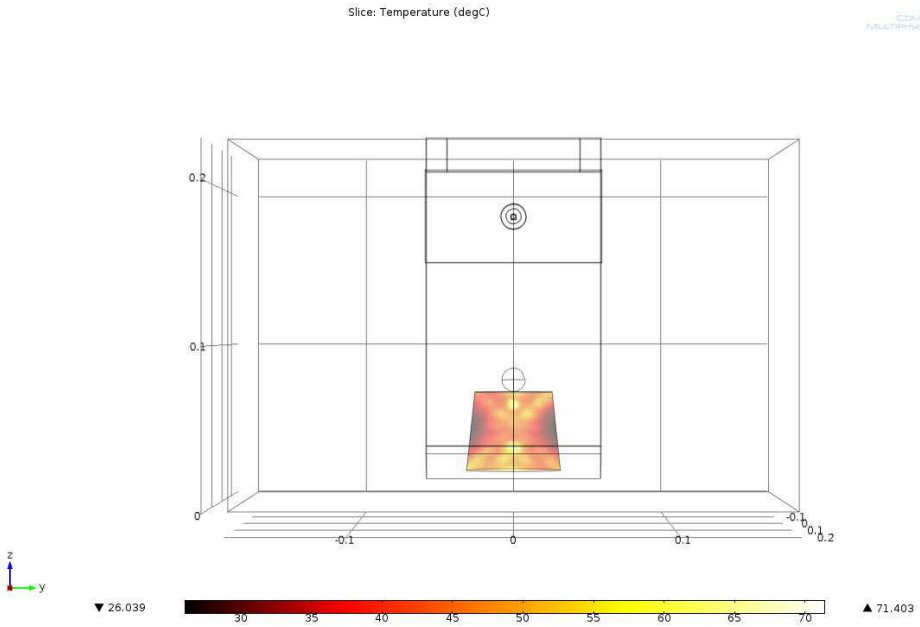

Fig. 20: Lateral view of MWO 3 with the heated load.

Also for MWO 3 has been simulated, finally, the time taken to perform the measurement. So through a heat transfer in solid was possible to simulate with a convective cooling, for the duration relative to the measure, that is 15 seconds, the initial cooling of the sample.

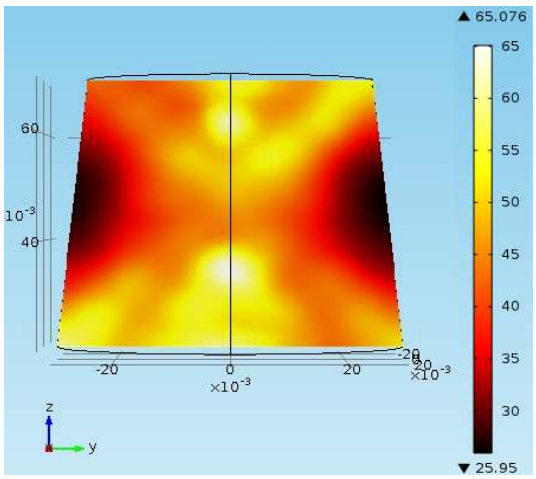

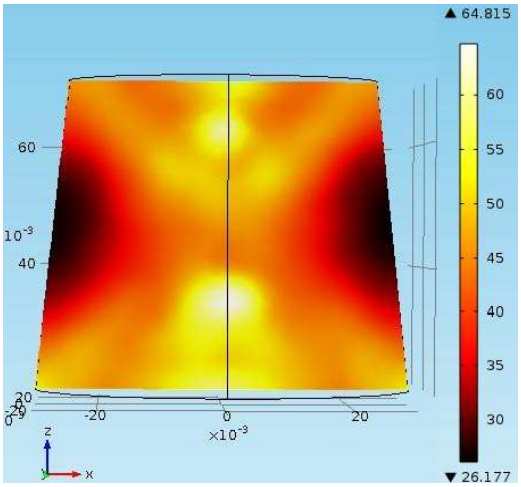

Fig. 21: Final temperature distribution of section 1-5-2. **Fig. 22:** Final temperature distribution of section 3-5-4.

Thus also in this case with the simulation on the convection cooling there is a decrease in temperature of a few Celsius degrees, so that the hot spots fall from 71°C to 65°C approximately.

- MWO 2:

The case on the MWO 2 was more complex to deal with. In fact the results are not satisfactory. The study on the frequency domain shows (see graph below) that the trend of power consumption as a function of frequency is very variable. Furthermore, compared with 2 cases seen previously, the preliminary calculation, leads to a distribution of the field, within the piece, which, as we shall see in the conclusions, does not reflect the reality.

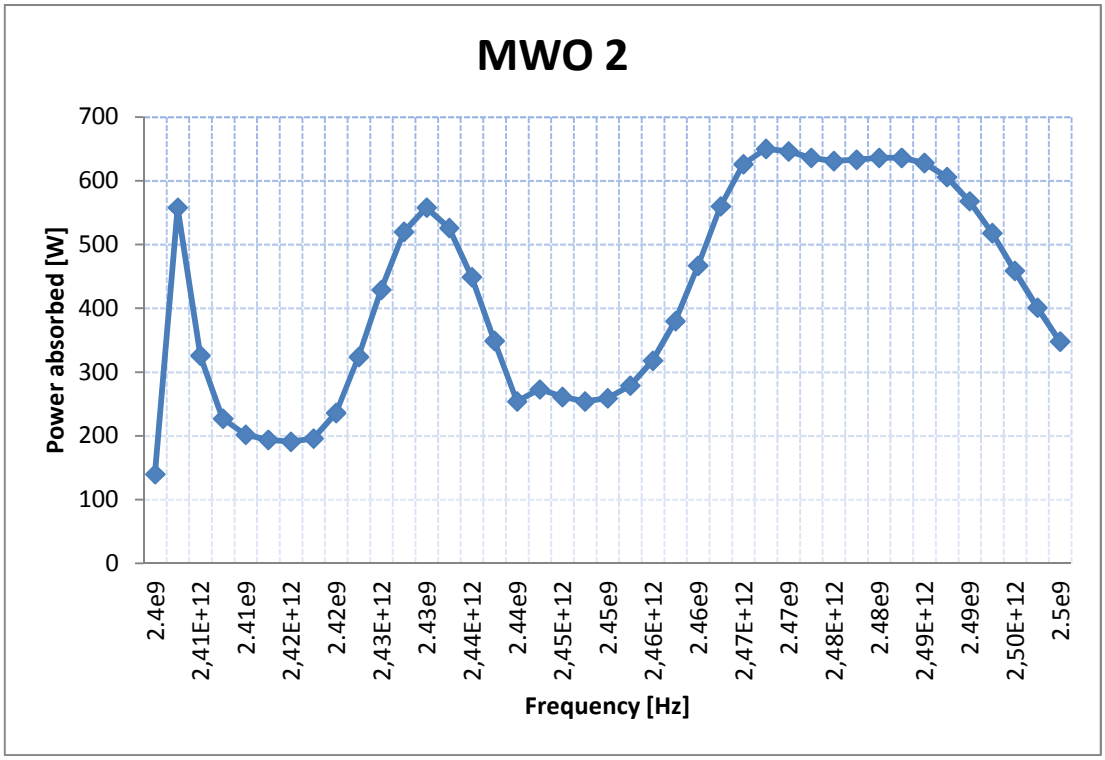

As can be seen from the graph there is a trend of the power absorbed as a function of the frequency highly variable even compared to the previous cases. Following are some field distributions related to certain frequencies to point out the diversity of their cases:

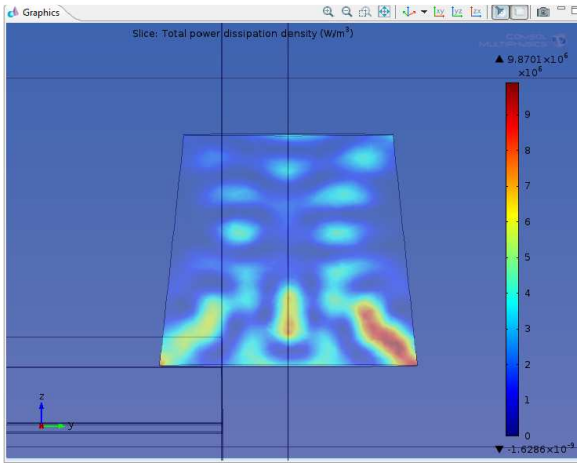

Fig. 23: Field distribution at 2.4 GHz.

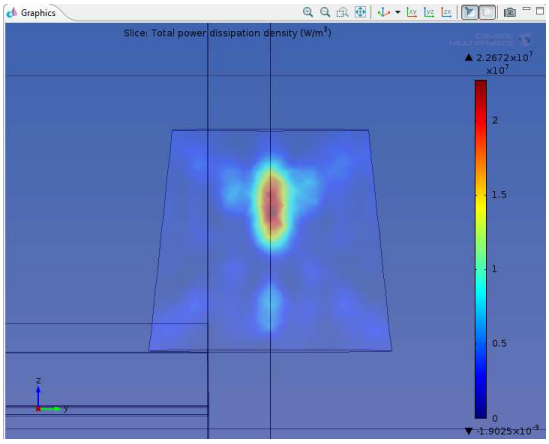

Fig. 24: Field distribution at 2.41 GHz.

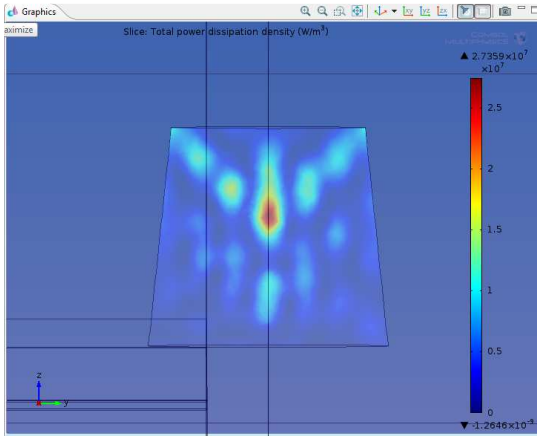

Fig. 25: Field distribution at 2.45 GHz.

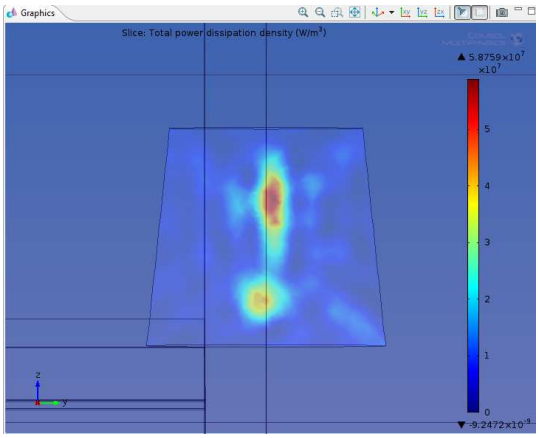

Fig. 26: Field distribution at 2.47 GHz.

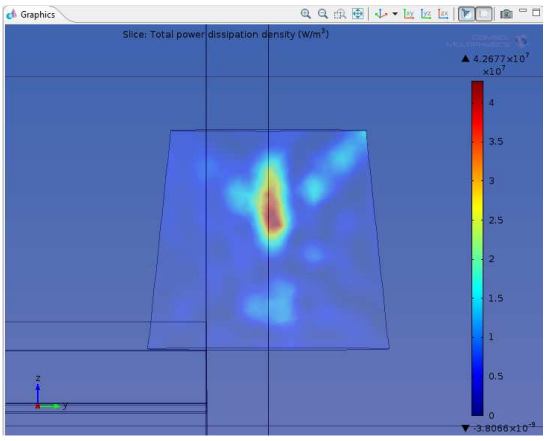

Fig. 27: Field distribution at 2.5 GHz.

So it was not chosen to complete the simulation, including the heating load for 20 seconds, by turning the turntable, but to explain the problems encountered relating to the case:

- First, there is to say that both as regards the MWO 2 and 3 will have the MWO two waveguides. So this is certainly to influence the field distribution that is random, ie there is no way to understand the field wisely prefer to leave a gap over the other.
- The geometry of the MWO 2 is very particular with respect to a traditional oven (see figure 28): the cavity has a semi-cylindrical shape which affects certainly on the type of reflection which takes place inside it. Also the waveguide with the corresponding input of the antenna is singular. In fact, the magnetron is disposed at the bottom of the oven. All that far removed from such a simple configuration MWO 1, where it has an antenna placed on the lateral side of the guide placed in the oven and with a single outlet for the "leakage" of the field.

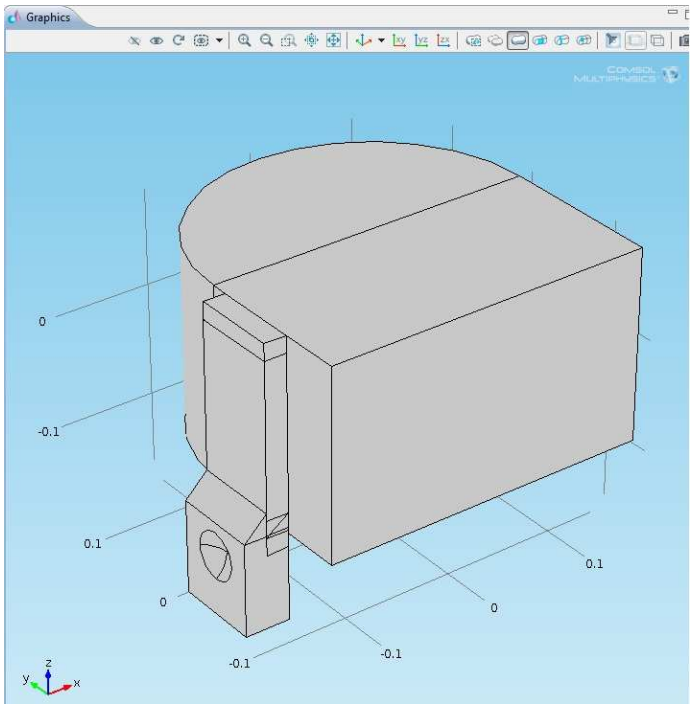

Fig. 28: Geometry of MWO 2: semi-cylindrical cavity shape.

Chapter 6

Conclusions

6.1 – Comparison between numerical models and experimental tests

Below are the results obtained by experimental tests and simulation with the numerical code COMSOL Multi-physics; this to see if there is some correspondence and whether it is possible to obtain reliable results using software, knowing only the initial parameters of the single problem.

The following are the results of the methods used or thermocouple measurements, infrared camera detections and COMSOL Multi-physics validation.

- MWO 1:

Initial Temperature ϑ_0	19	°C
Average Temperature measured ϑ_{ave}	53	°C
Efficiency η	55	%

Initial Temperature ϑ_0	19	°C
Average Temperature measured ϑ_{ave}	56	°C
Efficiency η	60	%

Table 1: Results obtained by using thermocouple. **Table 2:** Results obtained by using infrared camera.

The results obtained by the two experimental methods are very close together. In fact, the calculations for the measurements taken with the thermocouple led to an efficiency, in the cavity, of 55% while those with the camera to an efficiency of 60%. Finally, as regards the comparison with the results obtained using the software is that the efficiency is 57%.

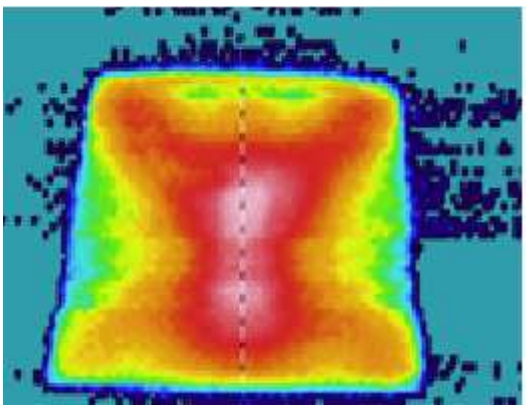

Fig. 1: Infrared camera view: section 1-5-2

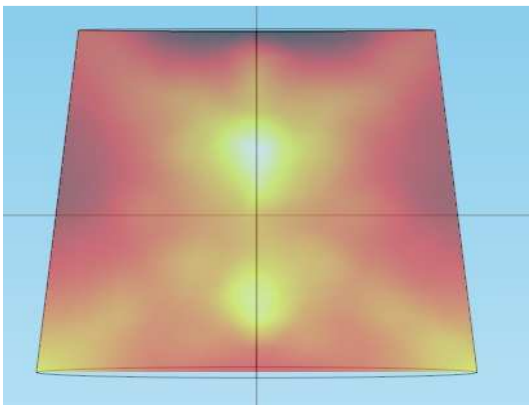

Fig. 2: COMSOL Multi-physic result: section 1-5-2.

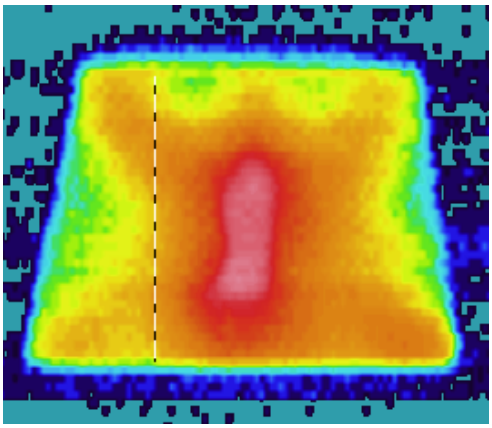

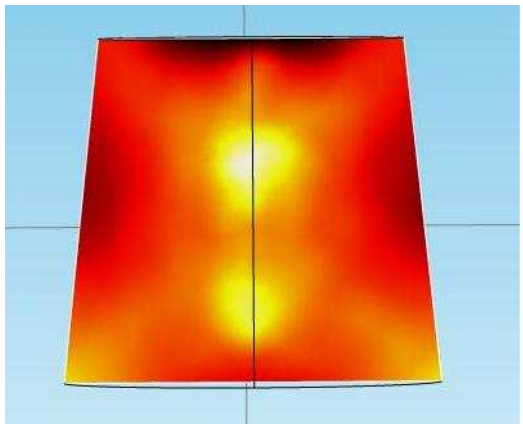

Fig. 3: Infrared camera view: section 3-5-4

Fig. 4: COMSOL Multi-physic result: section 3-5-4.

The simulations carried out, using COMSOL Multi-physics, have been very satisfactory in the case of MWO 1 where it can be said that the validation is successful. Indeed, as one can see from figure 1-2 and 3-4, the temperature distribution between the experimental case (section through infrared camera) and simulation (by software) are very close together. It meets the temperature distribution in an "X" and will also have the two hot spots along the center line where it reaches a temperature of approximately 80°C, somewhat less after cooling (see fig. 8-9 chapter 4.4 and 15-16 chapter 5.3).

Keep in mind that the color scale refers to the temperature measured is different between thermographies and COMSOL. It can be noted, however, as the orange area for the thermography indicates a temperature between 50-60°C which is the red area for the image of COMSOL; this means that the trend detected by the software is very close to the real one.

A final comparison is shown below where are reported the temperature/depth graphics of the measurement for the individual lines respectively for each of the methods used; therefore on the measurements taken with the thermocouple (Tc), those found with the infrared camera (IR) and those extracted from the results obtained by the numerical code COMSOL Multi-physics (C).

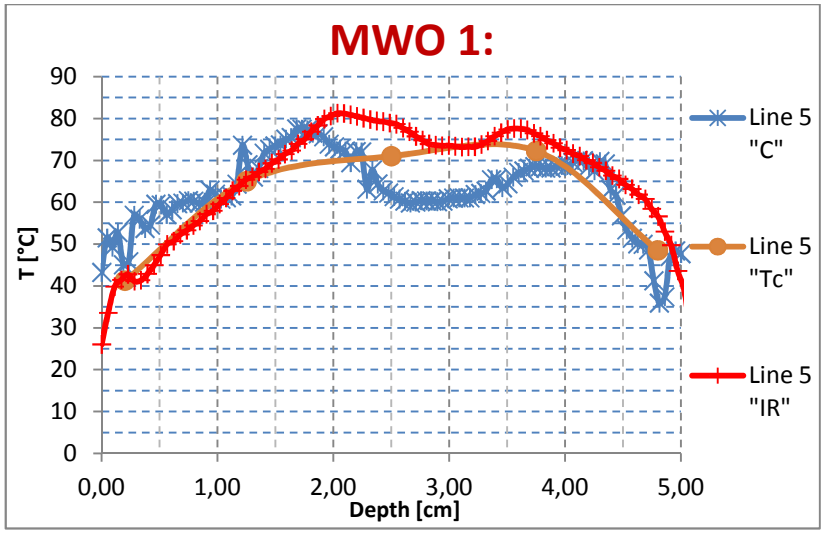

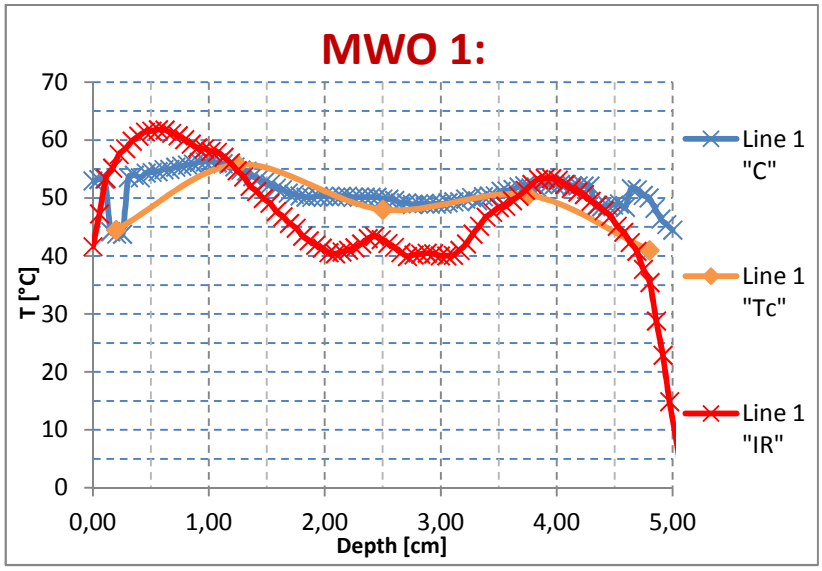
MWO 1:
70
60
50
40
30
20
10
0
T [°C]
0,00
1,00
2,00
3,00
4,00
5,00
Depth [cm]
Line 1 "C"
Line 1 "Tc"
Line 1 "IR"

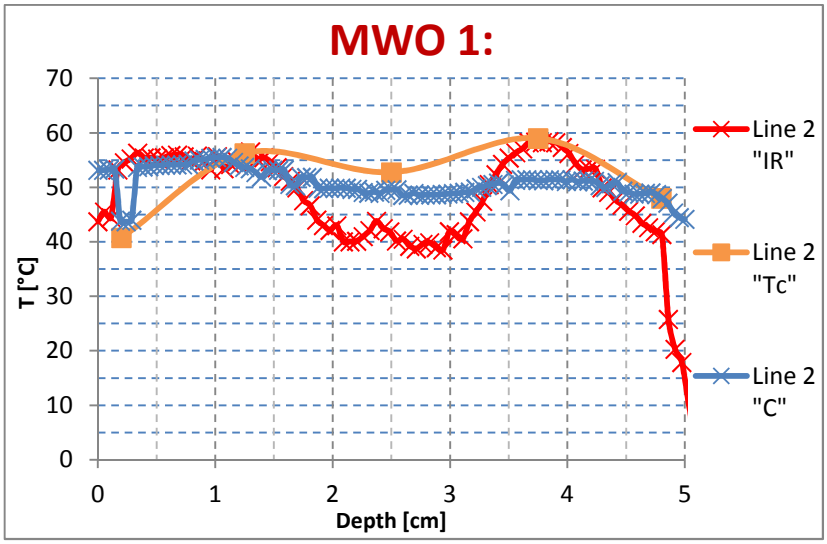
MWO 1:
70
60
50
40
30
20
10
0
T [°C]
0
1
2
3
4
5
Depth [cm]
Line 2 "IR"
Line 2 "Tc"
Line 2 "C"

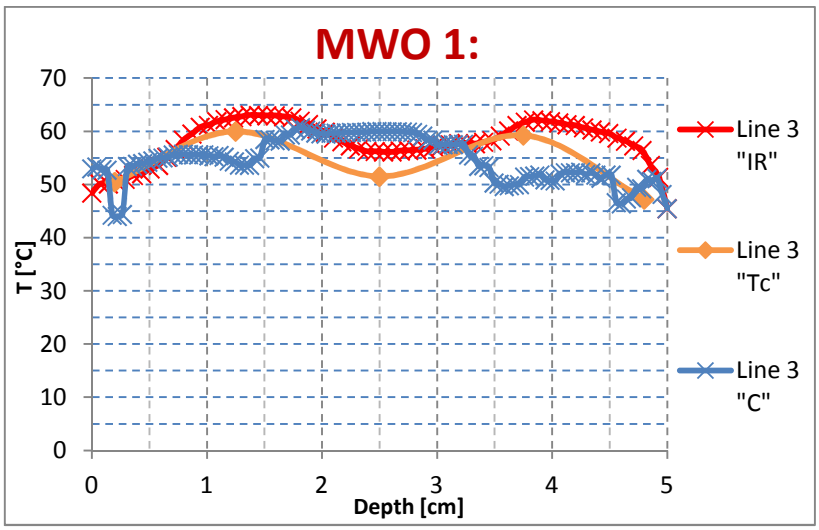
MWO 1:
70
60
50
40
30
20
10
0
T [°C]
0
1
2
3
4
5
Depth [cm]
Line 3 "IR"
Line 3 "Tc"
Line 3 "C"

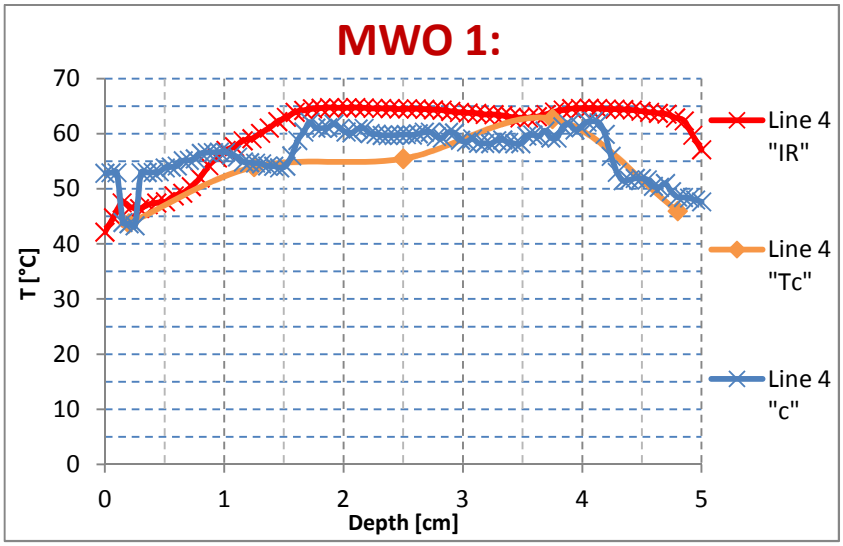

- MWO 3:

Initial Temperature ϑ_0	19	°C
Average Temperature measured ϑ_{ave}	44	°C
Efficiency η	52	%

Initial Temperature ϑ_0	19	°C
Average Temperature measured ϑ_{ave}	48	°C
Efficiency η	59	%

Table 3: Results obtained by using thermocouple. **Table 4:** Results obtained by using infrared camera.

The results obtained by the two experimental methods show two efficiencies that deviate from 52% to that obtained with the thermocouple to 59% by infrared camera; as mentioned earlier, this is probably due to the fact that on the thermocouple temperature readings there is a margin of error due to the accuracy of the measure that may have influenced the results. So it is more realistic to think of an efficiency that is close to the value obtained by the infrared camera. As regards the comparison with the numerical code we have an efficiency of 52%. This taking into account the fact that the value obtained from the preliminary assessment made, descends through the frequency domain; in fact, doing a parametric sweeps with the frequency of work, it was possible to detect which field distribution was the closest to the case and hence which value of power absorbed, and thus efficiency in cavity, was the most appropriate. These considerations lead to the conclusion that it was not easy, especially in the case of the two ovens with the double guide, to set the problem with COMSOL; this may be due to the fact that, compared to MWO 1, where there was a single guide which leads to a simulation easier, in this case the configuration with two guides, with the consequent problem of cross-talking between the phases, make more complex the study.

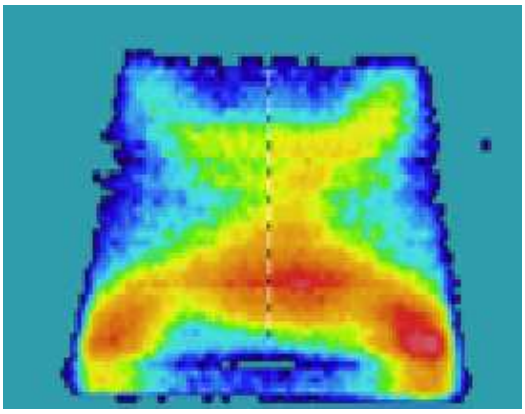

Fig. 5: Infrared camera view: section 1-5-2.

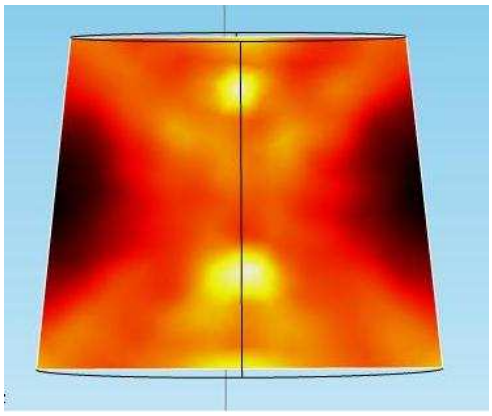

Fig. 6: COMSOL Multi-physics result: section 1-5-2.

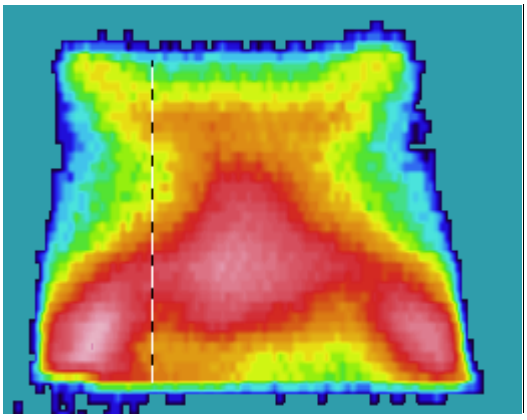

Fig. 7: Infrared camera view: section 3-5-4.

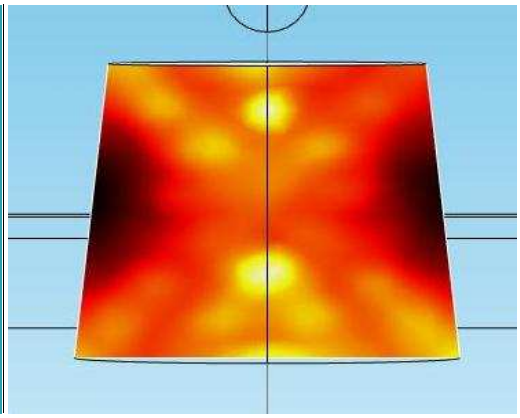

Fig. 8: COMSOL Multi-physics result: section 3-5-4.

Compared to the previous case, that relating to the MWO 3 presents diversity. Indeed, as shown in figures 5-6 and 7-8, the software detects that the hot spot at the top of the piece there, but should instead be two hot spots in the lower ends. That which corresponds is certainly the hot spot just under the center of the load and also remains correct the temperature distribution in an "X".

The temperature reached, in the hot spots, in the experimental test is 70°C which is what is achieved through the simulation with COMSOL at the point just below the center of the sample; while the ends do not reach just the same values of temperature but are close enough cause the termographic camera marked 70-75°C (fig. 12-13 chapter 4.3) while the software's simulation reported 60-65°C, always considering the cooling of the piece. (fig. 21-22 chapter 5.3).

- MWO 2:

In this case it was even chosen not to make the simulation complete with software, which includes the rotation of the load for the required time, and this because the results obtained from the frequency domain, as seen in the previous chapter, were not acceptable. The fact is due, as for the MWO 3, to the more complex geometry comprising the double guide and in this case also a semi-circular shape of the cavity which may have led the software to an incorrect calculation. This leads us to think of studying the physics of a problem than; for example, make the antenna of the magnetron in a different way trying to reach, if possible, to simplify the problem.

6.2 – Outlooks

The results obtained leads us to affirm that the use of the agar-gel, such as experimental load, is valid, also in substitution of water, provided by the Standard IEC 60705, relating to methods for the measurement of performance in household microwave ovens.

As already mentioned, the problems seen especially in the case of MWO 2 lead us to think that we need to improve the simulations with a more accurate model of the physics, especially with regard to the source. Moreover, it would be interesting to investigate about simplified models, especially regarding the geometry and physics of the problem.

Furthermore, the microwave ovens viewed, with the magnetron as source, have a configuration that has come to the end as development. The machines of the future will have, instead of the magnetron source, other types of feeding that will lead to increase efficiency and the distribution of the temperature in the load.

Bibliography

[1] G. Dilda, *"Microonde"* , Torino, Libreria Editrice Universitaria Levrotto & Bella, 1956, chapter 4-5 (first part) and chapter 4 (second part).

[2] "*Il Magnetron*", http://www.cirocarbone.it/MyJobs/magnetron.htm, 25/10/2011.

[3] S. Lupi, *"Appunti di Elettrotermia"*, 2005-2006, chapter 6.

[4] H. W. Yang, S. Gunasekaran, "Comparison of temperature distribution in model food cylinders based on Maxwell's equations and Lambert's law during pulsed microwave heating", *Journal of Food Engineering*, 64, 445–453, 2004.

[5] M.W. Lorence, P.S. Pesheck, *"Development of packaging and products for use in microwave ovens"*, Boca Raton Boston New York Washington, DC, CRC Press, 2009, chapter 1-2-4.

[6] D. M. Pozar, "Microwave Engineering", New York, Chichester, Weinheim, Brisbane, Singapore, Toronto, John Wiley & Sons, Inc., 1998, chapter 1.

[7] "Thermographic camera", http://en.wikipedia.org/wiki/Thermographic_camera, 10/01/2012.

[8] J. M. Osepchuk, "The history of microwave oven: a critical review", Full Spectrum Consulting, Concord MA,01742,U.S.,2009 IEEE.

Appendix A

MWO 1

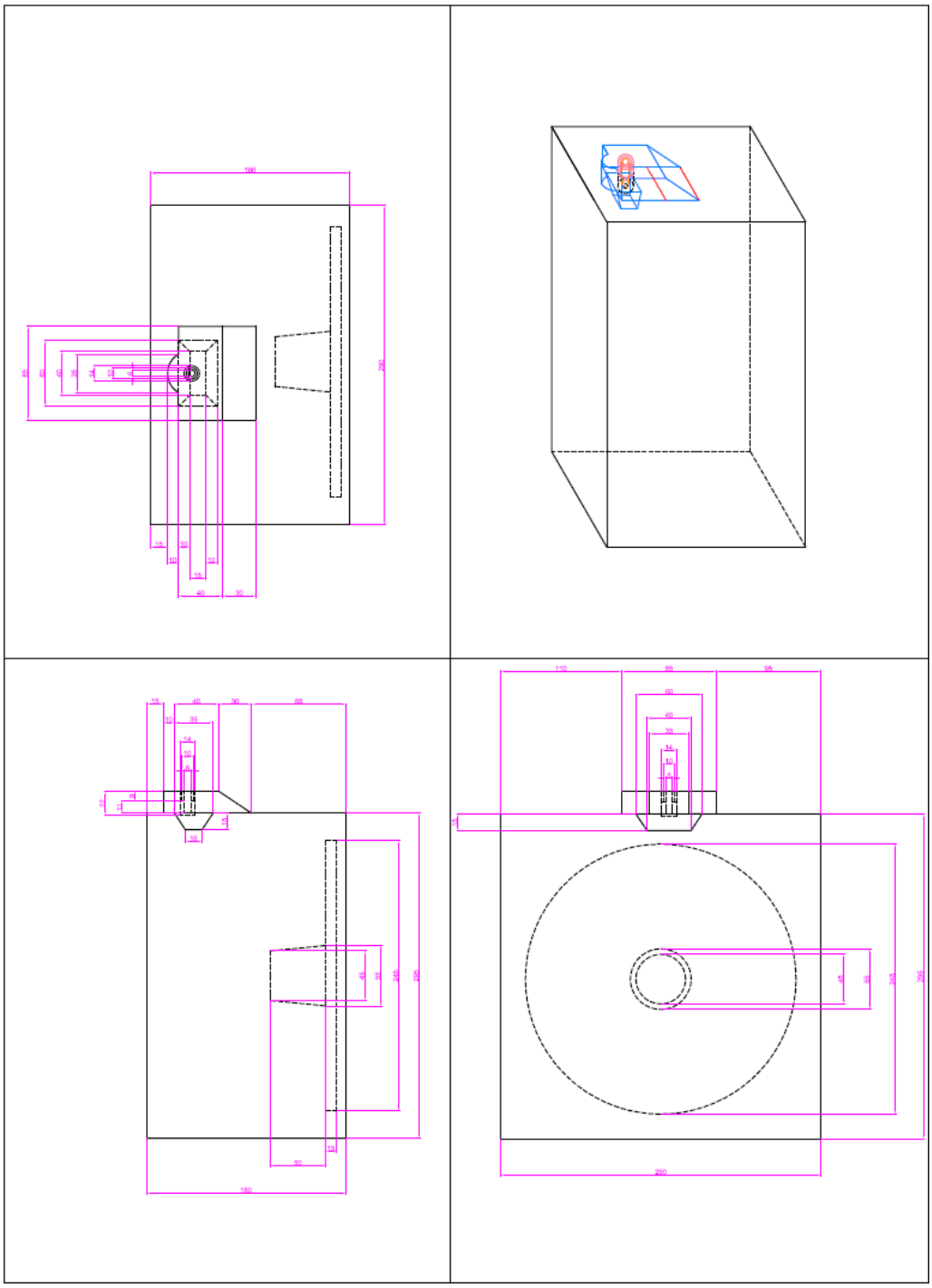

Appendix B

MWO 2

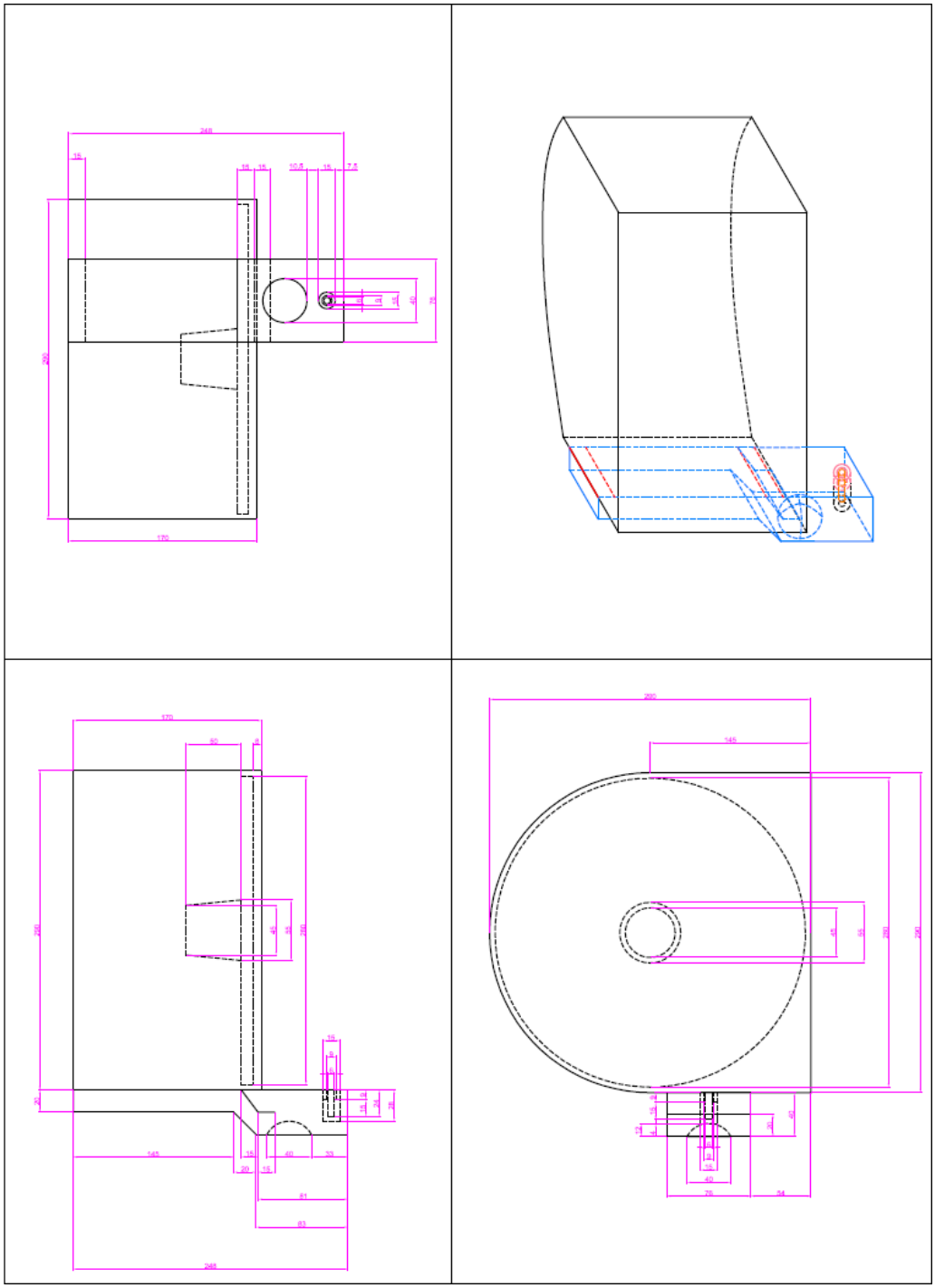

Appendix C

MWO 3

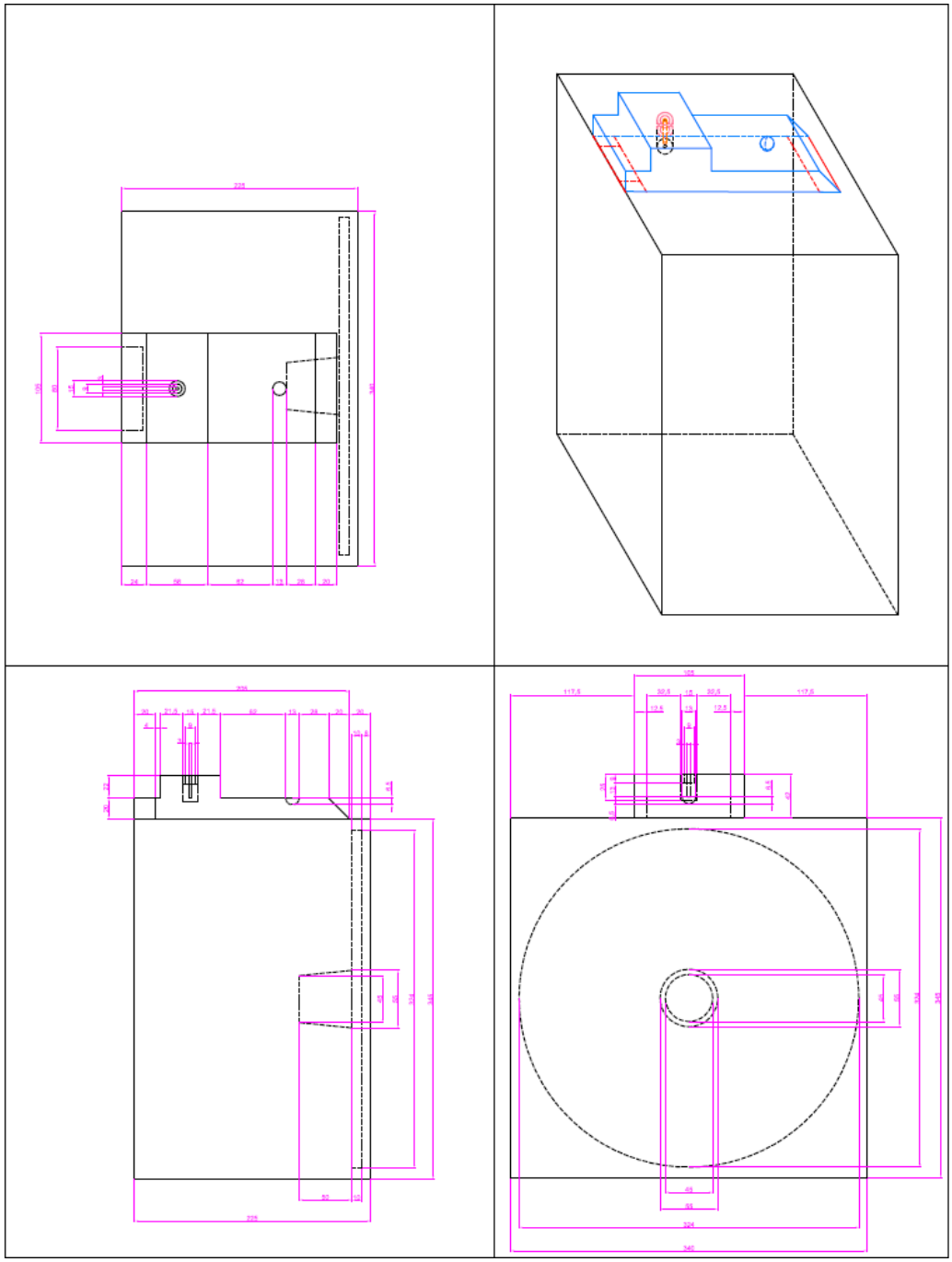

Acknowledgments

First of all, I would like to thank Prof. Fabrizio Dughiero, who gave me the opportunity to develop this thesis.

I also thank Marco Bullo, and in particular, Fernando Bressan, who have followed my study giving me the advices and assistance necessary; thanks to the group of Laboratorio di Processi Elettrotermici (LEP), Cristian, Elisabetta, Alessandro, Mattia, Stefano, Ale to their availability and great company in the last six months of work.

A thought also goes to all my long-date friends, Andrea, Gianp, Pir, Amali, Alex, and Gian and to a person who is becoming every day more special, Elena. A Sincerely thanks also to Diego for the time we spent together and also to his family for the hospitality shown.

Finally, I would like to thank my family who always supported me in all my choices.

Ringraziamenti

Prima di tutto, vorrei ringraziare il Prof. Fabrizio Dughiero, che mi ha dato l'opportunità di svolgere questa tesi.

Ringrazio inoltre i correlatori Marco Bullo ed, in particolare, Fernando Bressan, che hanno seguito il mio percorso di studio ed elaborazione dandomi i consigli e gli aiuti necessari in ogni occasione; un grazie anche al gruppo del LEP ovvero a Cristian, Elisabetta, Alessandro, Mattia, Stefano e Ale per la loro disponibilità e ottima compagnia in questi sei mesi di lavoro.

Un pensiero va anche ai mie amici di vecchia data Andrea, Gianp, Pir, Amali, Alex, Gian e ad una persona che sta diventando ogni giorno più speciale, Elena. Un grazie sincero anche a Diego per gli anni di studio passati assieme e inoltre alla sua famiglia per l'accoglienza mostrata.

Infine, vorrei ringraziare la mia famiglia che mi ha sempre sostenuto ed appoggiato in tutte le mie scelte.